Efficiency and Linearity Enhancement of Microwave GaN Power Amplifiers using Harmonic Injection

by

Asmita Rajiv Dani

B.S., University of Mumbai, India, 2008

M.S., University of Colorado, 2010

A thesis submitted to the

Faculty of the Graduate School of the

University of Colorado in partial fulfillment

of the requirements for the degree of

Doctor of Philosophy

Department of Electrical, Computer and Energy Engineering

2013

This thesis entitled:

Efficiency and Linearity Enhancement of Microwave GaN Power Amplifiers using Harmonic Injection

written by Asmita Rajiv Dani

has been approved for the Department of Electrical, Computer and Energy Engineering

Zoya Popović

Dragan Maksimović

Date

The final copy of this thesis has been examined by the signatories, and we

Find that both the content and the form meet acceptable presentation standards

Of scholarly work in the above mentioned discipline.

Dani, Asmita Rajiv (Ph.D., Electrical Engineering)

Efficiency and Linearity Enhancement of Microwave GaN Power Amplifiers using Harmonic Injection

Thesis directed by Professor Zoya Popović

This thesis addresses an architecture for enhancing efficiency and linearity of GaN power amplifiers using external second harmonic injection at the output. This transmitter architecture has potential uses in communication and radar systems which have stringent requirements of low DC power dissipation and minimum out of band interference. An idealized theoretical analysis based on expansions of the nonlinear transfer function of a PA predicts the measured improvements in linearity and efficiency.

The experimental demostration is performed with both hybrid and integrated harmonically-injected PA using discrete GaN 6 W transistors in class-AB mode with 55% PAE at a fundamental frequency of 2.45 GHz. Harmonic injection at the output is shown to enhance the efficiency of the PA to 89%. For a slightly reduced efficiency of 78%, the linearity can be improved and > 15 dB reduction of third and fifth order intermodulation distortion tones is measured in compression.

Integration of a dynamic supply of the harmonically-injected PA is also investigated in order to achieve high efficiency and linearity for signals with Peak-to-Average ratios (PARs) of 6 dB and higher. Experimental results demonstrate a 70-80% efficient HI-PA for an output power variation of 6 dB. Reduction in third order nonlinear products and AM-PM distortion shows improved linearity of the PA over the entire range of power levels.

Finally, the concept is extended to an X-band GaN MMIC to demonstrate integration and efficiency enhancement at 10 GHz with a 4 W, 47% efficient class-AB PA, with an expected final efficiency of over 60% with harmonic injection.

Dedication

To my family

Personal Acknowledgments

I would like to thank my parents who have taught me to be independent, strong willed and encouraged me to pursue higher studies. I want to thank my entire family for being so supportive and loving. Next, I would like to thank my husband, Gokul for being there for me always and supporting me throughout my graduate school career. I am blessed to have you in my life. I would like to thank my best friend, Urvi for helping me adapt to the culture in a different country and also getting me through the tough times. I want to thank my college friends for giving me fun moments in my undergraduate studies and helping me in my studies in India. I would like to acknowledge my teacher, Mrs. Tulsi Rao for teaching me mathematical analysis of problems and showing me how to answer questions with details and accuracy. Finally, I would like to thank Prof. Vakil for exposing me to the magical world of electronics and keeping me interested in design and analysis of communication systems.

Professional Acknowledgments

I extend my deepest regards and thanks to Professor Zoya Popović for having encouraged me, shown faith in me and tapping my interests in the field of RF/Microwave circuit design. I am extremely lucky to have worked with you and I will always apply the professionalism you have taught me in my career. I would also like to thank the U.S. Airforce for funding this project and TriQuint Semiconductor for providing access to their GaAs and GaN MMIC foundary. A special thanks to Dr. Charles Campbell for providing teaching us design tricks and providing knowledgable feedback on the MMIC design. I want to thank Dr. Michael Roberg for teaching me practical microwave circuit design and power amplifier basics. I would specially like to thank Dr. Erez Falkenstein, Dr. Rob Scheeler, Dr. Jonathan Chisum, Dr. Frank Trang, and Michael Litchfield for making me feel so welcome in the lab and helping me get through my research with useful discussions and inputs. I would like to acknowledge Dr. Tibault Reveyrand and Dr. Jose Angel Garcia for giving useful ideas and input on the project and help me take measurements. I would also like to thank Dr. Luke Sankey for teaching me how to design MMIC circuits. I would like to extend a special thanks to Lavanya P., for being a good friend and being there for me. Finally, I would like to thank all the past and present group members for being great friends and providing inputs and discussions related to the thesis and other projects in the lab.

Contents

List of Tables

List of Figures

Chapter 1

Introduction

Happiness is not something ready made. It comes from your own actions.

—Dalai Lama

Do not go where the path may lead,

go instead where there is no path and leave a trail.

—Ralph Waldo Emerson

Contents

1.1 Overview

Power amplifiers used in modern RF/microwave transmitters are required to have extremely low levels of distortion in order to transmit complex, broadband and high number of channels with acceptable levels of intermodulation and spectral regrowth. Also, high efficiency is an important criterion since transmitters used for communication and radar applications usually consume a large fraction of the available power in the transmitter. The power amplifier is located directly behind the antenna and is often operated in a saturated regime in order to be more efficient as shown in Fig.1.1. This results in nonlinearity and signal distortion at the output of the transmitter.

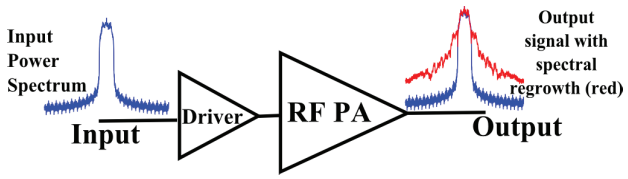

Figure 1.1: Nonlinear distortion characterisitc of a power amplifier showing the original signal (blue) and the spectral regrowth (red) caused due to distortion in the PA.

A large portion of current research in high-power amplification of signals with carriers in the microwave range focuses on improving efficiency and linearity. There are many power amplifier (PA) topologies that achieve high efficiency by driving the active device into a nonlinear region and shaping voltage and current waveforms across the device via proper selection of the output loading network at harmonic frequencies. These techniques, such as class-F and F^{-1} PA topologies, rely on the nonlinear active device for harmonic current or voltage generation and have been heavily researched, eg. in [10, 11, 12, 13]. Modern communication systems utilize amplitude and phase modulation schemes with high peak-to-average ratios (PARs) and bandwidths. The primary challenge of a transmitter design is to achieve high efficiency and maintain linearity over the entire range of power levels and bandwidth [14, 15]. Some of the solutions which address this requirement include outphasing (LINC), Doherty PA with DPD and envelope tracking PA with DPD [16, 17]. In this thesis, an architecture in which power at one or more harmonics of the operating frequency is supplied externally to either the input, output, or both input and output of the active device, referred to as harmonically-injected

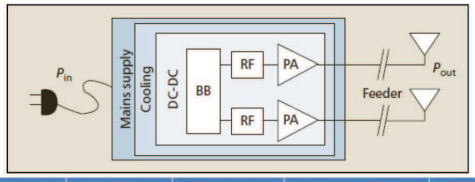

Typical base-station	Power amplifier	Air conditioning	Analog and digital signal processing	Power supply loss
% power consumption	50-80%	10-40%	5-15%	5-15%
Approximate power	1200W	300W	200W	100W

Figure 1.2: DC power consumption in various stages of a radio base station transmitter.

PAs or HI-PAs is studied as a possible solution.

Why is power amplifier design so critical in transmitters? According to a study performed by Energy Efficient Radio Access Network Technologies, Alcatel-Lucent in 2009, the PA including feeder network consumes almost 50-80% of DC power in a transmitter as shown in Fig.1.2. In 2009, the total number of cell phone users were estimated to be around 3 billion across the globe which required almost 4 million Radio base stations (RBS). Each RBS consumes 1 KW of power along with network contol consuming 1 KW and servers consuming 10 kW of DC power. Therefore, it is of the highest prority to reduce the DC power consumption in order to have energy efficient use of cell phones and base stations. In satellite transmitters, tens of watts of microwave power is required. As mentioned in [18], during eclipses, the satellite gets powered by onboard batteries which loose lifetime due to unecessary waste of power in power amplifiers. Various device technologies have been researched and are being used to design PAs for transmitters which include GaAs, LDMOS, CMOS, BiCMOS, GaN, InP, etc. However, these solid state technologies have their limitations which do not yield an optimal performance required in terms of PAs. Out of these solid state technologies, the most common ones used in the wireless and cellular frequency bands (700-2.45 GHz) are LDMOS, GaAs and CMOS technologies. GaAs and CMOS have a severe ouput power density limitation with GaAs transistors providing a maximum of 1-2 W. These devices also have a frequency limitation with lower cut-off frequencies, f_t which results in lower gain at high frequencies and hence limits the usage of the devices for high efficiency and output power. Also, technologies like GaAs and LDMOS require better thermal power management since these devices have detrimental self-heating effects [19, 20, 21].

Table 1.1: Comparison of GaAs and GaN properties

Property	GaAs	GaN
Bandgap Energy	1.4 eV	3.4 eV
Permittivity	13.1	9.6
Operating voltage	5-24 V	20-60 V
Current Density	0.5A/mm	1-2A/mm
Breakdown Field	0.4x10^6V/cm	5x10^6V/cm
Thermal Conductivity	47 W/m.K	150 W/m.k

1.2 GaN Microwave Devices

In recent years, GaN has become a prime material for research in order to build powerful devices which can deliver high performance in terms of power, efficiency and linearity. GaN has several advantages over other solid state technologies in use today such as LDMOS, GaAs, CMOS, etc. Gallium Nitride or GaN wafer technology is not as developed and therefore the devices made from GaN are based on a Silicon or Silicon Carbide substrate (SiC) which provides high thermal conductivity on the order of 490 W/m.K. A comaprison of GaAs with GaN devices is shown in table 6.1. Since GaN devices have a much higher bandgap energy which is 2 eV higher than that of GaAs, more energy is required for conduction which results in GaN handling higher voltages and hence having high P_{sat} values compared to GaAs. Also as reported in [22], one of the potential advantagess of using wide bandgap devices is to have higher junction temperatures and thinner drifting regions which can result in lower on state resistance.

The superior performance of GaN in terms of current density, thermal conductivity and wide bandgap gives it a superior advantage over the use of GaAs devices for high power microwave power amplifier applications. Another advantage of GaN is its high cutoff frequency, f_t which results in high gain at frequencies well above the ones which devices like GaAs and LDMOS can handle. Fig.1.3 shows a comparison of various solid state technologies as a function of frequency and power. It is seen that although devices made from Indium Phosphide, InP can work up in the 100s of GHz range, however, the power density is lower as compared to GaN devices.

Most of the GaN devices use the High electron mobility transistor (HEMT) technology for current research. One of the first works reported in [23] for GaN HEMTs at X band showed devices fabricated on two inch Si

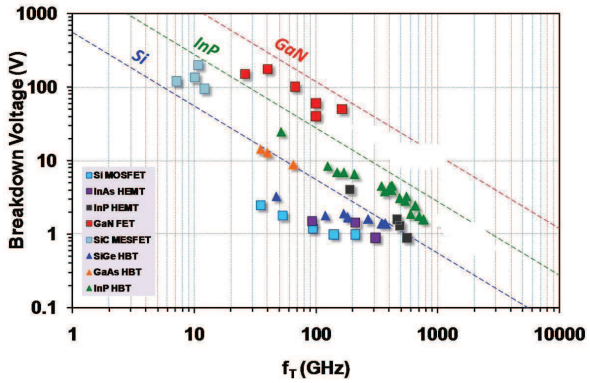

Figure 1.3: Comparion of various solid state technologies in terms of maximum frequency of operation and breakdown voltages [1].

substrate with CW power densities of 3.9 and 6.2 W/mm. These devices were tested at three different drain bias levels of 20, 35 and 40 V with a I_{dq} of 200mA/mm. The measured PAEs for the two power densities were reported to be 52 and 36% respectively. A reliability study in [23] showed that low cost, large area MMICs on Si could be realized for GaN devices at X band. However, since SiC is a better thermal conductor and provides a good lattice match for AlGaN/GaN heterojunction, GaN on SiC devices are more popular. A comparison between various substrates for GaN devices has been reported in [22] where the electron and hole mobility along with critical breakdown field, thermal conductivity and coefficent of thermal expansion is studied for various substrate materials such as Si, SiC, Diamond and Sapphire. Of these substrates, diamond has been found to be the best in terms on thermal conductivity and lattice constant. However, the material and fabrication techonology is much less mature as compared to SiC and GaN. Also, it would be extremely expensive process to produce GaN on diamond for commercial applications. A clear comparison in [24] between GaN and GaAs HEMTs shows that GaN HEMTs have a power density in W/mm which is 23 times more than GaAs HEMTs along with a breakdown voltage which is five times higher than GaAs devices.

Even though GaN on SiC devices have exhibited superior performance in terms on power density, cut-off frequency limits, etc., these devices have limitations in terms of output power density at microwave frequencies and performance degradation with temperature as shown in [25, 26]. In [27], thermal characterization of high performance millimeter-wave GaN on SiC devices is presented where changes in output power, pinch-off voltage , knee voltage and saturated drain current is measured. The drain current drops by almost 44%

with a temperature variation from -25 to 125 ∘C and the on-resistance changes by 2-3 Ω/mm over the entire temperature range. A time dependent model to examine current power and temperature in pulsed and CW mode is shown in citeWu2007. In[28, 29, 30], thermal analysis of GaN FETs is shown with critical voltage levels due to electronic degradation. In this paper, the drain current dispersion effects are investigated in AlGaN/GaN HEMTs by measuring pulsed and small signal variations. The gate and drain current lags are related to the traps formed in the heterojunction as explained in [31] where the DC, small signal and microwave output power characteristics in AlGaN/GaN HEMTs are studied.

In [31], a maximum drain current of > 1 A/mm and gate-drain breakdown voltage of > 80 V is achieved for devices with gate lengths of 0.4 μm, f_t of 30 GHz and f_{max} of 70 GHz. It is reported that at high drain voltages, the electrons injected into the GaN buffer layer get trapped resulting in depletion of the 2-D electron gas layer at the heterojunction and a reduction in drain current. It is shown that reduction of these trapping effects result in a CW power density of 3.3 W/mm and pulsed power density of 6.7 W/mm at 3.8 GHz. These trapping effects cause self heating which can be detrimental to the reliability of GaN devices as shown in [32]. A time dependent model to examine current power and temperature under pulsed operation for GaN devices is studied in [33]. The self-heating of GaN devices is studied which shows that as the SiC substrate thickness is increased along with the GaN buffer layer thickness, the thermal resistance also increases. A comparison in the reduction of transconductance for both SiC and sapphire substrates shows that the transconductance, g_m reduces by nearly 100mS/mm due to heating in both the substrates.

Variations in the chemical composition of the heterojunctions have also been investigated. For example, In [34], performances of AlInN/GaN heterojunction transistors exhibited 10 W/mm power density with 60% associated PAE at 3.5 GHz, 6.6 W/mm power density with 39% PAE at 10.34 GHz and 4.2 W/mm power density with 43% PAE at 18 GHz. In order to operate these devices at higher frequencies and have greater f_t, the gate lengths for the devices can be scaled and reduces in order to achieve optimal performance at higher frequencies. In [35], the author mentions that in order to achieve high gain and efficiency at Ka band and above, the gate lengths should be scaled well below 0.2 μm. In [35], the short channel effects on gate lengths less than 0.05 μm are presented. A comparison of various wafers with different thicknesses ranging from 207 to 240 A∘ and gate length of 0.32 μm in terms of the f_t and f_{max} is shown in this paper. The aspect ratio of

gate length, L_g to substrate thickness t is a crucial factor in deciding the output resistance and heating effects with exponential increase in these parameters with increase in the ratio. It is concluded that the breakdown voltage and output resistance benefit from high aspect ratio greater than 15. In [24], performance capabilities for AlGaN/GaN HEMTs and HBTs at mm-waves is shown. Studies cited in [24] show that a 20% increase in cut-off frequency, f_t will result in a 20% improvement in transconductance, g_m. Also, higher values of g_m can be achievable with thin AlGaN barrier layer and low contact resistance.

In recent years, there has been lot of successful work published for GaN power amplifiers at microwave frequencies with high efficiency and output power and several companies which manufacture commercial GaN devices today are listed in Table 1.2. A C-band GaN based high power amplifier was shown to have achieved a CW power of 208 W with 12 dB of small signal gain and 34% efficiency at 5 GHz in [36]. C band PAs with over140 W of output power using 0.8 μm GaN HEMTs and X band PA with 100 W of output power using 0.25 μm GaN devices has been reported in [37, 38]. A wideband amplifier working in the S-band from 1.9-4.3 GHz with PAE ranging from 50% - 62% is demonstrated with output power of 10 W over the entire bandwidth. Also, it is shown that the linearity specifications related to the ACPR of the PA in the entire band ranges from -44 to -42 dBc for a 11.2 dB peak to average ratio and PAE ranging from 25-27% for this ACPR. GaN PAs designed for frequencies $>$ 70 GHz have been demonstrated in [39, 40] where the devices are developed at HRL laboratories. The gate peripheries for these devices range from 150 to 1200 μm. The PAE at 90 GHz ranges from 13-20% with output power ranging from 1.5 W to 2 W. In [41], X-band MMICs PAs using TriQuint GaN on SiC 0.25 μm process are presented with PAEs ranging from 45-69% with output powers ranging from 2.5-13 W and upto 20 dB of large signal gain.

Several companies which manufacture GaN devices today are listed in Table 1.2.

1.3 PA CLASSES OF OPERATION

A general block diagram of a power amplifier is shown in Fig.1.4. The gate and drain bias voltages are denoted as V_{gg} and V_{dd} respectively. The drain current is denoted as I_{dd} where as the quiescent drain bias current is denoted as I_{dq}. There are three reference planes shown at the output of the transistor. Reference plane P1 is known as the virtual drain of the amplifier. Output impedance matching results in a real impedance,

Table 1.2: Several manufacturers of high performance GaN devices for commercial and military applications.

Manufracturer	*Device*
TriQuint Semiconductor	Discrete devices (GaN on SiC) with cutoff at 32 GHz
Cree	Packaged devices upto 6 GHz
Nitronex	Packaged devices (GaN on Si)
RFMD	Discrete and packaged devices (GaN on SiC) upto 10 GHz
Northrup Grumman, BAE systems, Raytheon, etc	High performance GaN devices for Military applications
RFHIC	GaN hybrid and wideband amplifiers upto 3 GHz
Fujitsu	GaN Power transistors upto 3 GHz
Mitsubishi Electric	L to C band packaged GaN devices with highest PAE of 50%
United Monolithic Semiconductors (UMS)	GaN power transistors upto 6 GHz with 50% PAE and 11 dB gain in C band.

R_{opt} at this reference plane. Plane P2 represents the reference plane after the output nonlinear capacitance. Impedance matching at this reference plane results in complex impedance Z_{opt} and is capacitve. Reference plane P3 denotes a packaged transistor which includes the package parasitics. The fundamental input and output powers are denoted as P_{in} and P_{out} with the total DC power dissipated, $P_{DC} = V_{dd} \cdot I_{dd}$.

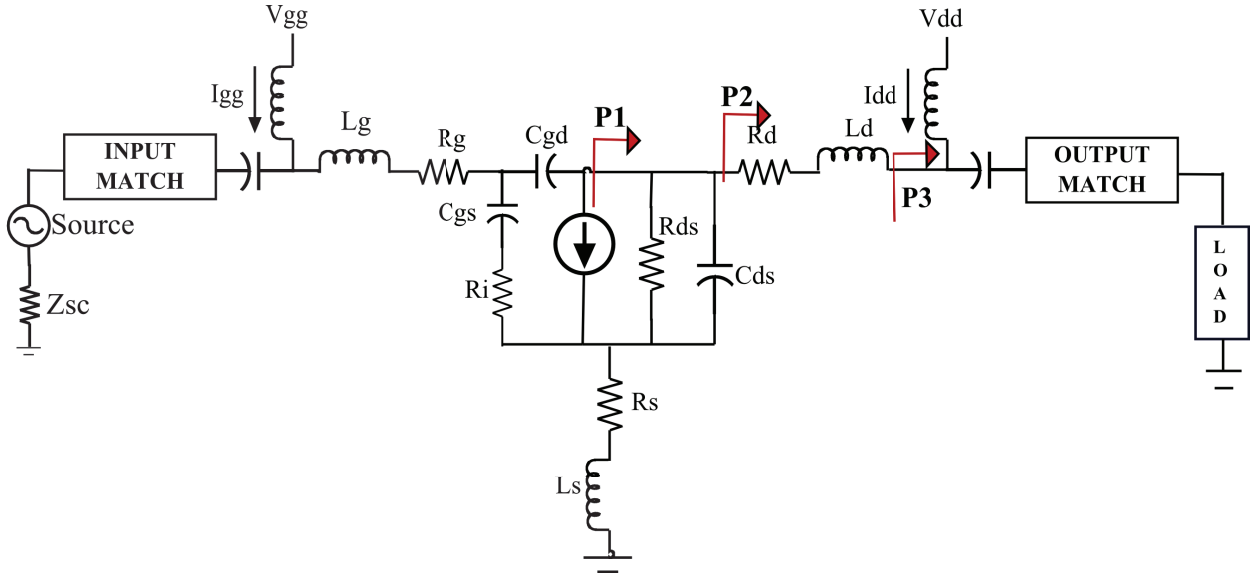

Figure 1.4: Block diagram of a general power amplifier [2].

The knee voltage, V_{knee} is the minimum voltage required for the device to operate in the linear region. This voltage limits the lower values for an RF signal with sinusoidal waveforms and is a cause of distortion.

Fig.1.5 shows a typical plot of IV curves for a GaN on SiC device with thermal heating effects. The red curve shows a trace of DC load line which represents the response of the device to DC and RF input signals.

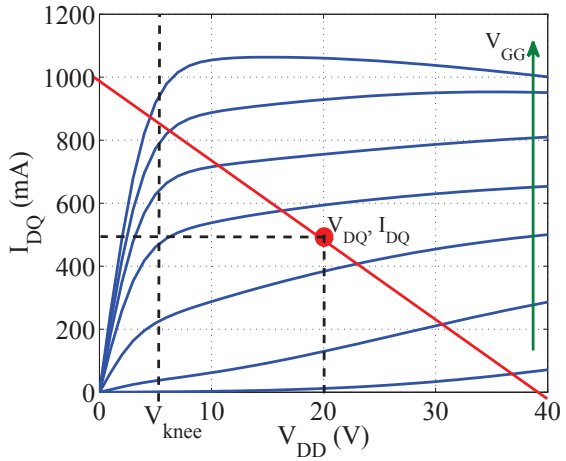

Figure 1.5: IV-curves for a 6 W GaN on SiC HEMT by TriQuint Semiconductor, TGF2023-01 showing a class-A bias point condition and load line.

Two definitions of efficiency for a normal mode of operation for a power amplifier are used in the work presented. These can be defined as the following:

- The drain efficiency, η_D is defined as:

$$\eta_D = \frac{P_{out}(f_0)}{P_{DC}} \tag{1.1}$$

- The power added efficiency or PAE takes into account the gain of the amplifier:

$$PAE = \frac{P_{out}(f_0) - P_{in}(f_0)}{P_{DC}} \tag{1.2}$$

$$PAE = (1 - \frac{1}{G})\eta_D \tag{1.3}$$

Note that the RF and DC power levels used in the calculation of efficiencies are in Watts. A power amplifier is designed to operate in a specific class of operation depending on the bias voltage and current waveform shaping at the virtual drain of the PA which is the reference plane at the current source within the transistor and does not take into account the nonlinear output capacitance. In order to design a power amplifier with a

specific class of operation, the transistor has to be terminated with the optimal load impedance, Z_{load} as shown in [42]. The real part of this load impedance, R_{load} has to be presented at the reference plane P1 as shown in Fig.1.4.

There are four basic power amplifier classes of operation defined as class A, AB, B and C. These classes of operation can be distinguished based on the gate bias turn on voltage and the DC quiescent current for the device. The DC load line for each of the classes of operations varies resulting in different current waveforms. The efficiency and maximum output power is also a function of class of operation for the PA. A PA is designed to operate at a certain input drive level in order to achieve one of the basic classes of operation. These modes of a PA can be distinguished by the current conduction angle α. which is defined as the time for which the current conducts in the postive cycle and is shown in Figure 1.6.

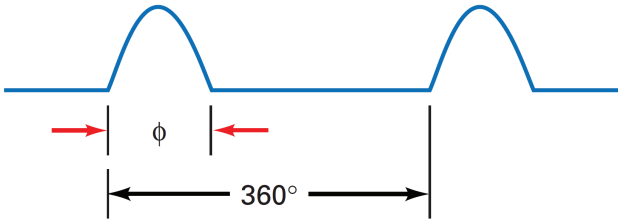

Figure 1.6: Pictorial representation of current conduction angle, α in a transistor.

1.3.1 Standard PA classes of operation

A summary of the standard PA classes of operation normalized to maximum current I_{max} and drain voltage V_{dd} is presented in Table.1.3.

Table 1.3: Basic PA modes of operation.

$Mode$	V_{dq}	I_{dq}	α	$Max.\eta$
A	0.5	0.5	2π	50%
AB	0-0.5	0-0.5	$\pi - 2\pi$	50-78.5%
B	0	0	π	78.5%
C	<0	0	0-π	100%

When a PA is operating in class-A mode of operation, the Q point defined by drain voltage (V_{dq}) and quiescent drain current (I_{dq}) is picked at the center of the DC load-line where the DC quiescent current, I_{dq}

and DC voltage, V_{dq} to be set to 50% of the I_{max} and V_{dd} values respectively. This allows the current to have maximum swing for a complete ac cycle of 360°. The load, R_L can now be defined as follows [2, 43]:

$$R_L = \frac{(V_{max} - V_{knee})}{I_{max}} \tag{1.4}$$

The theoretical analysis of reduced conduction angle modes of operation assume that all the harmonics are presented with short circuit at the virtual drain or reference plane P1 of the transistor. In class-B mode of operation, the bias point is at cut-off i.e.minimum quiescent drain current. This results in only the positive half of the ac current cycle to conduct and the resultant conduction angle for the current is 180°. The maximum theoretical efficiency for a class-B mode of operation is 78.5%.

Class-AB can be defined as class of operation with gate bias between class-A and class-B mode. The conduction angle is therefore greater than π but less than 2π as shown in Fig.1.7. The theoretical maximum efficiency for a class-AB mode of operation is 65% with the maximum output power 1 dB more than that for a class-A mode of operation.

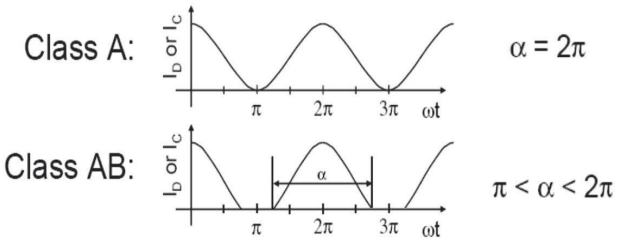

Figure 1.7: Current conduction angle for class-A and AB modes of operation for the PA.

In Class-C mode of operation, the transistor is biased below the cut-off region resulting in the current conduction angle to be less than 180°. Therefore, theoretically, this class of operation is designed to achiveve a 100% efficiency since there is no overlap between the current and voltage ac waveforms resulting in zero DC power dissipation. However, this class of operation is not practical, since the output power of the device now reduces significantly. A comparison of the efficiency and fundamental output power normalized to class-A mode of operation for the lower conduction angle classes (AB,B and C) is shown in Fig.1.8 from [2].

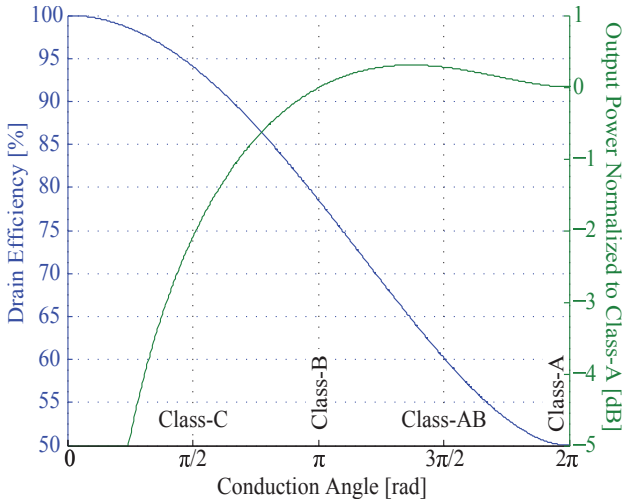

Figure 1.8: Theoretical efficiency and output power for reduced conduction angle modes of PA w.r.t class-A PA efficiency and output power [2].

1.3.2 Harmonically-tuned and Switched Mode PAs

In switched-mode PAs, wave shaping is done by directly controlling the time-domain voltage and current transients after a change in the switching state. The completely on state is a perfect short circuit and the off state is a perfect open. In order to achieve swtiched-mode of operation , the transistor should be biased at cut-off (class B) to prevent the current from flowing in the off state. Also, the input drive level must be large enough to transition from cut-off to saturation very quickly. The ideal switching PA avoids power dissipation in the switch resulting in a 100% efficient PA. However, this class of operation is nonlinear since almost 20% of the output power is in the harmonics of the fundamental frequency [2]. Some of the common classes of switched-mode PAs are class-D, E and S.

In harmonically-tuned PAs, such as class F and F^{-1}, waveform shaping is done at the virtual drain of the amplifier by terminating the harmonics in a specific manner as shown in [44, 45, 46]. This results in reduced DC power dissipation by squaring either voltage (F) or current (F^{-1}) and resulting in high efficiency PAs. Fig.1.9 shows waveform squaring by addition of third harmonic content to the fundamental sinusoidal waveforms which results in voltage squaring and current peaking for class-F and vice-versa for class F^{-1} mode.

As explained in [44], in class F mode of operation, the even order harmonics are short circuited and the odd order harmonics are open circuited at the virtual drain of the PA with a class-B bias condition. This

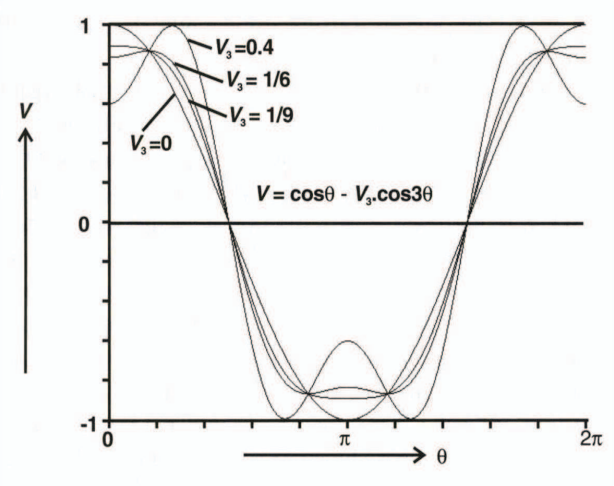

Figure 1.9: Current peaking and voltage squaring in class-F mode of a power amplifier.

results in current peaking and voltage squaring waveforms as shown in Fig.1.9. In class F^{-1}, the odd order harmonics are short circuited where as the even order harmonics are open circuited resulting in current squaring and voltage peaking. However, in practice, it is not possible to achieve ideal square waveforms for either voltage or current because this will require infinite number of odd harmonics to be terminated. If only the second and third harmonic is terminated for F/F^{-1} mode of operation, the maximum theoretical efficiency is 88.4% with a 0.5 dB increase in the output power as compared to class-B PA. If the terminations are increased to fifth harmonic, this efficiency increases to 94.8% with 0.82 dB increase in the output power. However, in order to drive a PA in class-F/F^{-1}, the PA needs to compressed beyong 1 dB compression so that it produces significant harmonic content which can then be used to shape the waveforms. Therefore, this mode of operation, even if highly efficient, is nonlinear by itself. The maximum theoretical efficiency for class-F mode of operation with addition of third and fifth harmonic is 94.8% with output power comparable to class-A mode.

1.4 PA Trade-off Characteristics

As shown in Fig.1.10, a PA design always involves trade-off between efficiency and linearity. If the PA is designed to be highly efficient, then PA needs to generate harmonics which makes it very nonlinear. If the input vs. output power characteristic of the PA is observed in Fig.1.10, the PA has maximum drain efficiency,

η_D and PAE at the 1 dB compression point where the output power of the PA is maximum and the PA is higly nonlinear. Therefore, the output spectrum is distorted due to spectral regrowth and intermodulation products. This is a significant issue with PA design in industry today since distortion causes band interference. In order to minimize this distortion, the PA is backed-off in input power. However, at this point, the PA looses efficiency significantly. Therefore, design of PA for communication and radar systems involves a trade-off between high efficiency and linearity.

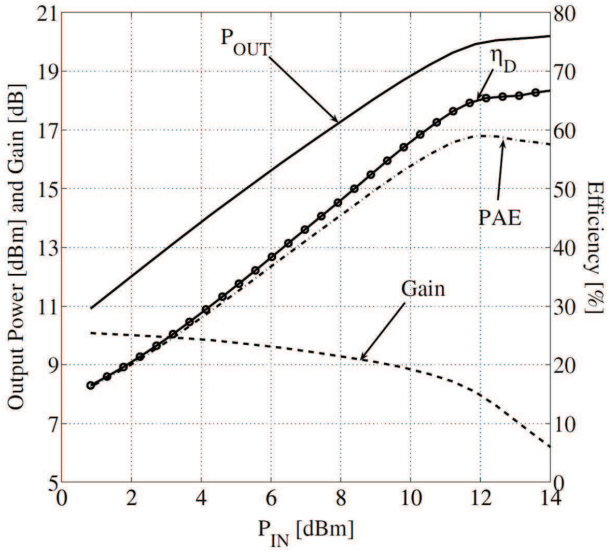

Figure 1.10: Efficiency, gain and output power characteristics of a power amplifier.

Also, modern communication signals have Peak-to-average ratios of > 6 dB which requires the PA to not only be efficient at a signal drive level but to be consistently efficient and linear for a variation in input power. This problem can be addressed by designing complex transmitter architectures such as envelope tracking, Doherty PA design, etc.

1.5 Transmitter architectures

The stringent requirements in the transmitter designs for handset and base stations require complex PA architecures to be implemented as explained in [3]. A brief summary of these PA architectures is presented in Table1.4 with a general block diagram shown in Fig.1.11. The general transmitter architectures consists of four blocks representing an input signal division between the main PA and secondary PA with a final block

for combining the signals from the two PAs at the output.

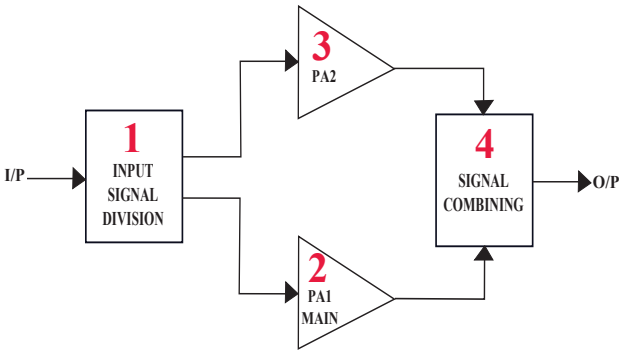

Figure 1.11: General block diagram of a PA architecture in transmitters to achieve high efficiency for high Peak-to-average ratios.

Table 1.4: Transmitter Architectures

Block	*DohertyPA*	*LINC*	*EER*	$HI-PA$
1	Digital, hybrid	Digital phase split	Digital baseband, both magnitude and phase (polar)	Baseband and RF upconversion
2	Class AB RFPA at f_0	Class-E high efficiency at f_0, highly saturated	high efficiency class of RFPA at f_0, optimized over V_{dd}	Class A/AB linear RFPA at f_0
3	Peaking amplifier, class-C at f_0	Identical to 2	High efficiency, high slew-rate PA at envelope bandwidth	Linear PA at $2f_0$ with gain $> 15\,\mathrm{dB}$ and PAE $> 40\%$
4	Doherty combiner	Isolated/Chireix combiner	Active, low-inductance bias line in RFPA	3-port diplexer network
Efficiency enhancement method	Load-pull, impedance transformation from $2Z_0$ (low power state) to Z_0 (high power state)	Load-pull with conjucate impedances	Supply modulation	2^{nd}harmonic active load pull

The Kahn envelope elimination and restoration (EER) technique uses a highly efficient but nonlinear RF PA and a highy efficient envelope amplifier in order to achieve high efficiency PA architecture for high peak to average ratios. The block diagram of this technique is shown in Fig.1.12. As explained in [3, 47], the EER approach is based on the fact that a narrow band signal can be produced by simultaneous amplitude and phase modulations and the transmitters based on Kahn technique provide high efficiency for wide range of signals and power levels. In this technique, the two most important parameters affecting linearity of the system are the envelope bandwidth and the alignment of envelope and phase modulators. The envelope tracking technique is similar to Kahn EER method, except that the supply voltage is changed dynamically.

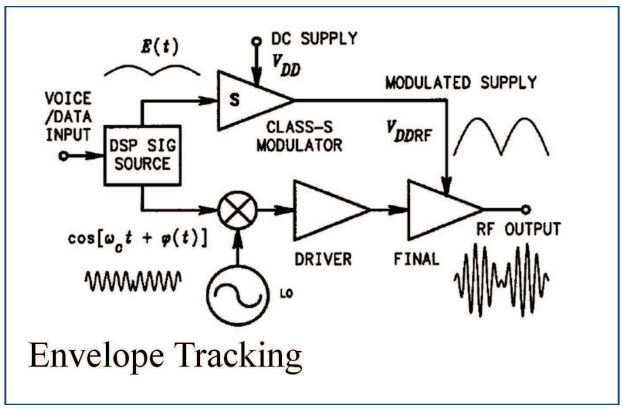

Figure 1.12: General block diagram for a envelope tracking transmitter system [3].

In the outphasing or LINC technique invented by Chireix, the transmitter produces an amplitude-modulated signal by combining the outputs of two PAs which are driven by signals with different phases [48, 49]. The phase modulation causes the instantaneous vector sum of the two output signals to follow the desired signal amplitude. Fig.1.13 shows a basic block diagram of the system architecture.

In the Doherty PA design technique explained in [50, 51], two PAs are combined with equal power through quarter-wavelength lines or networks. The main PA is biased in class B mode, while the second PA also known as the peaking amplifier is biased in class-C. Only the first PA is active when the signal amplitude is half or less than the peak amplitude. The PA architecture is operated in three different modes with low power, medium power and peak power. In the low power regions, the peaking PA is off. As the signal amplitude increases, the peaking PA starts becoming active. The additional current sent to the load of the peaking PA now causes load modulation at the first PA while maintaining the system efficiency at a constant level.

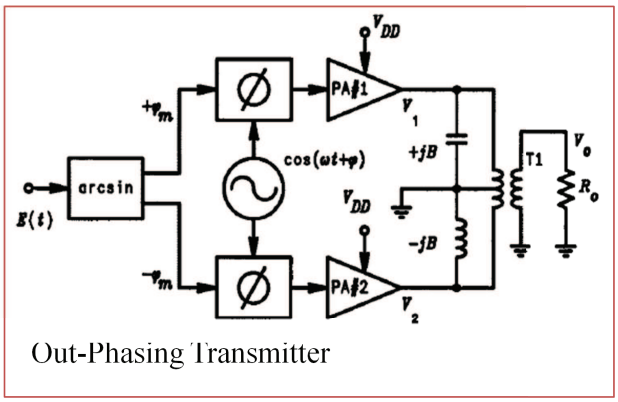

Figure 1.13: General block diagram for an outphasing transmitter system [3].

Fig.1.14, shows a block diagram and the resultant efficiency curve due to Doherty PA design.

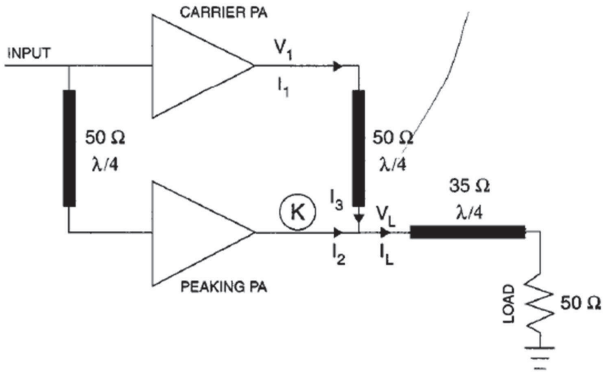

Figure 1.14: General block diagram for a Doherty PA transmitter system [3].

All the above mentioned architectures are complex and require more than one PA in order to operate efficiently for signals with high peak-to-average ratios. The design for these architectures requires challenging design steps to be taken in terms of efficiency of individual PAs, isolation and maintaining constant load for the PAs. In order to provide linearization, digital pre-distortion is required in all the architectures as shown in [52, 53, 54, 55]. Some of the other linearization techniques involves feedback where a portion of the RF-output signal from the amplifier is fed back to the RF input signal and substracted from it without detection. In this technique, the delays involved should be small in order to have system stability and loss of gain is also an issue. Another technique to achieve linearization involves the feedforward technique where the input signal is split into two paths, with one going to the main PA and other going to a delay element. The output signal from the main PA then consists of both desired and distorted signal. This signal is then combined with the delayed

input part of the signal to eliminate the error signal. Analog pre-distortion technique as explained in [56], can also be used to achieve linearization. Some of the recent work has been concentrated towards integration of supply modulation with other transmitter architectures to achieve high efficiency for >6 dB Peak-to-Average ratio signals. It is shown in [57] that a Doherty PA topology integrated with supply modulation results in PAE ranging from 51 - 70% with 8 dB back-off in input power level.

However, all these techniques require large system considerations and design challenges so as to integrate linearization techniques and achieve high efficiency for high Peak-to-Average Ratio signals. Some of the newer techniques being researched involve active load modulation which can help achieve high efficiency as well as reduce the intermodulation distortion to a certain level so that linearization as baseband does not provide high complexity and design challenges for a PA designer. This thesis talks about one of the active load modulation techniques known as second harmonic injection at the output of a PA where a external second harmonic signal with optimal phase and amplitude is injected into the drain of a PA with a diplexer network. However, even in this approach, the efficiency of the injector circuit can play a crucial role and result in design challenges at the desired input drive level. In the work presented, results from integration of harmonic injection PA architecture with supply variation are also analyzed and presented in Ch.6.

Chapter 2

Theoretical Basis for PAs with Harmonic Injection

Progress is impossible without change, and those who cannot change their minds cannot change anything.

—George Bernard Shaw

Contents

2.1 Concept of Harmonic Injection PA (HI-PA)

The concept of harmonic injection refers to architectures in which power at one or more harmonics of the operating frequency is supplied externally to either the input, output or both of an active device. A general block diagram describing the concept for harmonic injection at the output of a PA is shown in Fig.2.1. This concept incorporates the use of the fundamental frequency input signal to create the harmonics using frequency doublers which are then injected into the output of the PA at an optimal amplitude and phase. The amplitude and phase of these harmonics can be adjusted using phase shifters and attenuators. The concept of injection at the second harmonic is shown in theory and experiment in this work.

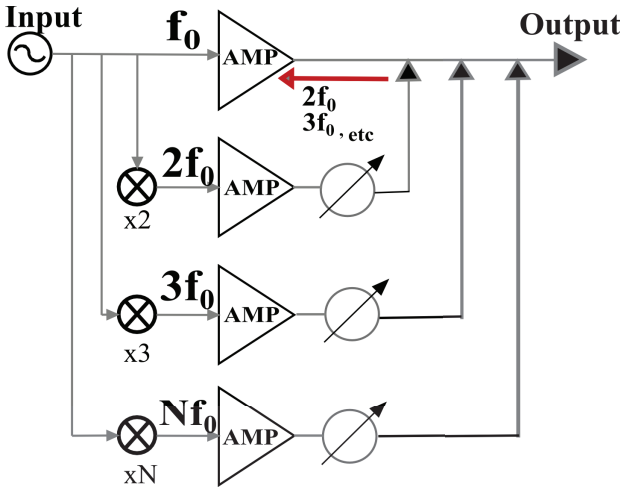

Figure 2.1: Block diagram of a harmonic-injection power amplifier (HI-PA) with 2^{nd} harmonic injection at the output. A three-port network at the output allows isolation between waves at f_0 and $2f_0$ between ports 2 and 3, while allowing low loss at f_0 between ports 1 and 2. The phase of the injected harmonic is critical to obtaining high efficiency.

Harmonic injection has been performed at the second harmonic at both input and output of an amplifier in order to achieve high efficiency or linearity criteria for the designed PA. In 1992, a patent was issued for a harmonic injection amplifier in which the harmonic signal created using a frequency multiplier is injected into the transistor output [58]. Analysis of efficiency improvement of tube PAs using harmonic injection into both the grid (input) and plate (output) has been presented in [59, 60, 61]. A harmonic injection scheme referred to as a harmonic reaction amplifier was presented in [4]. In this PA architecture, PAE of 75% is achieved for a 3-W GaAs PA at 1.7 GHz. The architecture uses two similar PAs in parallel which utilize the second harmonic produced by each of the PAs to enhance the efficiency. Signal rejection filters for fundamental and

second harmonic are integrated in the output network to provide isolation between the PAs. Fig.2.2 shows the variation in PAE and draine efficiency with 2^{nd} harmonic path length variation.

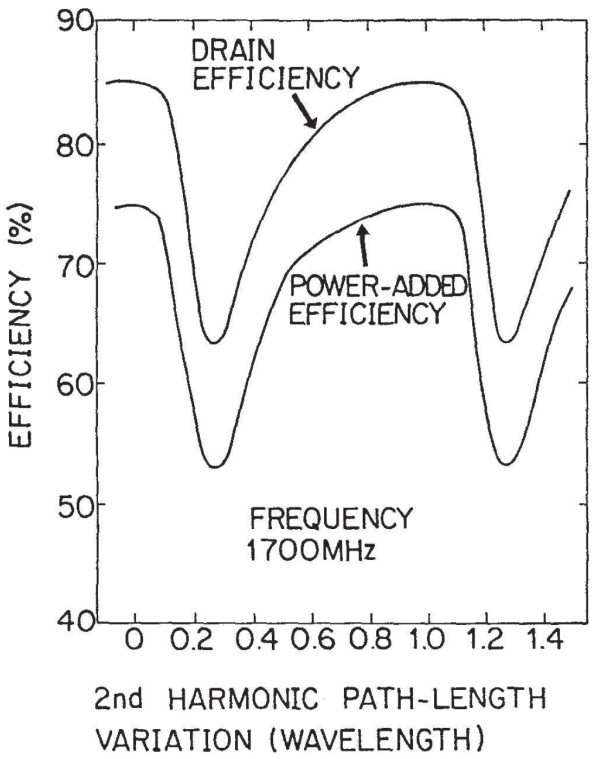

Figure 2.2: Variation in PAE and drain efficiency with change in second harmonic path length [4].

Harmonic injection technique has also been used at the input of a PA for enhancement of linearity in the PA. [62] showed theoretical analysis for linearization of power amplifiers based on second harmonic injection and base-band frequency injection at the input of the PA. In this method, the second-order frequency components generated by the predistortion circuits are provided at the input of the PA in order to generate mixing products for $IMD3$ cancellation. However, the practical limitations shown are subject to the gain and phase error associated with RF and baseband circuitry. Demonstration of reduction in third order intermodulation distortion products or IMD3, by over 24 dB for the upper sideband using a two tone signal with 5 MHz spacing is shown in [5] with harmonic injection at the input of a TWT amplifier. Fig.2.3 shows the measured results for a two-tone test on TWT with harmonic injection showing a 21.3 dB reduction in upper IMD3 levels.

In [63], a design concept of the PA's load impedance and bias network with second harmonic injection is

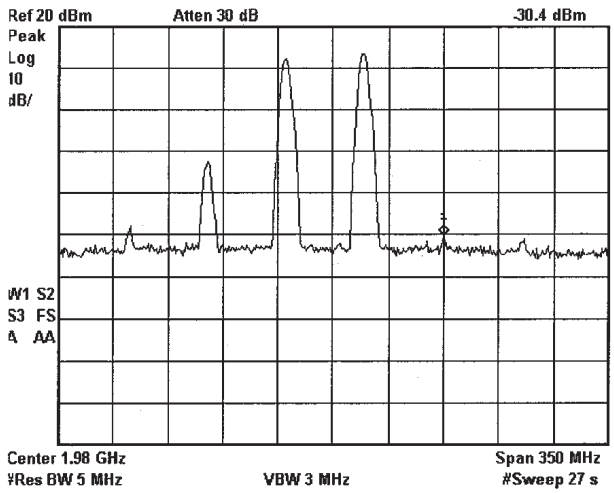

Figure 2.3: TWT output spectrum for a two-tone 15 dBm/tone input signal with harmonic injection showing a 21.3 dB reduction in upper IMD3 levels [5].

shown using volterra-series analysis. The design presented here shows a final stage PA with drain efficiency of 53% and output power of 21 dBm. It is shown in [6] that the second harmonic injection at the input reduced the IMD3 levels by 43 dB at 835 MHz resulting in a linear power amplifier. Also, it was shown that injection at the difference frequency can also result in high linearity with a 20 dB improvement in $IMD3$ and 30 dB improvement in $IMD5$ as shown in Fig.2.4. Second harmonic injection using feedback from output to the input of a PA resulting in 16 dB reduction of IMD3 levels has also been demostrated in [64].

More recently, An experiment demonstrating 15.2% efficiency improvement of a 2 GHz GaN PA using second harmonic injection at the input is reported in [65]. More recently, a concept for efficiency improvement via injection of harmonics into the output of a narrowband and broadband class-B/J amplifier was demonstrated [7, 66]. Fig.2.5 shows the measured efficiency for a class-B/J PA with second harmonic injection at the output. A novel scheme of efficiency improvement of a class-E amplifier using input harmonic injection via a feedback loop was shown in [67]. Also, a class-E VHF PA at 3.5 MHz with a secondary class-E 7 MHz PA injector is

(a) (b)

Figure 2.4: Two-tone response of 880 MHz amplifier without (a) and with (b) injection of difference frequency showing $IMD3$ and $IMD5$ improvement of 20 and 30 dB respectively [6].

presented in [68].

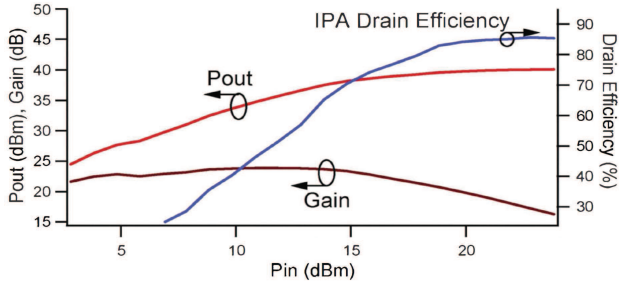

Figure 2.5: Harmonic injection class-J PA results for a constant magnitude and phase offset between the input and injected signals [7].

As shown in [69, 70, 6, 5, 71], second harmonic injected at the input of a power amplifier results in null points in the intermodulation distortion products or IMDs resulting in linear PAs. However, harmonic injection at the output of the PA, as shown in [9, 7] results in a highly efficient power amplifier with total drain efficiencies ranging from 70-80% in compression. Harmonic injection at the output of the PA also results in direct impedance synthesis at the harmonics resulting in lower distortion content. This results in higher linearity as well. In the next section, a theoretical explanation for the concept of second harmonic injection at the output of the PA is derived using fourier waveforms expansion [43].

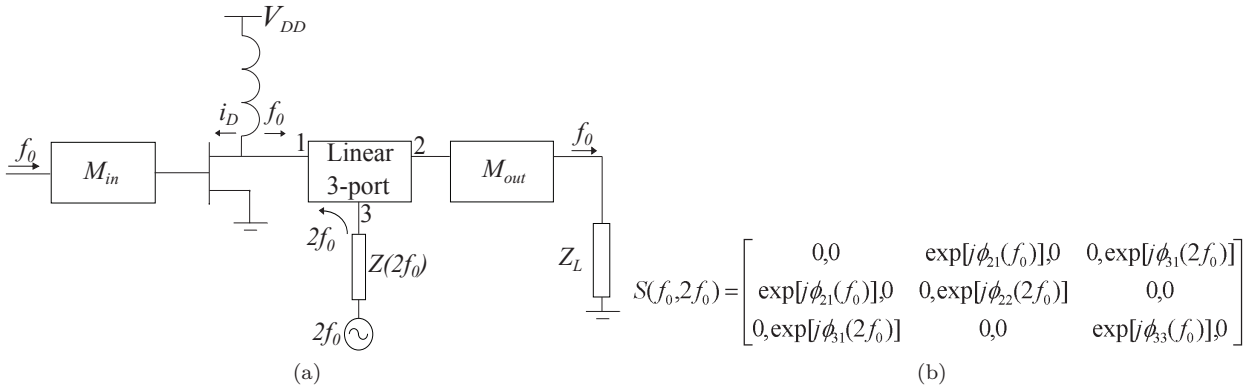

(a) (b)

Figure 2.6: (a) Block diagram of a harmonic-injection power amplifier (HI-PA) with 2^{nd} harmonic injection at the output. A three-port network at the output allows isolation between waves at f_0 and $2f_0$ between ports 2 and 3, while allowing low loss at f_0 between ports 1 and 2. The phase of the injected harmonic is critical to obtaining high efficiency. (b) Ideal S parameters for the three port injection network.

2.2 Theoretical Analysis

The theoretical analysis of the efficiency for a harmonically injected PA (HI-PA) shown in Fig.2.6 is developed based on Fourier expansions of the voltage and current waveforms at the current source of the transistor, detailed in [7, 72]. First, expressions are derived for injected voltage which optimizes efficiency, followed by the analysis of total dissipated power and a discussion of linearity. This analysis, though ideal, reveals the main purpose of the HI-PA and is summarized here for completeness from[43]. Following an overview of efficiency and power, a theoretical development of linearity for the HI-PA using taylor series expansion of the PA nonlinear characteristics is shown.

2.2.1 Waveform Analysis

In the discussion of the efficiency and power for an HI-PA shown in M. Roberg's thesis [43] and similar discussions in [73], the normalized drain voltage and current waveforms at the virtual drain of a linear FET PA are considered:

$$\bar{v}_D(\theta) = \bar{V}_{DD} + \sqrt{2}\sin\theta \tag{2.1}$$

$$\bar{i}_D(\theta) = \bar{I}_{DD} - \sqrt{2}\sin\theta \tag{2.2}$$

where $\theta = 2\pi f_0 t$, and the bar indicates a normalized quantity. For instance, when $\bar{V}_{DD} = \bar{I}_{DD} = \sqrt{2}$, the normalized class-A output power is 1W and the waveforms result in 50% efficiency. If the drain waveforms

can be shaped by harmonic content in a manner such that the overlap of the voltage and current is minimized for a given fundamental frequency output power, then drain efficiency will be maximized.

Consider the addition of only the second harmonic term in (2.1) and (2.2). In order to maintain waveform symmetry, only co-sinusoidal components are added. Such a condition will result in the voltage waveform of the same shape but 180° out of phase with the current waveform. The waveforms following addition of a second harmonic term become:

$$\bar{v}_D(\theta) = \bar{V}_{DD} + \sqrt{2}\sin\theta + a_2\cos(2\theta) \tag{2.3}$$

$$\bar{i}_D(\theta) = \bar{I}_{DD} - \sqrt{2}\sin\theta + a_2\cos(2\theta) \tag{2.4}$$

as shown in Fig.2.7, showing minimal overlap of the voltage and current waveforms.

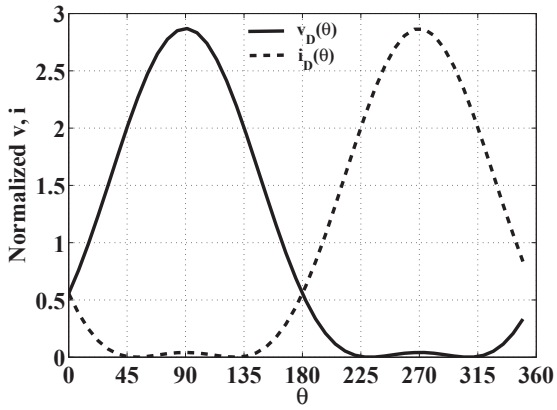

Figure 2.7: Optimal drain current and voltage waveforms for second harmonic injection amplifier, normalized to 1 W output power.

From (2.3) and (2.4), it can be concluded that the impedance at $2f_0$ is the negative of that at f_0. Effectively, this requires that power is delivered to the transistor at the second harmonic. An optimal value of a_2 that maximizes the efficiency can be found by analyzing the critical points of the drain current and voltage waveforms. The resultant optimal values of a_2 are then calculated to be:

$$a_2 > +\sqrt{2}/4, \quad \bar{v}_D(\theta_{critical,v}) \text{ is a minimum} \tag{2.5}$$

$$a_2 < -\sqrt{2}/4, \quad \bar{v}_D(\theta_{critical,v}) \text{ is a maximum} \tag{2.6}$$

2.2.2 Efficiency Analysis

The normalized total DC power consumed by the amplifier is expressed as

$$\bar{P}_{DC} = \bar{V}_{DD}\bar{I}_{DD} + \frac{a_2^2}{2\eta_{inj}} = \bar{V}_{DD}^2 + \frac{a_2^2}{2\eta_{inj}} \tag{2.7}$$

where η_{inj} is the efficiency of the injector circuit. Note that due to the symmetry of the current and voltage waveforms, $\bar{V}_{DD} = \bar{I}_{DD}$, the optimal DC supply voltage is that which results in a drain voltage waveform with minimum of zero. Therefore, from (2.3),

$$\bar{V}_{DD} = -\sqrt{2}\sin\theta_{min,v} - a_2\cos(2\theta_{min,v}) \tag{2.8}$$

The total DC power may now be expanded to the form

$$\bar{P}_{DC} = \left(\frac{1+4a_2^2}{4a_2}\right)^2 + \frac{a_2^2}{2\eta_{inj}}, \quad a_2 \leq \frac{-\sqrt{2}}{4} \tag{2.9}$$

and

$$\bar{P}_{DC} = (\sqrt{2}+a_2)^2 + \frac{a_2^2}{2\eta_{inj}}, \quad a_2 > \frac{-\sqrt{2}}{4} \tag{2.10}$$

Since we use a normalization that sets the fundamental output power to 1 W, the total efficiency is calculated as the inverse of the normalized DC power.

$$\eta_{total}(a_2, \eta_{inj}) = \frac{1}{\bar{P}_{DC}} \tag{2.11}$$

Fig.2.8 shows the total efficiency plotted as a function of both injector efficiency, (η_{inj}) and normalized magnitude of 2^{nd} harmonic (a_2).

The value of a_2 is optimized by setting the partial derivative of P_{DC} w.r.t. the Fourier coefficient a_2 to zero and solving for a_2:

$$a_2 = -\frac{1}{\sqrt[4]{8(2+\frac{1}{\eta_{inj}})}}, \quad a_2 \leq \frac{-\sqrt{2}}{4} \tag{2.12}$$

$$a_2 = -\frac{2\sqrt{2}}{2+\frac{1}{\eta_{inj}}}, \quad a_2 > \frac{-\sqrt{2}}{4} \tag{2.13}$$

These values minimize P_{DC}. Given $\eta_{inj} = 1$, the optimal Fourier coefficient reduces to $-\frac{1}{\sqrt[4]{24}}$. A plot of a_2 which corresponds to the amplitude of the required injected 2^{nd} harmonic versus η_{inj} is shown in Fig.2.9. As one would expect, the magnitude of the Fourier coefficient decreases as the injector efficiency decreases.

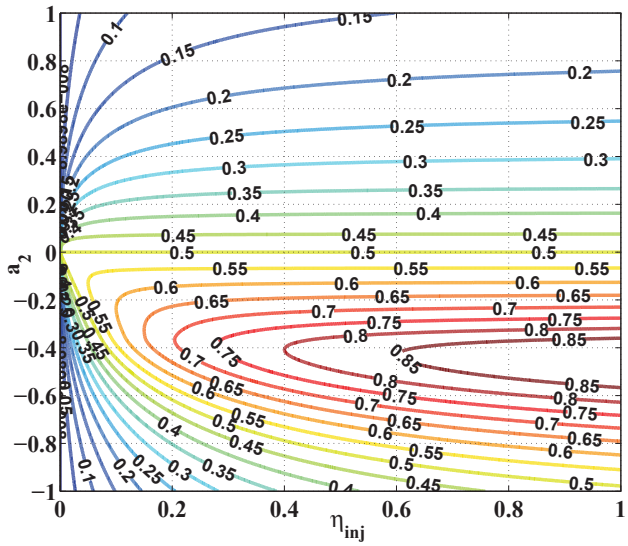

Figure 2.8: Contour plot for η_{total} as a function of a_2 and injector circuit efficiency η_{inj}.

Another interesting parameter to investigate is the ratio of the delivered fundamental output power to the required delivered second harmonic injected power, $20\log_{10}\left|\frac{a_2}{\sqrt{2}}\right|$, also shown in Fig.2.9. The PA efficiency is

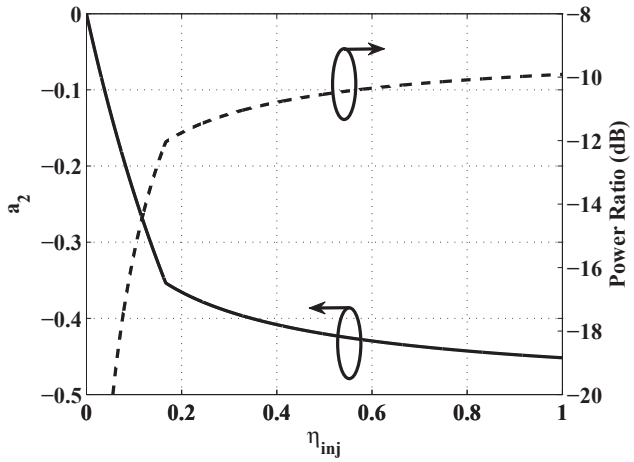

Figure 2.9: Optimal solution for Fourier coefficient a_2 and second harmonic delivered power relative to fundamental frequency output power versus second harmonic injector circuit efficiency η_{inj}.

determined by inserting a_2 into (2.9) and (2.10):

$$\bar{P}_{DC} = \frac{\left(2+\sqrt{2(2+\frac{1}{\eta_{inj}})}\right)^2+2}{8\sqrt{2(2+\frac{1}{\eta_{inj}})}}, \quad a_2 \le \frac{-\sqrt{2}}{4} \tag{2.14}$$

and

$$\bar{P}_{DC} = \frac{1}{\eta_{inj}\sqrt{\frac{8}{\eta_{inj}}+16}} + \frac{2}{\sqrt{\frac{8}{\eta_{inj}}+16}} + \frac{1}{2}, \quad a_2 > \frac{-\sqrt{2}}{4} \tag{2.15}$$

$$\eta_{total} = \frac{8\sqrt{2(2+\frac{1}{\eta_{inj}})}}{\left(2+\sqrt{2(2+\frac{1}{\eta_{inj}})}\right)^2+2}, \quad a_2 \leq \frac{-\sqrt{2}}{4} \tag{2.16}$$

and

$$\eta_{total} = \eta_{inj}\left(\sqrt{\frac{8}{\eta_{inj}}+16}-4\right), \quad a_2 > \frac{-\sqrt{2}}{4} \tag{2.17}$$

A plot of the total efficiency versus injector circuit efficiency, η_{inj} is shown in Fig.2.10 for optimized solution at a_2 and a plot for the total efficiency, η_{total} as a function of η_{inj} and a_2 is shown in Fig.2.8. The maximum value is 89.9%, and it rolls off reasonably slowly with decreasing injector efficiency. This is intuitive because the power required from the injector is significantly lower than the fundamental output power of the amplifier, as shown in Fig.2.9. As expected, when the amplifier efficiency reaches 50%, the injector circuit is turned off. In this case the amplifier degenerates to the canonical class-A mode.

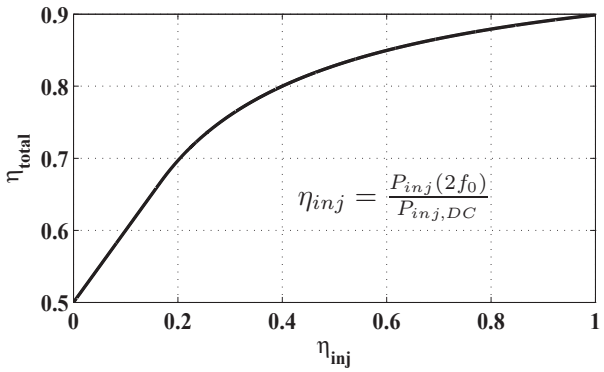

Figure 2.10: Total efficiency η_{total} versus injector circuit efficiency η_{inj}.

As previously mentioned, the load presented to at the second harmonic is the negative of that presented at the fundamental, so the load resistance normalized to the class-A fundamental load is -1. To find the output power of the PA normalized to class-A output power, normalization conditions corresponding to peak voltage and current constraints are enforced. $\bar{V}_{DD}$ and $\bar{I}_{DD}$ are now found, enabling determination of the maximum instantaneous normalized voltage $\bar{V}_{max}$ and current $\bar{I}_{max}$, and the output power normalized to the

class-A amplifier output power is determined. The normalized DC voltage is expressed as

$$\bar{V}_{DD} = -\frac{1+4a_2^2}{4a_2}, \quad a_2 \leq \frac{-\sqrt{2}}{4} \tag{2.18}$$

$$\bar{V}_{DD} = \sqrt{2} + a_2, \quad a_2 > \frac{-\sqrt{2}}{4} \tag{2.19}$$

Note that due to the symmetry of the current and voltage waveforms, $\bar{V}_{DD} = \bar{I}_{DD}$, the maximum normalized voltage is calculated as

$$\bar{V}_{max} = -\frac{1+8a_2^2-4\sqrt{2}a_2}{4a_2}, \quad a_2 \leq \frac{-\sqrt{2}}{4} \tag{2.20}$$

and

$$\bar{V}_{max} = 2\sqrt{2}, \quad a_2 > \frac{-\sqrt{2}}{4} \tag{2.21}$$

The output power normalized to class-A is then given by

$$p_{LA}(f_0) = \frac{8}{\left(\frac{1+8a_2^2-4\sqrt{2}a_2}{4a_2}\right)^2}, \quad a_2 \leq \frac{-\sqrt{2}}{4} \tag{2.22}$$

$$p_{LA}(f_0) = \frac{8}{(2\sqrt{2})^2} = 1, \quad a_2 > \frac{-\sqrt{2}}{4} \tag{2.23}$$

Fig.2.11 depicts the fundamental frequency output power reduction relative to a class-A amplifier versus the injector efficiency. This was calculated by computing a_2 as a function of η_{inj}, then computing the output power from a_2 and determining the ratio relative to 1 W. When $\eta_{inj} = 1$, the output power is only reduced by only 0.13 dB relative to the class-A amplifier.

Also, it is of practical interest to find the supply voltage and current normalized to class-A:

$$v_{DD,A} = \frac{\bar{V}_{DD}}{\sqrt{2}} \tag{2.24}$$

Fig.2.11 shows the normalized supply voltage which is approximately 0.7107 for $\eta_{inj} = 1$.

A similar analysis can be performed for third harmonic injection at the output, since symmetric square waveforms can be achieved using odd harmonics only. In the case of third harmonic injection, the impedance at the third harmonic is positive rather than negative, so the ideal waveforms can be realized with a passive set of output terminations. The analysis shows, however, that the total efficiency given by (2.16)-(2.17) is around 65% for injector efficiencies above 40% and does not reach the high efficiencies of the second harmonic

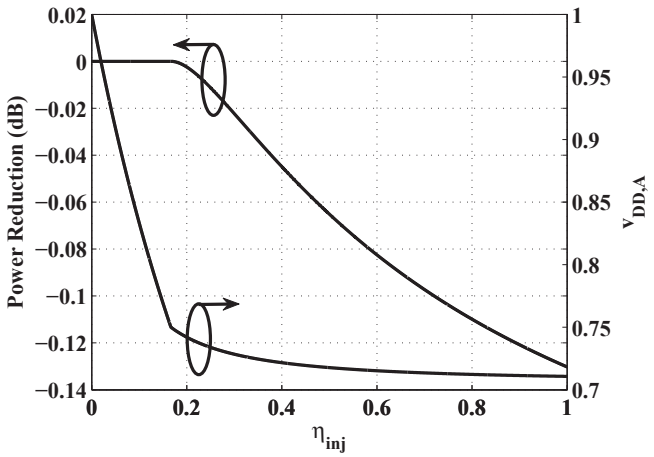

Figure 2.11: Power reduction and normalized supply voltage relative to class-A $v_{DD,A}$ versus injector efficiency η_{inj}.

injection case. The complete theoretical analysis for third harmonic injection at the output can be found in [43].

Since doing second harmonic injection at the output of the amplifier requires additional power at second harmonic to be generated, the efficiency calculation cannot be done by just taking into account, the fundamental output power and DC power dissipated in the main PA. Now the DC power dissipated in the injection circuit is critical and needs to be considered for overall efficiency of the harmonically-injected PA. This drain efficiency can be described as follows:

$$\eta_D = \frac{P_{out}(f_0)}{P_{DC_{f_0}} + P_{DC_{inj}}} P_{DC_{inj}} = \frac{P_{inj}(2f_0)}{\eta_{inj}} \tag{2.25}$$

where $P_{DC_{f_0}}$ is the DC power dissipated in the fundamental PA and $P_{DC_{inj}}$ is the DC power dissipated in the injection circuit. Since, the injector circuit not only consists of driver amplifiers, but also other components such as phase shifters, variable attenuators and mixers, the DC power dissipated in the injector circuit is defined as function of the injection circuit efficiency, η_{inj} and the total RF power delivered at second harmonic, $P_{inj}(2f_0)$.

2.3 Linearity

Transistors exhibit nonlinearities due to various factors such as input and output device capacitance, transconductance and drain-source resistance resulting in nonlinear transfer function which can be described in terms of input gate voltage, v_{gs} and drain current, i_d as follows:

$$g_m = \frac{\partial i_d}{\partial v_{gs}} \tag{2.26}$$

where g_m is the transconductance of the amplifier. As shown in Fig.2.12, this transconductance varies as a function of gate bias for each of the harmonics produced by the PA in a specific manner. The fundamental frequency transconductance, g_{m1}, increases as the PA gate voltage increases from pinch-off voltage. However, the third harmonic transconductance, g_{m3} has negative values in the class-A/AB region where as it is positive when the PA is biased at pinched-off. The interaction of harmonics in the PA with different transconductance values with the fundamental frequency results in waveform shaping and power compression.

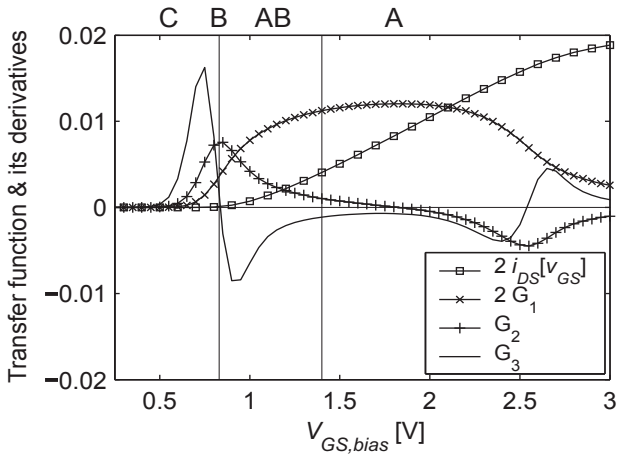

Figure 2.12: Typical transfer function and its derivatives for different gate bias voltages in FET power amplifier. The corresponding classes of operatiion are shown on top of the figure [8].

The general transfer function for a PA output system in terms of input and output voltage can be defined with the power series as follows:

$$
\begin{aligned}
v_{out} &= k_1 v_{in} + k_2 {v_{in}}^2 + k_3 {v_{in}}^3 + ... \\
&= \frac{1}{2} k_2 A^2 + \left(k_1 A + \frac{3}{4} k_3 A^3 \right) \cos \omega_o t + \\
&\quad \frac{1}{2} k_2 A^2 \cos 2\omega_o t + \frac{1}{4} k_3 A^3 \cos 3\omega_o t
\end{aligned} \tag{2.27}
$$

where $v_{in} = A \cos \omega_0 t$. k represents the general transfer function for the entire PA system.

As seen in (2.27), the second order nonlinearity causes an additional DC component and a signal at twice the fundamental frequency to appear in the output voltage. For a two tone signal, the second order nonlinearity can be easily filtered out and does not cause any in-band distortion of the signal. However, the third order nonlinearity results in in-band distortion products. The gain of the fundamental component under nonlinear operation can be expressed in terms of the fundamental gain and the third order gain and amplitude and the derivation is given in [74]. The analysis in [74] also shows that the amplitude of the second harmonic output signal is inversely proportional to the magnitude of the transfer characteristic of the amplifier at the third harmonic, which is referred to in section IV. A good discussion on extracting linearity information from a CW-fed amplifier by measuring the third harmonic output content is presented in [75]. Based on this theory, in this paper, a CW signal is used for harmonic injection analysis as the device enters saturation. In particular, we measure 2^{nd} and 3^{rd} harmonic as a function of the injected power and phase in order to assess the linearity.

2.3.1 Waveform shaping

An amplifier's simplest form on nonlinearity can be described by adding the second term to the transfer characteristic as shown in Eq.2.27. When the PA starts compressing, the amplitude of the second harmonic increases as the square of the fundamental power. Therefore, the transconductance, g_{m2} also increases. From Fig.2.12, this transfer function is remains positive when the PA is operating in class-A/AB mode. Now consider a sinusoidal input fundamental signal to the PA with the fundamental transconductance value, g_{m1} = 10. If only the second order nonlinearity is considered, then for various values of g_{m2}, the output current waveform will distort as shown in Fig.2.13.

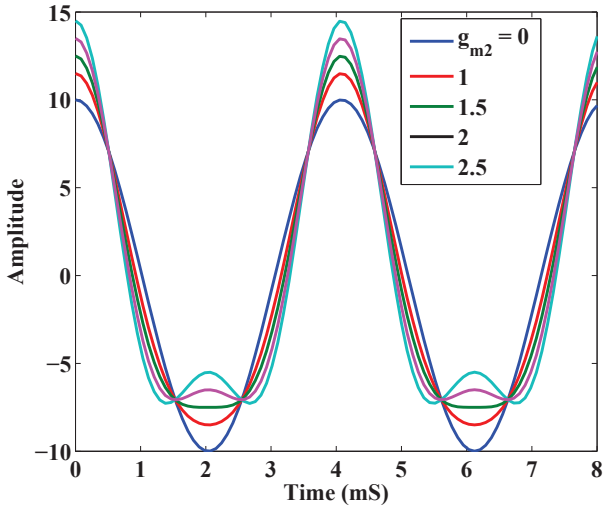

Figure 2.13: Effect of second order nonlinearity on sinusoidal waveform.

It is seen that as the value of g_{m2} increases, the sinusoidal signal becomes more asymmetric resembling half wave sinusoidal waveforms similar to class-B waveforms for a PA. This results in an additional DC component and the second harmonic due to the second order nonlinearity as shown in (2.27) and Fig.2.13. Therefore, the optimal amplitude required for the injected second harmonic depends on the input drive level and the power of the second harmonic produced by the PA itself.

In order to analyze third order nonlinearity, first lets consider the Fourier series approximation of a square wave which can be represented as follows:

$$x(t) = \frac{4}{\pi}(sin(2\pi ft) + \frac{1}{3}sin(6\pi ft) + \frac{1}{5}sin(10\pi ft) + ...) \tag{2.28}$$

where x(t) represents the square wave. The Fourier series representation of square wave is shown in Fig.2.14.

It is seen that ideal square wave results from infinite number of terms in the Fourier series expansion. However, with limited number of terms, the Fourier series representation of a square wave is non-ideal and results in flat waveforms with ripples. In a PA, odd order nonlinearities, such as 3^{rd}, 5^{th},... result in squaring of the fundamental sinusoidal signal resulting in power compression.

Now, if only addition of the third order nonlinearity of a PA with the transconductance, g_{m3} is considered, then depending on the polarity of g_{m3}, the power of the fundamental signal can either increase or decrease.

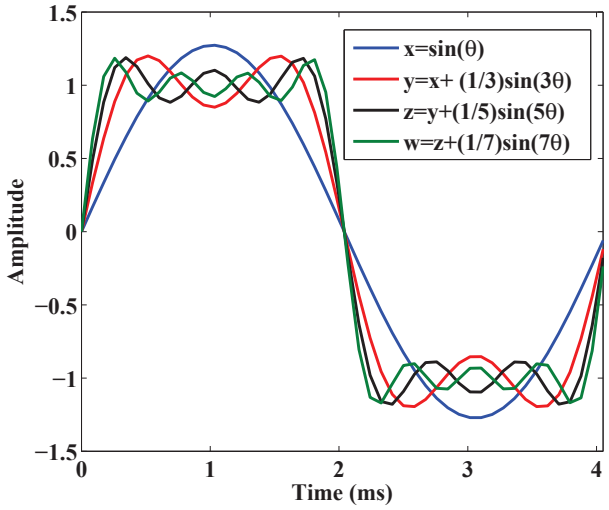

Figure 2.14: Square wave representation with the first four terms in the Fourier series.

From Fig.2.12, the values of g_{m3} for classA/AB conditions have negative sign. This results in waveform squaring and power compression in a PA as shown in Fig.2.15.

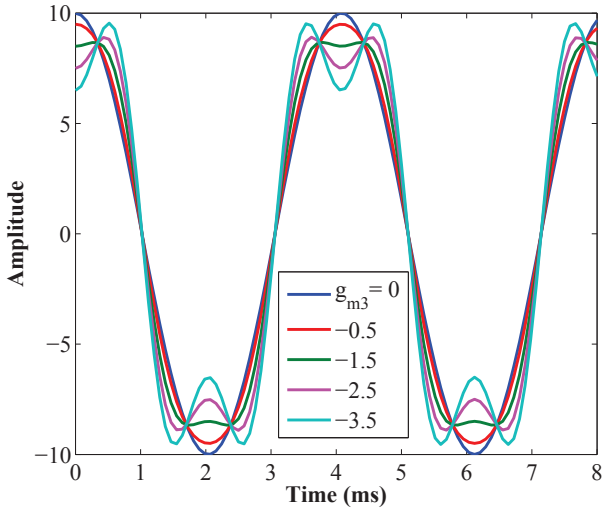

Figure 2.15: Effect of third order nonlinearity on sinusoidal waveform with negative g_{m3} values.

If the absolute values of g_{m3} are positive, then the sinusoidal waveform for various g_{m3} values results in waveform peaking and increase in power level as shown in Fig.2.16.

It is known from Fig.2.12 that the values for g_{m3} are negative for class-AB or deep class-A mode of operation. Therefore, in order to avoid squaring of fundamental waveforms resulting in reduced output power

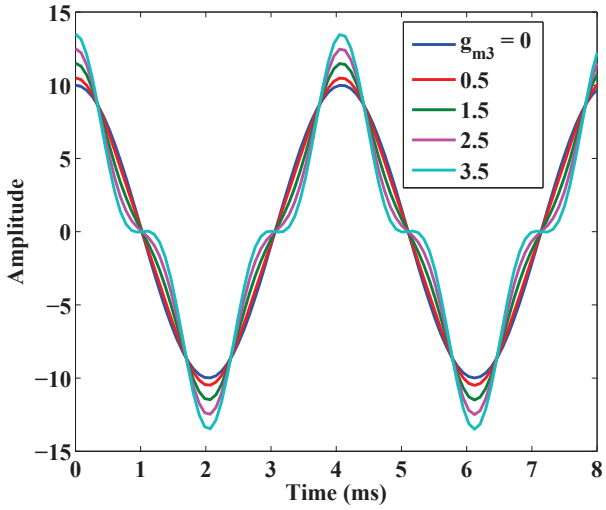

Figure 2.16: Effect of third order nonlinearity on sinusoidal waveform with positive g_{m3} values.

and shaping the waveforms such that the resultant response is similar to the one shown in Fig.2.16, the values og g_{m3} should be positive. From the theory presented in section 6.2, it is known that the injected second harmonic signal needs to be 180° out of phase w.r.t. the fundamental voltage and current waveforms. Therefore, when harmonic injection is performed on the PA, the mixing of the injected second harmonic and fundamental signal results in a third harmonic with opposite phase w.r.t. the third harmonic produced by the PA. This results in minimizing of the third harmonic and improving the linear performance of the PA.

Even though CW signal evaluation can give a general idea about the linearity of the PA, two-tone tests provide a better approximation of spectral regrowth and Adjacent channel power ratio (ACPR) with intermodulation distortion products or IMD products. First, the general behavior of PA with two-tones is analyzed w.r.t various gate bias levels. It is shown in [8, 76, 77] that the intermodulation distortion products characterisitcs vary as the gate voltage is swept from cut-off region to active region for transistors. The odd order distortion products are of relevance as they result in in-band distortion which is not easy to filter out. The third and fifth order distortion products (IMD3 and IMD5) are the most relevant parameters discussed in this work.

The intermodulation distortion products in an amplifier exhibit a behavior with sweet spots depending on the gate bias and input drive level. These sweet spots largely termed as large signal IMD sweet spots occur when the small signal IMD is in phase with the fundamental component. This behavior is associated with the

power expansion series as shown in [78].

Consider the simplified transfer function for a power amplifier based on Taylor series expansion with the output current i_d as a function of the input gate voltage, v_{gs} only. The power series can be written as:

$$i_d = g_{m1}.v_{gs} + g_{m2} \cdot {v_{gs}}^2 + g_{m3} \cdot {v_{gs}}^3 g_{mk} = \frac{\delta^k i_d}{\delta^k v_{gs}}, k = 1, 2, 3... \tag{2.29}$$

Assuming a two tone input signal with amplitude A_1, the input gate voltage can be written as:

$$v_{gs} = A_1 \cdot (cos(\omega_1 t) + cos(\omega_2 t)) \tag{2.30}$$

By substituting (2.30) in (2.29), the fundmental and third order IMD components of i_d are:

$$i_{fund} = [g_{m1} A_1 + \frac{9}{4} g_{m3} {A_1}^3] \cdot cos(\omega_1 t) \tag{2.31}$$

$$i_{imd3} = [\frac{3}{4} \cdot g_{m3} {A_1}^3] \cdot cos(2\omega_1 t - \omega_2 t) \tag{2.32}$$

Since the transconductance is strongly dependent on the gate bias and the current depends on the transconductance, g_{mk} which can take positive or negative values depending on the bias, it follows that for a particular v_{gs}, $g_{m3} = 0$. This results in nulling of IMD3 products resulting in the sweet spot condition.

As seen from Fig.2.12, in class-A bias, the initial value of g_{m3} is negative, so no sweet spots are expected for this class of operation. But for reduced conduction angle modes, the values of g_{m3} in small signal are positive, resulting in sign change at large signal power levels. Hence, a zero crossing takes place and there exists sweet spots. This condition described here is for the third order distortion product only. However, if we look at higher odd order nonlinearities, such as $g_{m5,7,9...}$, the resultant sweet spots will not follow the behavior for different classes of operation as the IMD3 products. Fig.2.17 shows the odd order distortion products calculated for a TriQuint 6 W GaN on SiC device in class-A mode.

When harmonic injection is performed on a PA at the output, the injected signal now mixes with the fundamental frequency and other harmonic frequencies, the PA produces by itself. As shown in [43], active impedance synthesis at second harmonic at the drain of the PA requires the PA also to produce harmonic

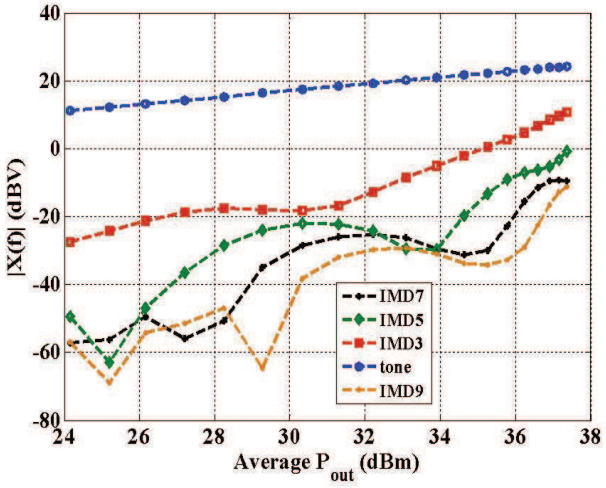

Figure 2.17: Measured voltage levels of odd order intermodulation distortion products for a two-tone signal with $f_1 = 2.45\,\text{GHz}$ and 1 MHz tone spacing.

content. Hence, the impedance synthesis at $2f_0$ now affects the other harmonic frequencies causing mixing products with different amplitude and phase. Fig.2.18 shows impact of second order products on the third and fifth order intermodulation distortion products.

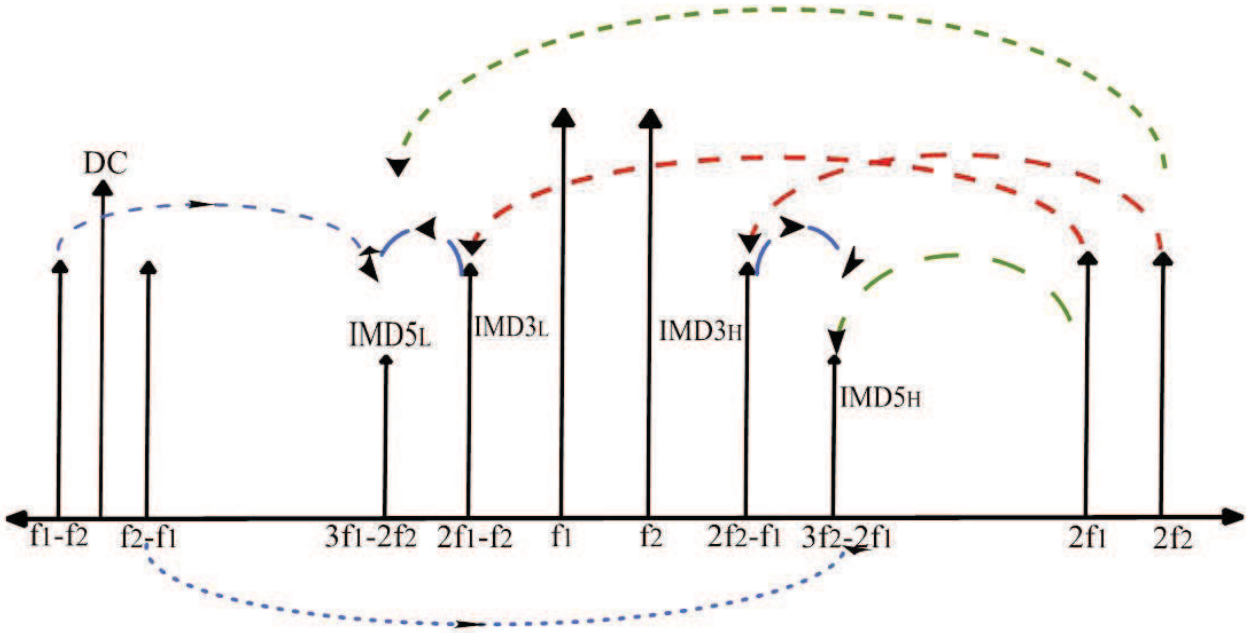

Figure 2.18: Effect on odd order distortion products (IMD3,5,...) due to mixing of fundamental, second and third order products.

From Fig.2.8, the second harmonic injection signal is 180° out of phase with the fundamental signal in

order to achieve high efficiency. Mixing of the second harmonic with other intermodulation products such as IMD3,5,.... also results in harmonic components with opposite phase as shown in Fig.2.19. This results in cancellation of the distortion products as an optimal phase and amplitude of the injected second harmonic.

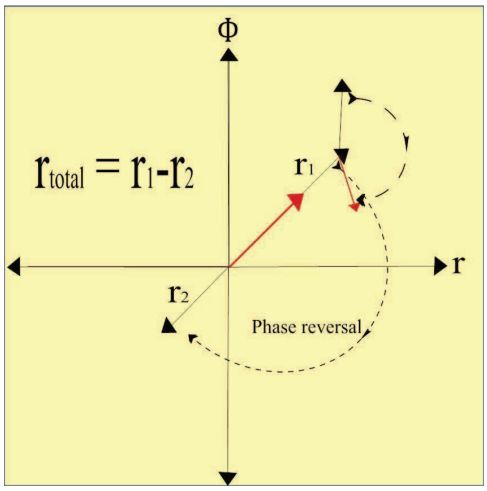

Figure 2.19: Cancellation in intermods due to mixing products formed from second harmonic injection with opposite phase. Here, r1 represents the IMD products from amplifier nonlinearity, r2 represents the IMD products created by mixing of fundamental and injected second harmonic signal. The resultant red phasor shows reduced amplitude resulting in reduction in overall distortion.

However, as shown in Fig.2.17, if the third and fifth order intermods are not increasing simultaneously with sweet spot conditions exhisting for either of the intermods at specific input drive levels, then reduction in both 3^{rd} and 5^{th} order intermods can be challenging. When the PA is operating in class-A mode, the sweet spot condition exhists only for fifth and higher order distortion products. Therefore, when the input power is swept, points in the input power sweep where sweet spots exhist for higher order intermods should be avoided in order to achieve simultaneous reduction in all odd order intermodulation products. Note that IMD7,9,... etc do not affect the perfomance of the PA as strongly as the third and fifth order distortion products due to extremely low power levels.

2.4 Conclusion

The theoretical foundations for harmonically-injected PAs presented in this thesis are derived for a highly idealized transistor model. Nevertheless, the fourier analysis predicts a maximum theoretical efficiency of 89.9% with a 0.13 dB reduction in output power and is able to predict trends in the optimal injected power

and phase for the second harmonic. The theory also predicts the required efficiency of the injector circuit of $>$ 40% in order to achieve significant overall improvement in efficiency. The power series expansion of transistor nonlinear characteristic gives insight into the linearity behavior of a harmonically-injected PA in terms of the even and odd harmonic content produced at the output of the PA.

Chapter 3

Proof-Of-Principle S-Band HI-PA

Excellence is not a skill. It is an attitude.

—Ralph Waldo Emerson

Contents

3.1 Introduction

In this chapter, a proof-of-concept harmonic injection PA or HI-PA is presented using a hybrid proto-type class-AB PA provided by Cree. The packaged device, CGH40006P has a maximum output power of 40 dBm or 10 W in class-A mode and 6 W in class-B mode. The 50 Ω PA is designed by Cree to operate from DC to 6 GHz. This PA is used to demostrate the harmonic injection concept at $f_0 = 2.45$ GHz with second harmonic,

$2f_0$ at 4.9 GHz. To this end, a three port injection network is designed in a 50Ω environment which allows the second harmonic to be injected into the output port of the PA. Initial experimental results demonstrate improvements in both efficiency and linearity.

3.2 3-Port output Injection Network

As shown in [43], a three-port output network satisfying the following conditions is required when injecting only the second harmonic at the output of the PA.

This network acts like a diplexer which is a combination of a high pass filter and a low pass filter in parallel. Such a three-port network is implemented in microstrip on a Rogers 4350B 30-mil thick substrate with relative dielectric constant, ϵ_r of 3.66 and loss tangent, $tan\delta$ of 0.0031, similar to the work reported in [7] at 900MHz and in [66] from 0.6-2.4 GHz. Fig.3.1 shows the relevant measured S-parameters extending beyond the second harmonic of the 2.45 GHz fundamental.

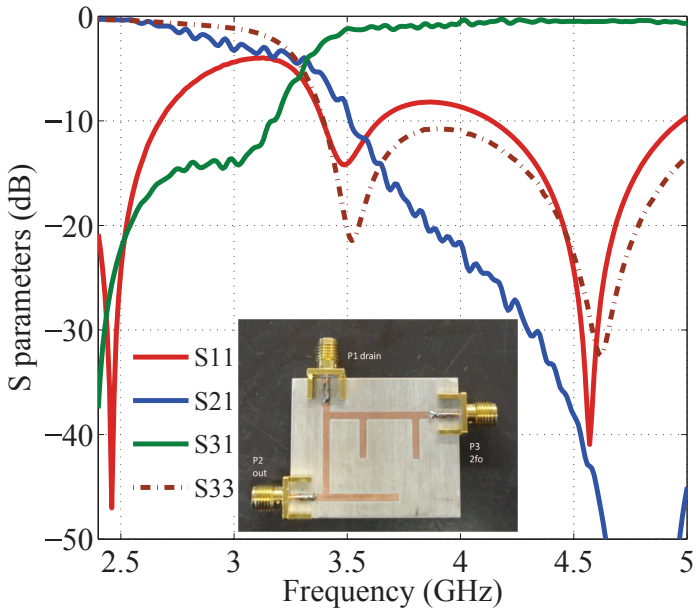

Figure 3.1: Measured S parameters for the three port injection network designed on Rogers 4350B substrate with a photograph of the circuit shown in the inset.Port 1 represents the drain of the fundamental PA, port 2 is the output of the PA and port 3 represents the injection port.

It is seen in Fig.3.1 that port 1 is matched for both the fundamental, f_0 = 2.45 GHz and second harmonic, $2f_0$, 4.9 GHz with $|S_{11}$ < -40 dB for both the frequencies. The plot also shows that the through path from

port 1 to port 2 for the fundamental frequency provides a very low loss where as the second harmonic is well isolated in this path since $|S21|(2f_0) <$ -25 dB. Therefore, the second harmonic will not leak into the fundamental low pass network resulting in negligible interference between fundamental output signal and injected second harmonic signal. Also, it is seen that port 3 is well isolated for f_0 with $|S31|(f_0) <$ -25 dB where as the second harmonic has extremely low loss in this path.

Once this network is designed, the concept of second harmonic injection is now validated by connecting the Cree CGH40006P-TB amplifier to the injection network at the output. As shown in [79], the PA has a flat gain of approximately 12 dB from 2.5 to 5 GHz at a drain voltage, $V_{DD} = 28$ V and quiescent drain current, $I_{DQ} = 100$ mA. The PA drain effiency is, $\eta_D = 60\%$ in class-B configuration at 2 GHz. The PA compresses at an input drive level of 32 dBm with a maximum output power, $P_{out} \simeq 9$ W at 2.45 GHz.

The harmonically-injected PA or HI-PA setup for $f_0 = 2.45$ GHz, $2f_0 = 4.9$ GHz utilizes two Cree GaN pHEMTs (CGH40006P) in broadband (DC-6 GHz) class-AB test-boards provided by the manufacturer. As shown in Fig.3.2, one of the PAs is used as the fundamental PA and the other PA is used as a driver in the second harmonic injection path. A single sweeper is used to generate the fundamental frequency signal at 2.45 GHz.

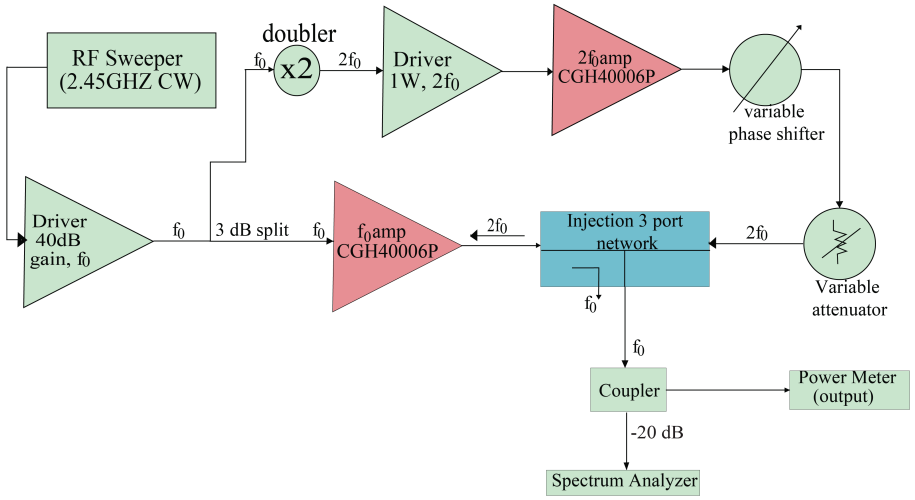

Figure 3.2: Block diagram for the experimental validation of a harmonically-injected PA concept using two pre-built broadband Cree PAs.

A 3 dB splitter,is used to divide the signal between the main PA and the second harmonic path. A low-efficiency commercial frequency doubler (Mini Circuits ZX90-2-36-S) is used to create the $2f_0$ CW signal

with a manual phase shifter and attenuator to adjust the phase and power level of the injected second harmonic signal in order to achieve active impedance synthesis at $2f_0$ at the drain of the amplifier. As shown in [43], the injected signal is required to have an optimal amplitude and phase w.r.t the output of the main PA. In order to achieve the desired power level, two driver stages are used in the second harmonic injection path. The three port injection network designed is used to inject the second harmonic into the output of the main PA.

Due to the low dynamic range of the frequency doubler, the input power to the main PA is limited and swept from P_{in} = 27 dBm to 34 dBm (linear to saturation region). A signle sweeper is used in order to preserve the relative phase in the two paths between measurements.

The drain supply is varied and measurements are performed at V_{DD} = 22, 25 and 28 V. The gate variation is also performed with V_{GG} = -1.6, -1.8 and -2 V. Since the harmonically-injected PA involves an external second harmonic signal being used to shape the fundamental voltage and current waveforms, the efficiency calculation of the entire PA system cannot just take into account the fundamental output signal and the DC power dissipated by the main PA only. In order to achieve the correct efficiency, the DC power dissipated in the second harmonic injection path needs to be taken into account. The harmonic injection circuit not only consists of amplifier, but also mixers with conversion loss and phase shifters. Hence, a better way to calcuate the DC power dissipated in the harmonic injection path is to take into account the amount of RF power being injected into the main PA at the second harmonic and the efficiency of the second harmonic injection circuit. The drain efficiency of HI-PA is therefore calculated as follows:

$$\eta_D = \frac{P_{out}(f_0)}{P_{DC} + P_{inj,DC}} \tag{3.1}$$

where $P_{inj,DC} = \frac{P_{inj}(2f_0)}{\eta_{inj}}$.

This efficiency calculation takes into account the $2f_0$ injected power and the DC power dissipated by the $2f_0$ generating amplifier.

Fig.3.3 compares the measured efficiency, output power and gain for the PA with and without harmonic injection. It is seen that the HI-PA saturates at a higher input power (32 dBm) as compared to the class-A PA (27 dBm), resulting in higher linearity. The gain of the HI PA is lower by about 1 dB as compared to the fundamental PA in the linear region, but remains higher in saturation.The drain efficiency is calculated at

the output terminal of the test board which is designed for a 50Ω system. Measured results show that higher efficiency can be achieved for a constant output power with HI PA by changing the operating bias point. For instance, the drain efficiency of the PA with no injection improves from 58% to 75% for an output power of 40 dBm by changing the drain bias from 28 V to 22 V for the HI-PA case.

The measurements in Fig.3.3 show the performance of the HI-PA in class-AB mode where a total drain efficiency improvement of 17% with the same output power as achieved for a class-AB PA without harmonic injection. In order to achieve higher efficiencies, the PA bias can be further reduces for the PA to operate in a class-B mode. In this case as shown in [7, 66], the output power of the fundamental signal is reduced by more than 1 dB and the PA is not as linear as in class-AB mode. Fig.3.4 shows a comparison of the efficiencies and output powers obtained for the HI-PA in various bias conditions.

As seen in Fig.3.4, the maximum output power is achieved at a gate bias of V_{GG} = -1.45 V and maximum drain efficiency is achieved with a gate bias of V_{GG} = -2.5 V. This just re-instates the behavior of nonlinear PAs where maximum output power is achieved in class-A mode and maximum efficiency is achieved when PA is operated close to cut-off.

As seen in the results shown above, external second harmonic injection to a PA works well to achieve high efficiency. But the question arises as to how much of the injected power is actually required in order to achieve the required performance from the PA? Is it possible to achieve 100% efficient PA if we keep injecting power into the PA? Note that in these measurements, the PA is not optimized for linear behavior. It is seen in simulations,that if the injected power to the PA increases, the efficiency of the PA also increases. However, the PA starts to become nonlinear after a certain power level of injected harmonic, since there is more than required harmonic content being produced due to mixing of the fundamental frequency and the injected second harmonic. Also, as the injected power is increased, the efficiency of the injection circuit also contributes to the total efficiency. Therefore, high total efficiency can only be achieved for an optimal level of injected harmonic power and phase. In this experiment, since we are using a pre-built PA, the loss in the output network of the PA is unknown at both fundamental and second harmonic frequencies. Therefore, measurements cannot be calibrated at the virtual drain of the amplifier. The calibration is, therefore performed at the 50Ω input and output ports of the PA. Fig.3.5 shows the magnitude of the injected power required in order to achieve the

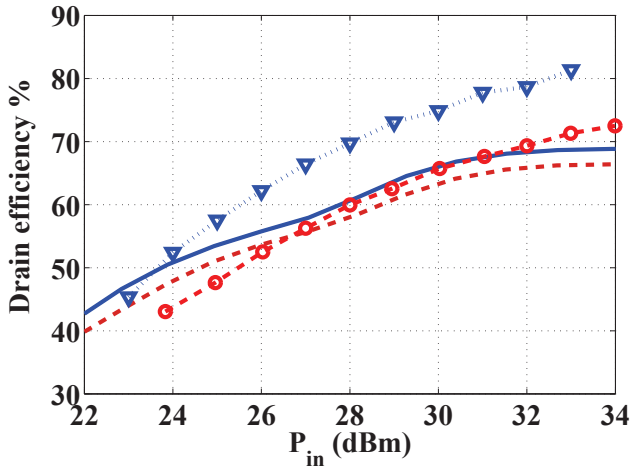

(a)

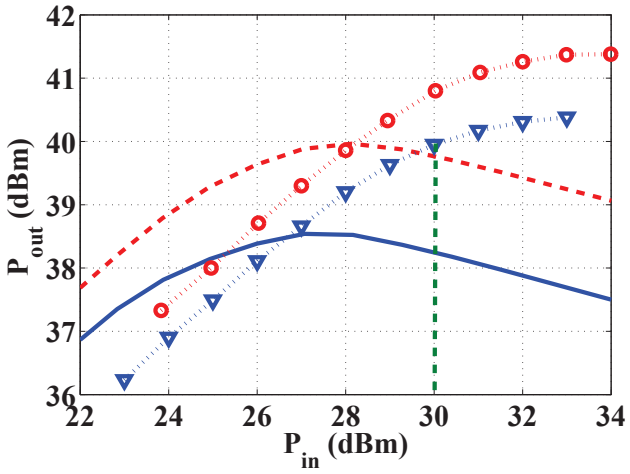

(b)

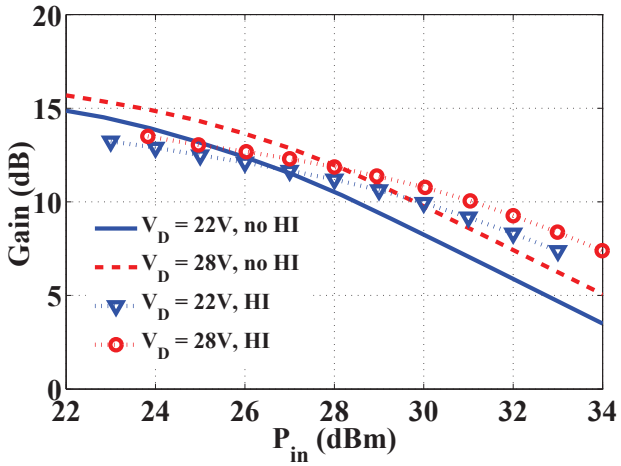

(c)

Figure 3.3: Comparison of measured (a) drain efficiency, (b) $P_{out}(f_0)$ and (c) gain for the HI-PA to the PA with no harmonic injection at V_{DD} = 22V, 28V and V_{GG} = -1.6V (class AB). Dashed green line indicates input power at which the PA becomes nonlinear.

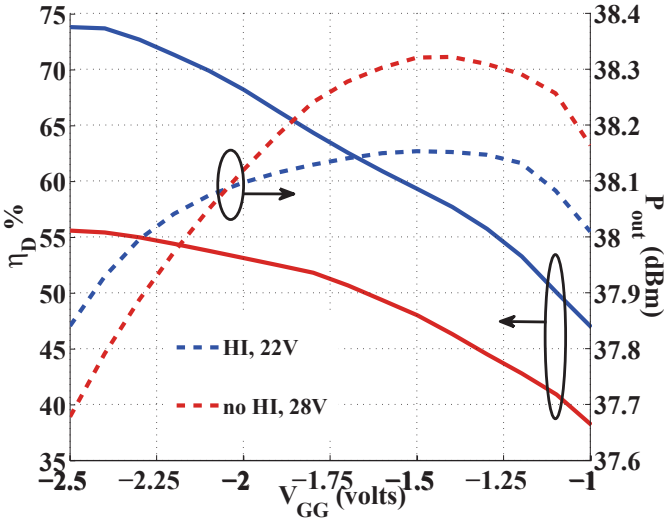

Figure 3.4: Efficiency and output power of HI-PA over a range of gate bias levels for V_{DD} = 22, 28 V and P_{in} = 30 dBm.

high efficiency in Fig.3.3.

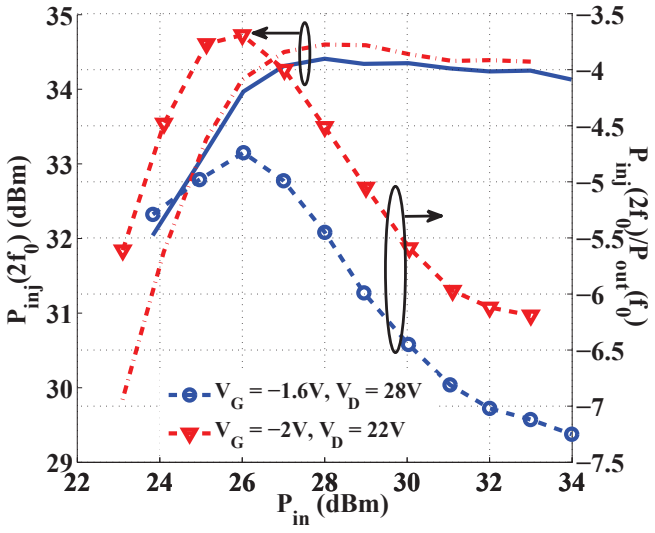

Figure 3.5: Measured ratio of injected 2nd harmonic power, $P_{inj}(2f_0)$, to output power at the fundamental, $P_{out}(f_0)$, for various bias points as a function of input power at the fundamental.

3.3 Linearity Measurements

In order to understand the nature of linearity for a harmonically-injected PA, a two-tone linearity test is performed at bias points: V_{DD} = 22 and 28V and V_{GG} = -1.8V. The two tones are kept 5 MHz apart with

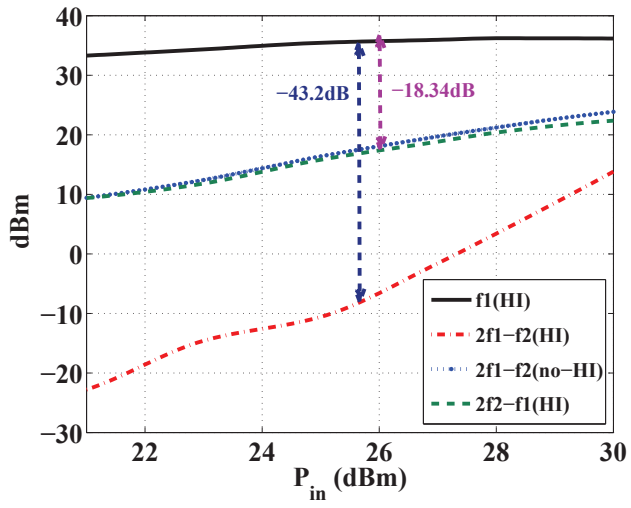

Figure 3.6: Comparison of power levels for single tone and 3^{rd} order IMD products for HI-PA and class-AB PA without harmonic injection.

f_1=2.45 GHz and f_2 = 2.455 GHz with the 3rd order intermodulation distortion products or IMD3 generated at $2f_1$-f_2 = 2.445 GHz and $2f_2$-f_1 = 2.46 GHz. In order to perform second harmonic injection for a PA with two-tones, both harmonic tones, $2f_1$ and $2f_2$ need to be injected at the output of the PA simultaneously. However, due to test setup limitations, the experiment is performed with harmonic injection at $2f_1$ (Fig.3.6), $2f_2$, orf_1+f_2 only, each requiring a different phase adjustment in order to achieve the optimal performance from the harmonically-injected PA (HI-PA). The measured results in Fig.3.6 show that the HIPA (red line) saturates at a higher input power than the PA with no HI (blue line). At lower input powers, the third order distortion product, $\text{IMD3}_{L/H}$ (3rd order intermodulation distortion) level is 30 dB lower for the HI-PA and remains 10 dB lower after the PA saturates. In Fig.3.6, only the $2f_1$ frequency is injected, resulting in a decrease in the $2f_1$-f_2 IMD_L while the $2f_2$-f_1 IMD_H is unchanged. Symmetrically, when $2f_2$ is injected, the $2f_2$-f_1 reduces. Both IMD products will be equally reduced for a signal injected at (f_1+f_2). However, the amount of reduction in this case is almost 10 dB lower than the case where either one of the two harmonic tones is injected at the output of the PA.

3.4 Conclusion

In summary, this chapter demonstrates efficiency and linearity improvements for a commercial broadband class A/AB PA with second harmonic injection at the output.

A 50 Ω diplexer network was designed with low loss in order to achieve second harmonic injection at the output of the PA. Because the harmonic content at the output is not generated by the device non-linearities, the HI PA has improved linearity compared to harmonically-terminated efficient PAs. A resultant 17% efficiency improvement with similar output power as compared to a class-AB PA is achieved for the HI-PA. Gain measurements show shift in the 1 dB compression point to a higher input drive level.

Two tone tests for the HI-PA result in > 30 dB improvement in $IMD3$ levels in the linear region and $>$ 10 dB improvement in saturation over a class-A/AB PA for a 5 MHz tone spacing with $f_0 = 2.45$ GHz. The harmonic injection at one of the two harmonic tone signals results in reduction of upper or lower sidebands which are directly related to the injected harmonic frequency. The measurements and analysis for the HI-PA in a 50 Ω environment with a commercial class-AB PA are reported in [72].

Chapter 4

Hybrid HI-PA integrated Design and Test

Accomplishments will prove to be a journey, not a destination.

—Dwight D. Eisenhower.

Contents

4.1 Hybrid HI-PA Integrated Design

As mentioned in Ch.3, a commerically built amplifier is difficult to characterize in terms of losses in both the through and the injection path at the output. In order to better understand the relationship between the fundamental and second harmonic injected powers, a hybrid power amplifier is designed with the three port injection network integrated within the output matching network of the PA along with the bias tee. The PA is designed using a 6 W GaN on SiC discrete die provided by TriQuint Semiconductor. The design of the PA is based on load-line analysis at drain voltage $V_{dd} = 28\,\text{V}$, with break apart TRL fixturing as explained in [2, 80]. The measurements are calibrated at plane P1 behind the output capacitance of the device, c_{ds} shown in Fig.4.1 which is also the virtual drain of the transistor. De-embedding to the virtual drain of the device id done by calculating the output capacitance of the device from the datasheet [81] and an EM model solution for gold bond wires simulated in Ansys HFSS.

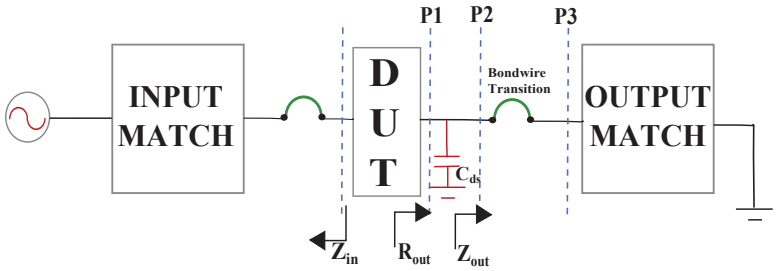

Figure 4.1: General block diagram of the designed amplifier with DUT representing the TriQuint 6 W GaN discrete die with reference planes, output capacitance, c_{ds} and bond wire transitions from die to copper on the input and output matching networks.

Based on the S parameters of the device, the input matching network of the PA is designed to have maximum small-signal gain at the fundamental frequency, $f_0 = 2.45\,\text{GHz}$ by doing conjugate matching at the input. The input matching network is designed to transform from $50\,\Omega$ to an input impedance, $Z_{in} = 10 + j * 12\,\Omega$. The second and third harmonics are shorted at the input of the PA although harmonic terminations at the input do not affect the performance of the PA in small signal regime. The input matching network consists of an input port which is $50\,\Omega$, a bias tee network to prevent the DC bias signal leaking into the input port, and impedance transformation from $50\,\Omega$ to $Z_{in} = 10 + j * 12\,\Omega$. The design of the input

matching network is done by considering a two-port passive network with port 1 terminated in 50 Ω and port 2 terminated in Z_{in}^{*}. Hence, the Z_{22} is matched to the Z_{in} impedance value and the Z_{11} is matched to 50 Ω. The input block is measured seperately using a break apart TRL calibration method. Fig.4.2 shows the measured S-parameters of the input network. An advantage in using break apart TRL calibration is that precise adjustments can be made to the circuit in order to achieve the exact impedances desired. This is due to small variations in the measured vs. simulated results due to milling tool tolerances.

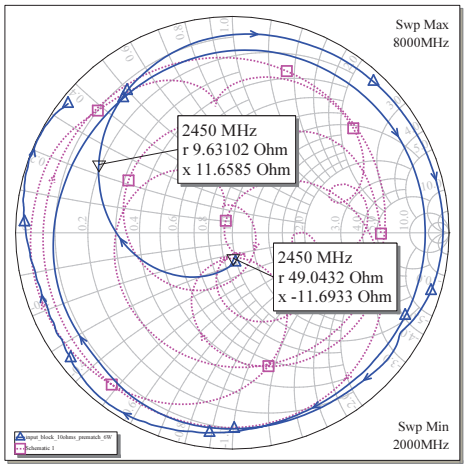

Figure 4.2: Measured input and output impedances, $Z_{11} = 49 - 11.6j\Omega$ and $Z_{22} = 9.6 + 11.6j\Omega$ for the passive 2-port input matching network.

The output network design for the PA is based on class-A bias design in [42] where the optimal impedance, R_{opt} is calculated from Eq.1.4 as 65Ω at the fundamental frequency, $f_0 = 2.45$ GHz. As shown in [43], in order to design a harmonicallly-injected PA with high efficiency, the impedance presented at P1 for the second harmonic, $Z_{out}(2f_0)$, should be equal to the fundamental output impedance, $Z_{out}(f_0)$. In order to achieve the optimal performance of the PA with harmonic injection, the impedance at the 2^{nd} harmonic was also matched close to R_{opt} at the fundamental frequency. The three port injection network which is a 3-port passive network is integrated into the output matching network with reference design from [7, 66]. Although, in this design, the matching at both fundamental and second harmonic is done in a non-50 Ω environment.

The output network is designed such that the three port injection network allows the impedances required to be presented at the virtual drain of the PA to be matched from a 50 Ω port in both the through and injection paths. The three port network can be seen as a low pass and a high pass filter connected in parallel

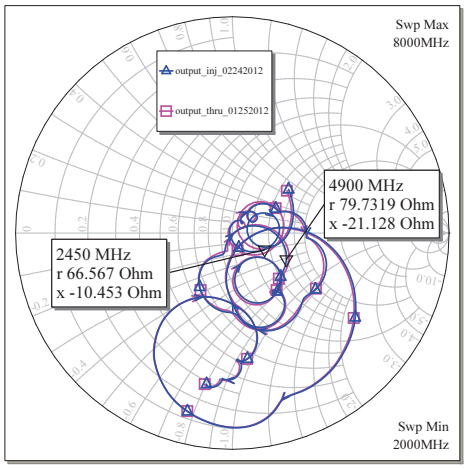

Figure 4.3: Measured Z_{11} for the output network at $f_0 = 2.45\,\text{GHz}$ and $2f_0 = 4.9\,\text{GHz}$.

with each other allowing the fundamental signal to pass through the low pass network to the output port while rejecting the second harmonic signal. Similarly, the high pass filter path allows the second harmonic to be injected into the drain of the PA while rejecting the fundamental signal coming from the output of the amplifier. Both paths have an isolation of $> 30\,\text{dB}$ between them. The measured loss for the output network in both the through and injection paths is shown in Fig.4.4. The loss in the through network is about $0.5\,\text{dB}$ as compared to a $0.9\,\text{dB}$ loss in the injection path. However, since the measurements are calibrated to the virtual drain of the device, these losses are calibrated out for measurements.

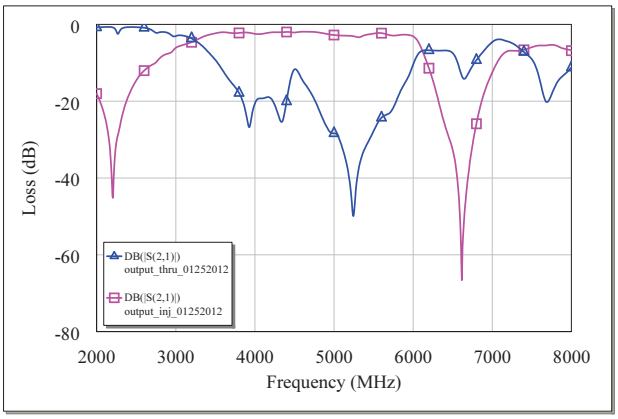

Figure 4.4: Measured loss in the output network low pass(blue) and high pass(pink) filter paths.

The design is based on the one presented in [7], although addtional stubs are used to do impedance transformation from R_{opt} to 50 Ω at both the output and injection ports. Bias tee is integrated with the output matching network providing high isolation between RF and DC paths. Measured S parameters of the output network are shown in Fig.4.3. This measurement is performed using break apart TRL method as explained in [43]. Due to fabrication tolerances, the fundamental f_0 impedance at the virtual drain of the device was found to be matched to 66 Ω and the $2f_0$ impedance to 79 Ω.

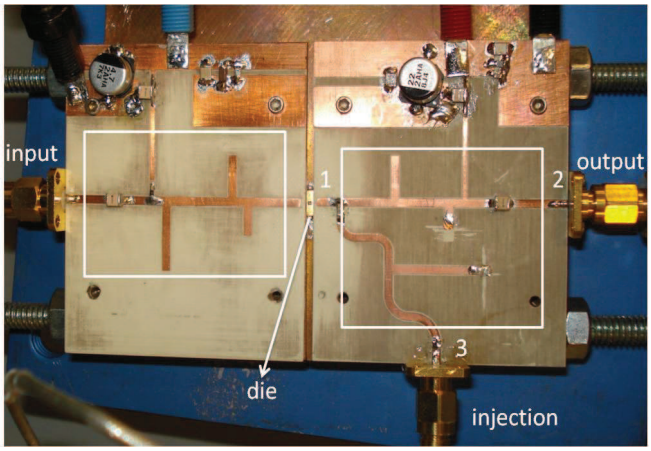

Figure 4.5: Hybrid harmonic injection power amplifier (HI-PA) with a 6W TriQuint TGF2023-01 die. The output network integrates the harmonic injection three port network with R_{opt} at f_0 matched to 65Ω and R_{opt} at $2f_0$ matched to 71 Ω. The input network does an impedance transformation from 50 Ω to 10 Ω in order to achieve high gain and P_{out} at the fundamental.

The class-AB PA is designed to have a 58% drain efficiency with an output power of 37 dBm without any harmonic injection at a drain bias voltage of V_{dd} = 28V and I_{dq} = 130 mA. Fig.4.6 shows the measured drain efficiency η_D, output power at fundamental ($P_{out}(f_0)$) and third harmonic ($P_{out}(3f_0)$), and the gain as a function of fundamental input drive power ($P_{in}(f_0)$).

4.2 Measurements

The block diagram shown in Fig.4.7 shows the modified measurement setup from Ch.3. A portion of the fundamental input is frequency doubled to create the second harmonic ($2f_0$) for injection. A voltage controlled phase shifter and variable gain amplifier are used to control the amplitude $P_{inj}(2f_0)$ and phase at $2f_0$.

All the measurements are de-embedded to the virtual drain of the transistor (reference plane P1 in Fig.4.1

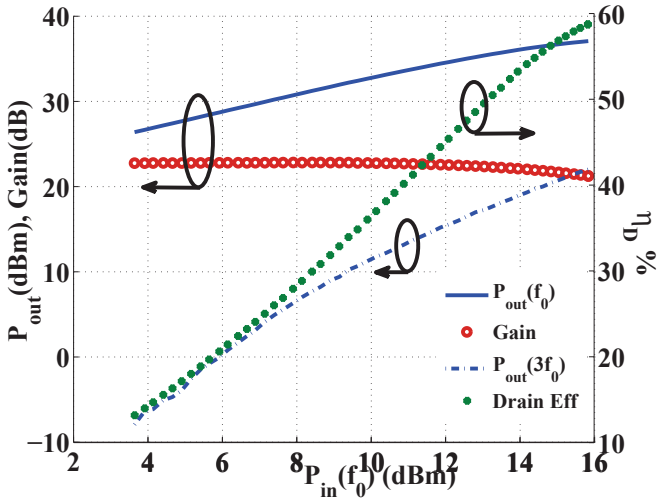

Figure 4.6: Measured drain efficiency, P_{out} at f_0 and $3f_0$ and gain for the class-AB PA shown in Fig.4.5 without injection.

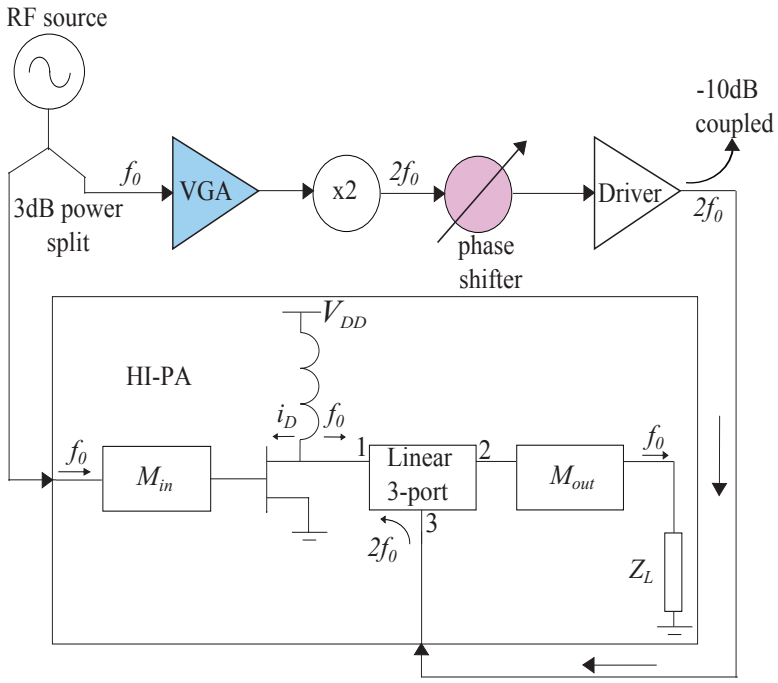

Figure 4.7: Block diagram of the HI-PA measurement setup. The input signal is split and frequency doubled to create the injected harmonic, $P_{inj}(2f_0)$. A voltage controlled phase shifter and variable gain amplifier are used to control the amplitude and phase of $P_{inj}(2f_0)$.

by calibrating the loss in the output network and taking into account the intrinsic device parasitics i.e. output capacitance of the device. A bondwire model in HFSS was simulated to consider the inductance loss in the bondwire transition for the hybrid PA design.

4.3 Maximum Efficiency Characteristic

The HI-PA using a TriQuint 6W GaN discrete HEMT in a class-AB PA achieves a high total drain efficiency of 89% with external second harmonic injection at the output at a bias voltage of $V_{dd} = 22\,\text{V}$. This efficiency is very close to the theoretical efficiency of 89.9% from Fig.2.8, though one would expect it to be lower, since the theory derived in Ch.2 for a device with ideal IV curves with no harmonic content and zero knee voltage. Note that in both the theoretical and experimental efficiency calculations here, the injection circuit efficiency is assumed to be 100%. But in practice, the PA always generates some harmonic content even at lower input power levels. The gain of the amplifier is reduced by 1 dB as compared to the amplifier without any harmonic injection. Fig.4.8 shows a comparison of the measured performance for the HI-PA and PA without harmonic injection. These measurements are optimized for high efficiency and hence the amplifier is nonlinear at P_{1dB}. It is seen that a better performance is achieved with the discrete device as compared to the results presented in Fig.3.3 for the packaged device, as expected. As seen in the theoretical analysis presented for harmonically-injected PAs in [43], harmonic injection implies a shift in the bias voltage in order to get the optimum performance from the amplifier.

Fig.4.9 shows the performance of the HI-PA at different drain bias voltages for a fundamental input drive ($P_{in}(f_0)$) of 16.2 dBm which is the 1 dB compression point for the class-AB GaN PA. This HI-PA is then optimized in order to achieve higher linearity.

As explained in section 2.3, for a CW amplifier, the values of $P_{out}(3f_0)$ can give an estimate on the linearity performance of the PA. It is seen from Fig.4.9 that at $V_{dd} = 24\,\text{V}$, the drain efficiency of the HI-PA is improved by over 20% as compared to the class-AB PA with no injection and the output power at the third harmonic($P_{out}(3f_0)$) is lowered by 30 dB for an input drive level of 16.2 dBm. At this bias point, conditions for high linearity and high drain efficiency are obtained with a nominal fundamental output power ($P_{out}(f_0)$) reduction of 0.26 dB over the PA without any injection. Note that when harmonic injection is performed, it results in higher fundamental output power due to reduction in other harmonic content.

In order to keep the output power constant and reduce the DC power dissipation, the drain supply voltage can be reduced to a certain extent, as shown in Fig.4.9. The supply voltage reduction is only advantageous up to a device-dependent lower value when the output power starts decreasing. As seen in Fig.4.9, $P_{out}(f_0)$

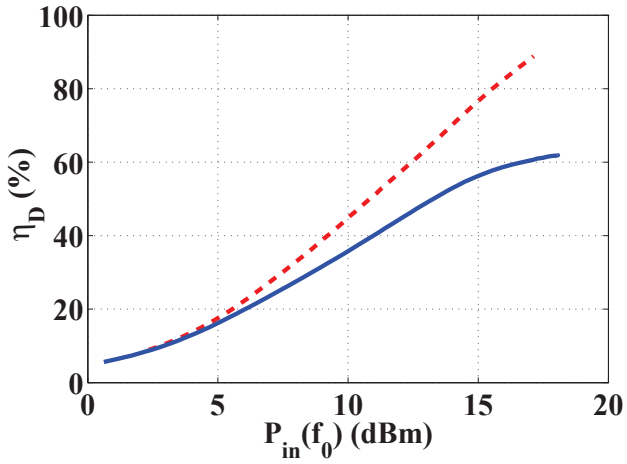

(a)

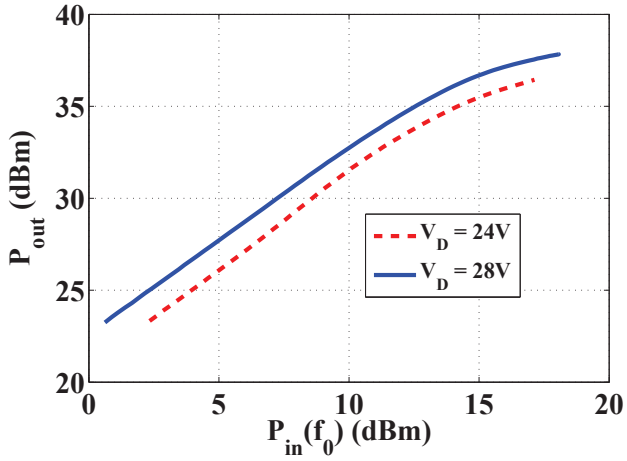

(b)

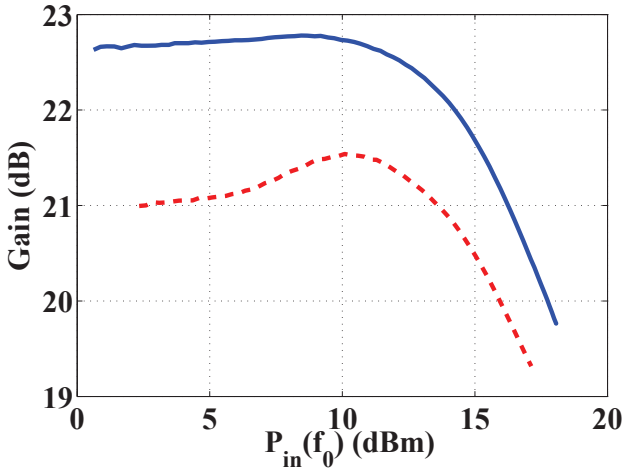

(c)

Figure 4.8: Comparison of measured (a) η_D, (b) $P_{out}(f_0)$ and (c) gain for discrete die protoype of HI-PA optimized for maximum efficiency.

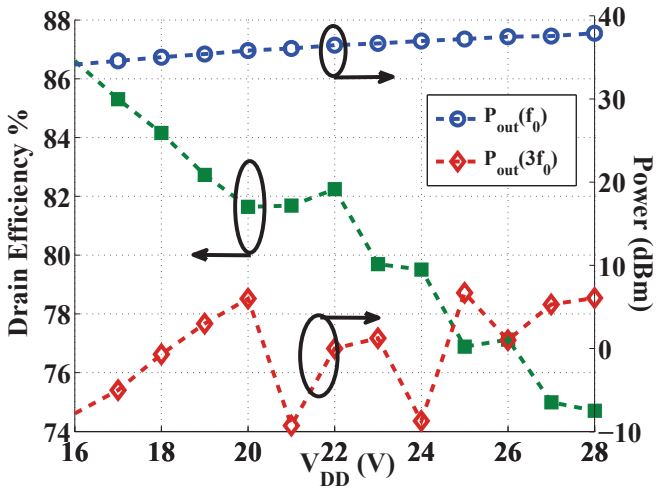

Figure 4.9: Drain efficiency, $P_{out}(f_0)$, $P_{out}(3f_0)$ for different V_{dd} bias voltages with the ratio $P_{inj}(2f_0)/P_{out}(f_0)$ = 0.1 and $P_{in}(f_0)$ = 16.2 dBm.

ranges from 32-38 dBm when the drain voltage is changed from 16 - 28 V. But, the output power remains almost at a constant value of 38 dBm at V_{dd} = 24 V to 28 V. Therefore, to achieve higher efficiency, lower voltage is selected. All the measurements presented in the next section are at a supply voltage V_{dd} = 24 V.

When the input power is swept on the fundamental PA, the required amplitude and phase of the injected second harmonic in order to achieve the optimal performance from the HI-PA at each power level varies. This is because the power levels of the harmonic content produced by the PA increases as the PA compresses. This charateristic of PA is explaned clearly in literature including [42, 74, 73]. A comparison of the fundamental output power, $P_{out}(f_0)$, drain efficiency, η_D, second and third harmonic output power, $P_{out}(2f_0)$, $P_{out}(3f_0)$ and drain current, I_{dd} is shown next.

4.3.1 Fundamental Output Power

Since a PA uses a nonlinear device and saturates with increasing input power, this results in squaring of the waveform and distortion at the output. The output power then reduces due to gain compression. But for a PA with harmonic injection, the output power can degrade severly or increase to the benefit of higher efficiency depending on the amplitude and phase of the injected signal. Theoretically, when the injected signal is 180° out of phase with the fundamental signal, the ideal conditions for harmonic injection exist. At this point, the output power is also higher than that for a non harmonically-injected PA. Fig.4.10 show

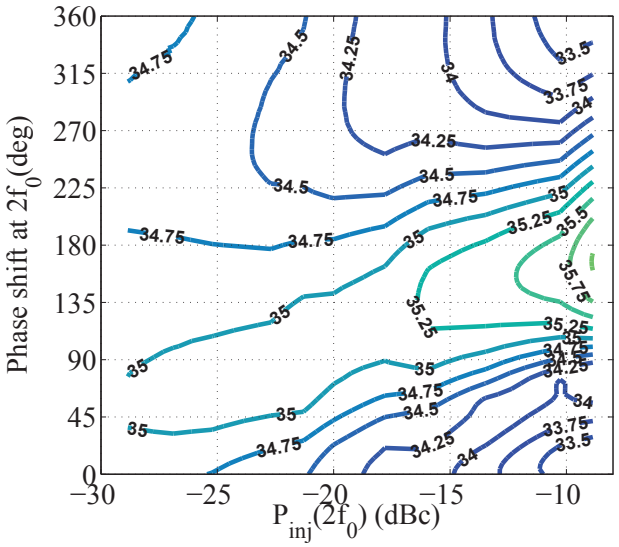

(a)

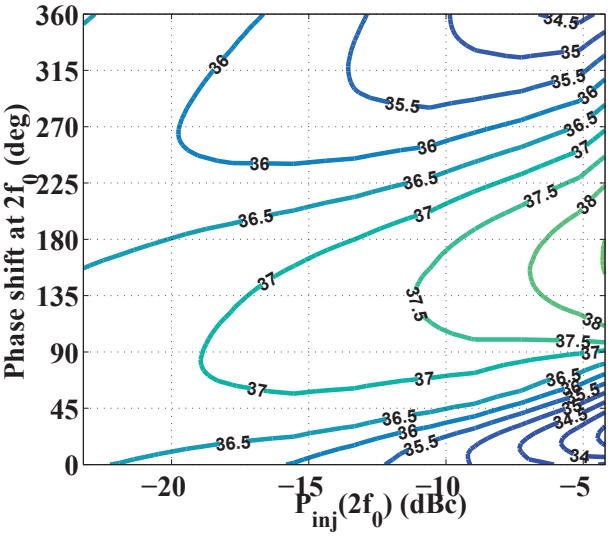

(b)

Figure 4.10: Contour plots of measured fundamental output power, $P_{out}(f_0)$ at (a) input power, $P_{in} = 10\,\text{dBm}$, (b) $P_{in} = 16\,\text{dBm}$.

the output power as a function of the injected signal amplitude and phase for different fundamental input drive levels. It is seen that as the input drive level increases, the optimal point for high output power shifts towards higher injection power level. The reason being that as the fundamental input power increases, the PA starts producing more harmonic content. In order to compensate for the internally produced harmonics and increase the fundamental output power, the required injected power also needs to increase. Also. since the PA degrades in phase with increasing input power, the optimal phase required to achieve high effciency and linearity also shifts with input drive level.

4.3.2 Drain Efficiency (η_D) Characterization

The drain efficiency for the HI-PA is calculated from (2.25) which is a function of the DC power dissipated in the main HI-PA and the DC power which is dissipated in the injection circuit. The drain efficiency for an HI-PA takes into account the amount of second harmonic power injected into the virtual drain of the device ($P_{inj}(2f_0)$) assuming $\eta_{inj} = 1$. Contour plots of variation in drain efficiency w.r.t. amplitude and phase of the injected signal is shown in Fig.4.11. It is seen that at a maximum amplitude of -5 dBc w.r.t. fundamental output power, the drain efficiency achieved in compression is 89%. However, at this point, the harmonic content in the PA also increases as will be shown in the next section resulting in nonlinear PA. Therefore, a trade-off between efficiency and linearity is required. It is seen that the total drain efficiency varies on the order of 10% for every 45° phase shift and 15-20 dB amplitude shift of the injected harmonic. However, the power reduces by > 1 dB for this range of values as seen in Fig.4.10.

4.3.3 Drain current

The optimal point for the amplitude and phase of the injected signal remains almost the same in terms of minimum drain current and maximum efficiency. This point varies by 20° in phase of the injected signal for maximum efficiency and minimum drain current. The current variation on the order of 10 mA for every 40° change in the phase and 2 dB change in the amplitude of the injected signal is shown in Fig.4.12. Also, it is seen that the minimum points obtained for drain current at input drive levels in linear and saturation region differ by almost 10 dB in amplitude.

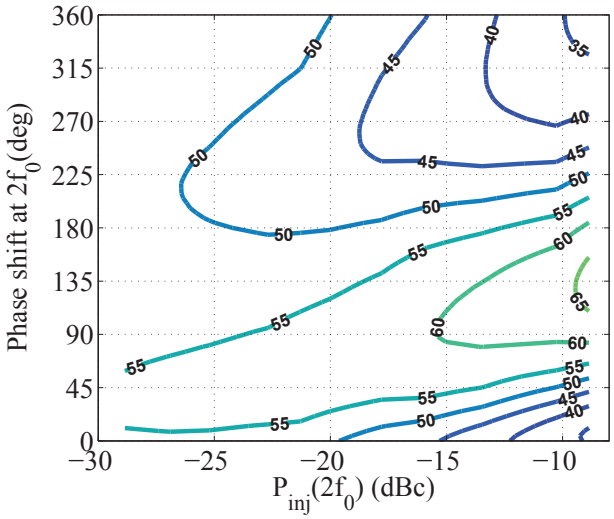

(a)

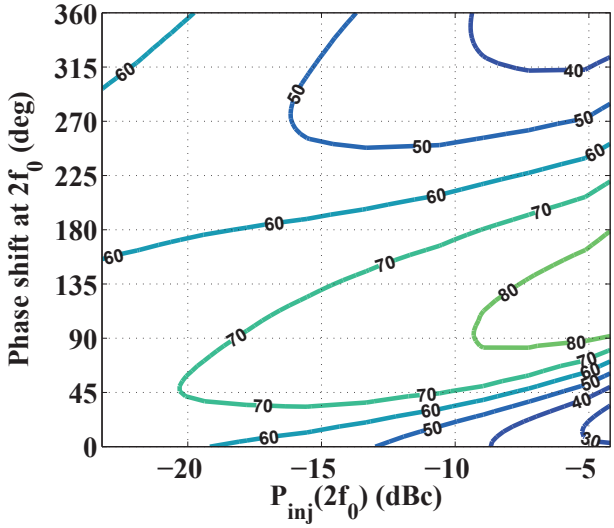

(b)

Figure 4.11: Contour plots for measured drain efficiency, η_D at (a) input power, $P_{in} = 10\,\text{dBm}$, (b) $P_{in} = 16\,\text{dBm}$.

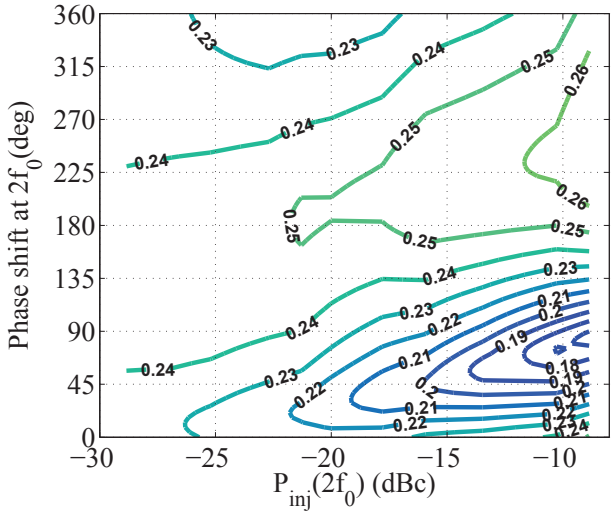

(a)

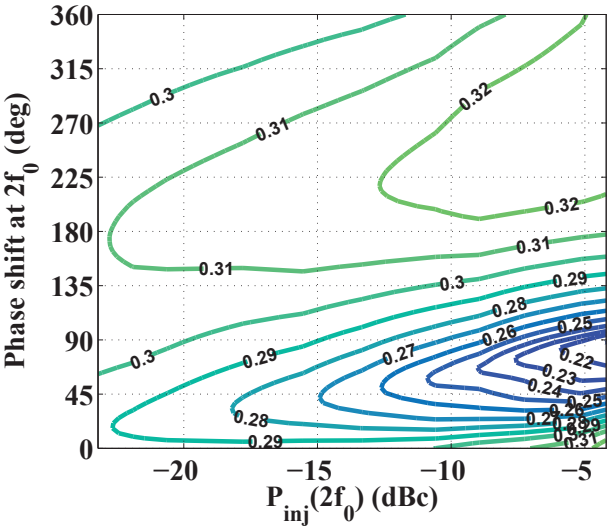

(b)

Figure 4.12: Contour plots for measured drain current, I_{dd} at (a) input power, P_{in} = 10 dBm, (b) P_{in} = 16 dBm.

4.3.4 Linearity Measurements and Characterization

As shown in Ch.2, linear behavior of an amplifier can be recognized with CW measurements by monitoring the even and odd order harmonic content in the PA. The third order nonlinearity creates the third harmonic at the output of the PA which can give an estimate on the linear performance of the PA. The analysis in [74] also shows that the amplitude of the second harmonic output signal is inversely proportional to the magnitude of the transfer characteristic of the amplifier at the third harmonic, which is given as:

$$G_{NL} = 20log(k_1 + \frac{3}{4}k_3A^2) \tag{4.1}$$

wherer k_1 and k_3 are the transfer functions at fundamental and third harmonic frequencies for a PA system and A is the amplitude of the fudamental input sinusoidal signal.

A good discussion on extracting linearity information from a CW-fed amplifier by measuring the third harmonic output content is presented in [75]. Based on this theory, here, a CW signal is used for harmonic injection analysis as the device enters saturation. In particular, we measure 2^{nd} and 3^{rd} harmonic as a function of the injected power and phase in order to assess the linearity characteristics of a PA. By performing second harmonic injection at the output, mixing between injected $2f_0$ signal and fundamental output f_0 signal results in third harmonic mixing product, $3f_0$. At the optimal phase and amplitude of the injected second harmonic, this mixing product will have a phase opposite to the third harmonic produced by the PA resulting in cancellation and higher linearity. Also, there will be an efficiency vs linearity trade-off since, from Fig.4.13, the level of second harmonic in the output signal is still significant. However, as shown in Fig.4.14, the efficiency degrades by 8-9% for the PA driven at 1 dB compression while maintaining extremely low levels of third order harmonic distortion.

From Fig.4.13 and 4.14, the optimal amplitude and phase of the injected signal also varies in order to achieve a null in either the 2^{nd} or 3^{rd} harmonic. At 1 dB compression, the maximum amplitude and optimal relative phase of the injected signal in order to achieve a null in the third harmonic is 10 dBc w.r.t. fundamental output power and 80 °, whereas it is 20 dBc and 110 ° for minimum second harmonic. This optimal phase for the injected signal also varies with input drive level since the power of the harmonics produced by the PA itself also increases with increasing input power. This can be directly related to the amplitude and phase modulation (AM-PM) distortion in the PA.

With increasing input drive levels, the harmonic content in the PA also increases by a factor of two for the second harmonic and a factor of three for the third harmonic. Also, the amplitude and phase modulation distortion, also known as AM-AM and AM-PM distortion results from increasing harmonic content in the main signal causing amplitude compression and phase deviation. Therefore, with increasing input drive levels, the optimal amplitude and phase of the injected signal required to reduce the 2^{nd} or 3^{rd} harmonics will

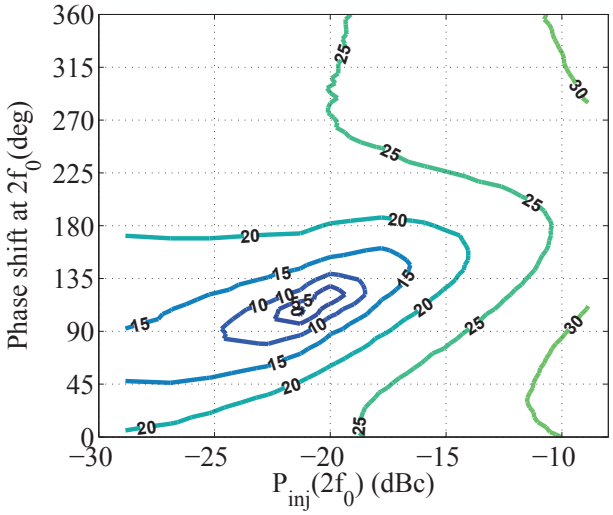

(a)

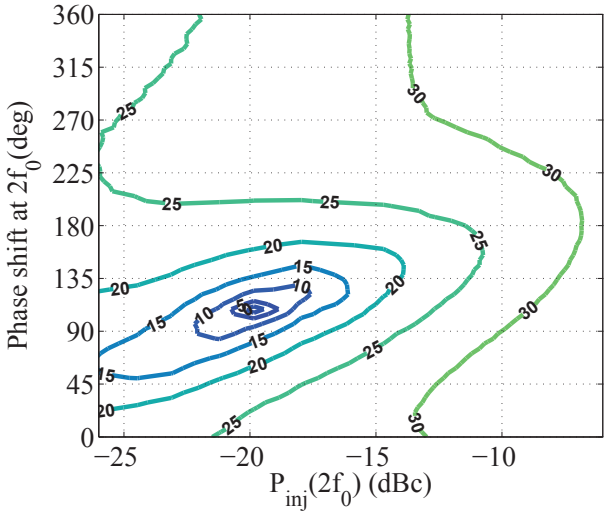

(b)

Figure 4.13: Contour plots for power measured at second harmonic, $P_{out}(2f_0)$ at (a) input power, $P_{in} = 10\,\text{dBm}$, (b) $P_{in} = 16\,\text{dBm}$.

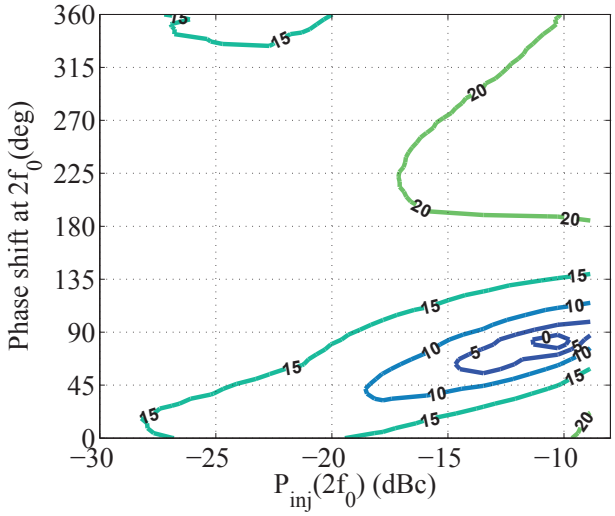

(a)

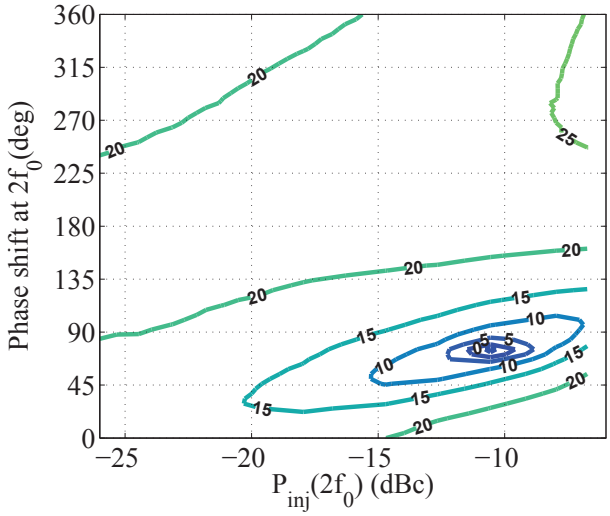

(b)

Figure 4.14: Contour plots for power measured at third harmonic, $P_{out}(3f_0)$ at (a) input power, $P_{in} = 10\,\text{dBm}$, (b) $P_{in} = 16\,\text{dBm}$.

change. Fig.4.15 shows the minima obtained in the second harmonic as well as the PA efficiency for different input drive levels from small signal to compression. At small signal, the PA efficiency and 2^{nd} harmonic produced by the PA are not affected by second harmonic injection. This is because in small signal regime, the PA itself does not produce any significant harmonic components. Therefore, active impedance synthesis is not achievable at these input drive levels. However, as the input power increases, the amount of injected power required to achieve maximum efficiency and minimum harmonic content also increases.

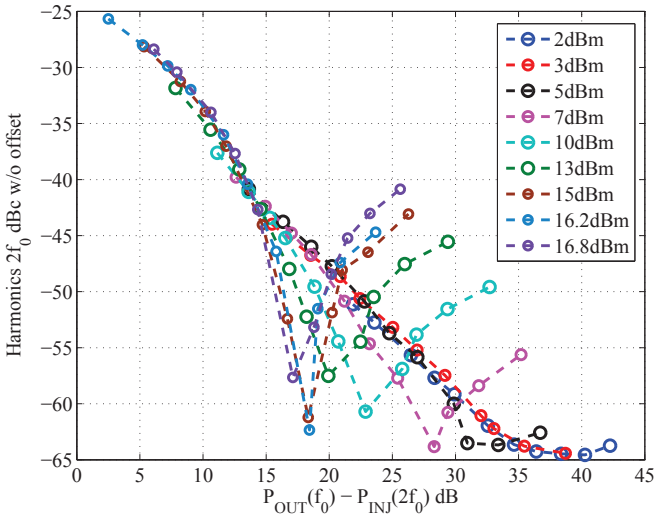

(a)

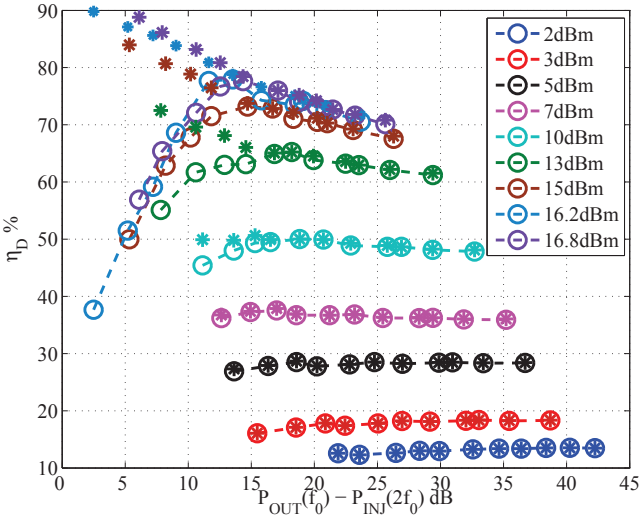

(b)

Figure 4.15: Total drain efficiency (b) and output power at second harmonic (a) as functions of the amplitude of the injected harmonic signal for various input drive levels. The phase of the injected signal is set to the optimal value for these measurements.

It is of interest to discuss some limitations on linearity and efficiency that are practically achievable. We have shown that the third harmonic, which directly affects IMD performance [75], is minimized for a specific phase and amplitude of the injected second harmonic. However, the injected signal also affects the nonlinear content in the waveform produced by the transistor, which can be evaluated by measuring the level of the second harmonic at the output. The amount of injected second harmonic power that results in a minimum of harmonic content in the output is shown in Fig.4.16. Note that the 2^{nd} and 3^{rd} harmonic have minima for different injected power levels of the second harmonic. The amplitude of $P_{inj}(2f_0)$ needed to lower $P_{out}(2f_0)$ is approximately 10 dB less than that needed to lower $P_{out}(3f_0)$. Also, the phase shift for $P_{inj}(2f_0)$ injection differs by 50°. As seen from Fig.4.11, the drain efficiency drops by approximately 10% between these two points in amplitude and phase.

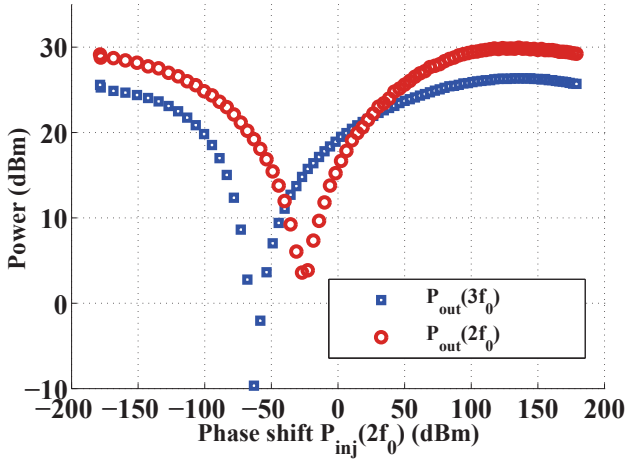

Figure 4.16: Minimum $P_{out}(2f_0)$ and $P_{out}(3f_0)$ measured at virtual drain of the HI-PA for $P_{in}(f_0) = 16.2$ dBm. The minimum for $P_{out}(2f_0)$ is obtained with $P_{inj}(2f_0)$ = -17.8 dBc w.r.t. $P_{out}(f_0)$, whereas minimum for $P_{out}(3f_0)$ is obtained for $P_{inj}(2f_0)$ = -8.9 dBc.

Fig.4.11 & 4.14 show that for $P_{inj}(2f_0)$ = -9 dBc and a phase shift of 80°, high drain efficiency of 79% is achieved using (2.25) along with extremely low values of $P_{out}(3f_0)$. Note that this efficiency takes into account the power of the injected signal. However, the effciency of the injector circuit is not included in this proof-of-concept experiment in which the HI-PA is not fully integrated. The value of $P_{out}(f_0)$ obtained at this point is approximately 37 dBm, only 0.2 dB lower than the fundamental output power obtained with no injection (Fig.4.6).

The measurements show that if $P_{inj}(2f_0)$ is not at the optimum phase and amplitude, the performance of

the amplifier can severely degrade. When the second harmonic voltage is out of phase relative to the optimal value, the amplitude of $P_{out}(3f_0)$ increases making the amplifier extremely nonlinear. The efficiency reduces from 80% to 40% while the output power drops more than 3 dB. If $P_{inj}(2f_0)$ is higher than the optimum value (in this case, $\geq$ -9 dBc), then even at the optimum phase of the injected harmonic, the HI-PA is highly nonlinear. This is due to undesired additional second harmonic content in the output voltage and current waveforms generated by the strongly driven.

4.4 Input Power Sweep

A sweep is performed at $P_{in}(f_0)$ in order to achieve the optimal performance of the HI-PA at various input drive levels. Since an amplifier undergoes AM-AM and AM-PM distortion, the optimal phase and amplitude of the injected second harmonic changes for different input drive levels. Fig.4.17 shows a comparison of the gain and drain efficiency obtained for HI-PA and PA without harmonic injection as a function of $P_{in}(f_0)$. The efficiency obtained at each input drive level is for an optimal value of amplitude and phase which are also dependent on $P_{in}(f_0)$. The overall gain of the HI-PA is reduced by 1 dB and the 1-dB compression point of the HI-PA is shifted to a higher $P_{in}(f_0)$ of 15.7 dBm implying improved linearity. The drain efficiency improvement ranges from 8% to 20% as the input drive level increases.

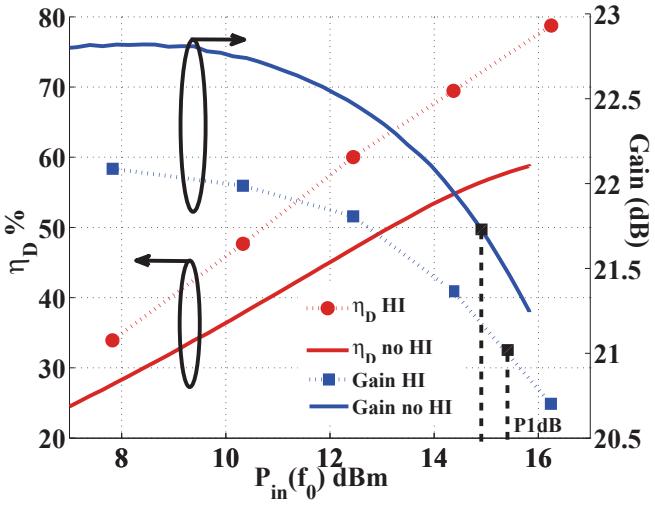

Figure 4.17: A comparison of drain efficiency and gain for HI and PA with no injection as a function of $P_{in}(f_0)$.

The comparison of $P_{out}(f_0)$ and $P_{out}(3f_0)$ for the HI-PA and PA with no injection is shown in Fig.4.18 along with $P_{inj}(2f_0)$ as a function of $P_{in}(f_0)$.

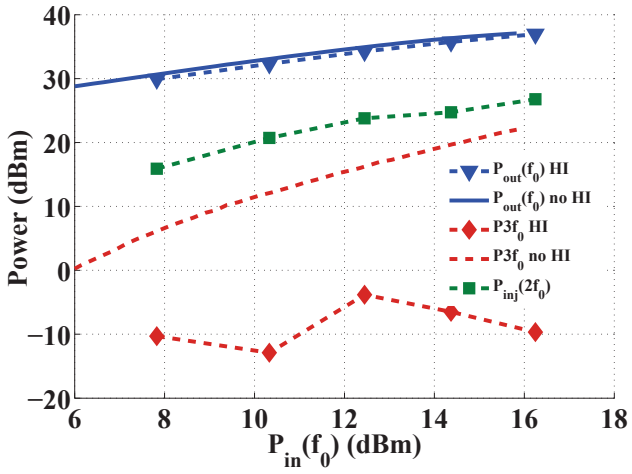

Figure 4.18: Comparison of $P_{out}(f_0)$ and $P_{out}(3f_0)$ as a function of $P_{in}(f_0)$ for HI and PA with no injection. The graph also shows the amplitude of $P_{inj}(2f_0)$ as function of $P_{in}(f_0)$ in order to achieve high efficiency and linearity performance for the HI-PA.

The nominal class-A operation of the PA without harmonic injection with a 50% drain efficiency is achieved at $P_{in}(f_0) = 13\,\text{dBm}$. Fig.4.18 shows that at this input drive level, the amplitude of $P_{inj}(2f_0)$ required in order to achieve an optimum performance in terms of efficiency and linearity for the HI-PA is -10 dBc. This result matches with the theoretical analysis presented in Fig.2.9 where for a 100% injector efficiency, the ratio of $P_{inj}(2f_0)$ to $P_{out}(f_0)$ is 0.1 for a class-A bias point.

It is seen that a total improvement of 8% to 20% is observed in the overall drain efficiency of HI-PA as compared to that of the class-AB PA without injection when the input power increases. Both the simulations and the measurements show that as the injected power is increased to the fundamental PA, the drain efficiency keeps increasing. However, after a certain level of injected signal, the PA again becomes extremely nonlinear due to additional harmonic content as shown in Fig.4.14.

4.5 Conclusion

In this chapter, a hybrid HI-PA is designed using a discrete GaN HEMT die with the diplexer integrated in the output matching network in a non-50 Ω environment at $f_0 = 2.45\,\text{GHz}$. The PA is designed for class-AB

mode of operation with large signal gain of 23 dB and $P_{out} = 5$ W. Optimization in efficiency and linearity is performed with second harmonic injection at the output of the PA. Variation in PA parameters such as P_{out} at fundamental and harmonics along with drain efficiency, η_D, gain and drain current, I_{dd} w.r.t. the amplitude and phase of the injected second harmonic are analyzed.

Measurements show maximum total efficiency improvement of 30% over class-AB PA with maximum η_D = 89% for the HI-PA. The power required at the injected harmonic to achieve this efficiency is -5.5 dBc. The PA performance is sensitive to the phase of the injected second harmonic with efficiencies reduced more than 5% for every 20° change in the relative phase of the injected second harmonic. The drain current is reduced by more than 100 mA at the optimal amplitude and phase of the injected second harmonic along with only a 0.26 dB reduction in output power as compared to the class-AB PA without harmonic injection.

Linearity analysis is performed in terms of second and third harmonic content for the HI-PA. Optimization for minimum third harmonic content results in total efficiency improvement of 20% for a CW signal with max $\eta_D = 78\%$ and third harmonic reduction of 15 dB in compression with the injected harmonic power 10 dBc w.r.t. fundamental output power. The design, analysis and comprehensive characterization of this integrated HI-PA demonstrating high efficiency and linearity is reported in [9].

Chapter 5

Linearization of HI-PAs

Our future discoveries must be looked for in the sixth place of decimals.

—A. A. Michelson, in *Light Waves and Their Uses*, 1903.

Contents

In this chapter, two-tone measurements are used to quantify linearity in terms of third and fifth order distortion products. Measurements with optimization for the amplitude and phase of the injected second harmonic in order to achieve lowest third and fifth order intermodulation products in both lower and upper sidebands ($IMD3_{L/H}$, $IMD5_{L/H}$) are performed. As shown in Ch.2, a harmonically-injected PA (HI-PA) can be linearized by injection of second harmonic tones at the output resulting in mixing products which cancel the ones produces by the PA itself. It was also shown in Ch.4 that the third order nonlinearities reduce

and the 1 dB gain compression point shifts to a higher input drive level resulting in linear behavior of the PA. However, the third order nonlinearities for a CW signal only provide an estimate of the PA's linear behavior. In order to understand the actual signal distortion, two-tone measurements give a comprehensive analysis for linearity behavior of a PA. In this measurement analysis , harmonic injection is performed with two tones having bandwidths of 1, 5, and 10 MHz with the fundamental tone, $f_1 = 2.45$ GHz. Due to setup limitations, the harmonic injection is performed at one of the two harmonic tone frequencies, $2f_1$ or $2f_2$. A basic block diagram of the measurement setup is shown in Fig.5.1. One of the two tones is split using a 3 dB power splitter, where one half of the tone is input to the PA and the other half is frequency doubled to create the second harmonic injection tone. This signal is then adjusted in amplitude and phase with a variable gain amplifier and a voltage controlled phase shifter.

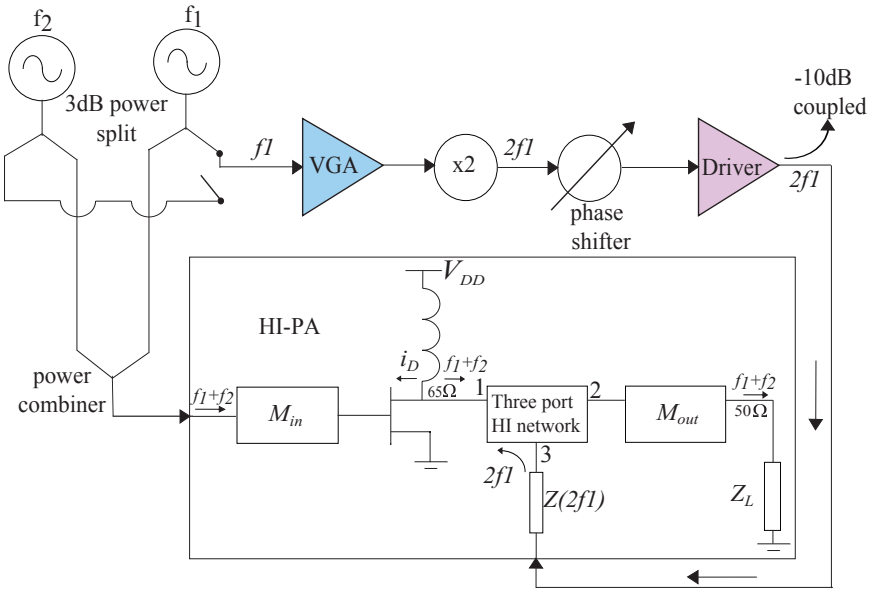

Figure 5.1: Block diagram of measurement setup for two tone test on the harmonic injection power amplifier.

External harmonic injection of $2f_1$ affects the performance of the third-order intermodulation distortion product, $IMD3_L$ at $2f_1$-f_2 and $IMD5_L$ at $3f_1$-$2f_2$ due to active impedance synthesis at the second harmonic tone frequency. It is important to note that the reduction in $IMD5_L$ results from mixing of $IMD3_L$ and distortion products caused due to second order nonlinearities as explained in Ch.2. Also, the injection at one of the two harmonic tone frequencies only affects either the lower or upper IMD products while the other side remains unaffected.

The measurement analysis is performed for various amplitude and phase values of the injected harmonic. The active impedance synthesis at the virtual drain of the PA results in an optimal impedance point for the odd-order intermodulation products to have minimum power levels with a simultaneous increase in the efficiency. Fig.5.2 shows the optimal amplitude and phase for injected second harmonic tone ($2f_1$) in order to achieve low $IMD3_L$ power levels for a fundamental input drive of $P_{in} = 16\,\text{dBm}$. It is seen that the minimum $IMD3_L$ is sensitive to both the amplitude and phase of the injected second harmonic with the $IMD3$ power levels varying by a margin of 10 dBm with a 5 dB increase in the injected signal amplitude. Also, since the variable phase shifter has a range from 0 to 450°, the optimal point with minimum IMD3 repeats itself at phase shifts of approximately 40 and 400°.

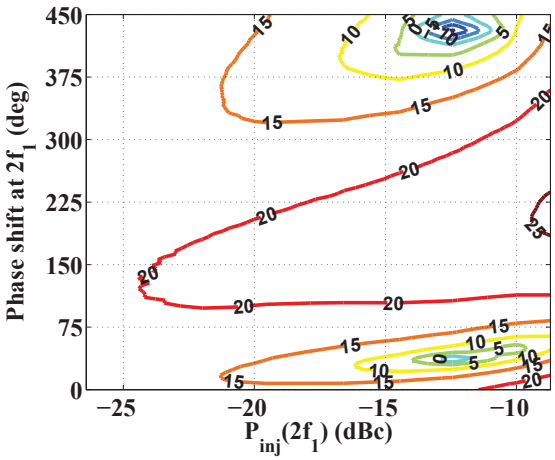

Figure 5.2: Measured power level of $IMD3_L$ ($2f_1$-f_2) as a function of the amplitude and phase of the injected second harmonic tone $2f_1$.

Similarly, a minimum for $IMD5_L$ is also a function of $P_{inj}(2f_1)$ as shown in Fig.5.3. However, it is seen that the amplitude and phase shift required at the injected second harmonic to achieve lowest $IMD5$ products differ by 2 dBm and 10° respectively as compared to the values for lowest IMD3 products as shown in Fig. 5.4. It is an expected result since $IMD3$ and $IMD5$ products produced by the PA itself differ in amplitude and phase w.r.t. each other when an input power sweep is performed on the PA.

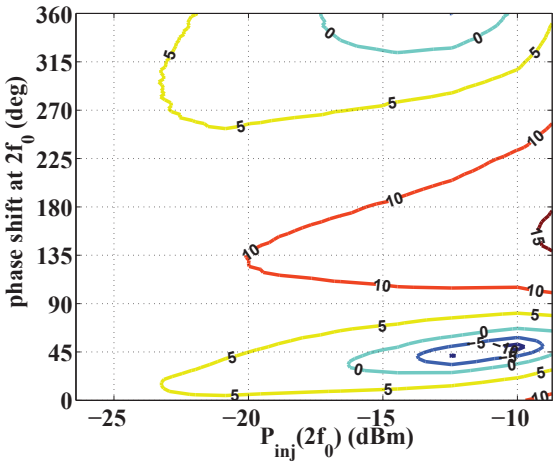

Figure 5.3: Measured power level of $IMD5_L$ ($3f_1$-$2f_2$) as a function of the amplitude and phase of the injected second harmonic tone $2f_1$.

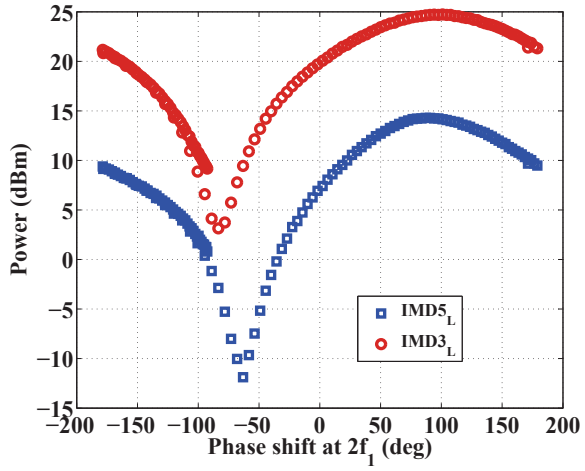

Figure 5.4: Measured power levels for $IMD3_L$ and $IMD5_L$ with harmonic injection at $2f_1$ and $P_{in} = 16$ dBm. The minima for $IMD3_L$ and $IMD5_L$ are obtained for $P_{inj}(2f_1)$ = -11.5 dBc and -9.5 dBc, respectively.

5.1 Variable tone spacing

Next, the performance of the HI-PA with tone spacings of 1, 10 and 20 MHz is studied with linearization using second harmonic tones. The PA is operated at two input drive levels in linear and saturated states. The measurements are presented for P_{in} = 10 and 16 dBm with the amplitude of the second harmonic maintained at -10 dBc w.r.t. the fundamental output power and an optimal phase shift between the injected and fundamental output frequency tones.

A comparison of the minimas obtained for odd order IMDs ranging from third to ninth order is shown

in Fig.5.5 - 5.7. Here, the measurements show the behavior of IMD products as a function of the change in phase for the injected second harmonic tone at the optimal amplitude which is 10 dBc w.r.t. the output power. Also, two different input drive levels are shown with $P_{in} = 10$ and 16 dBm. As seen from Fig.2.17, the fifth and higher order intermods have sweet spots or minima for the class-AB PA without injection at some specific input drive levels. For example, the fifth order intermodulation products have a minimum at an input drive level of $P_{in} = 11$ dBm or $P_{out} = 33$ dBm. Therefore, when harmonic injection is performed at that particular input drive level, from Ch.2, these intermodulation products will no longer have minimas and will increase in power levels. As shown in Fig.5.5a, the minimum obtained for the third order intermodulation product is not coincident with that obtained for the fifth and higher intermodulation products. Therefore, in order to have simultaneous reduction in all the odd order distortion products with harmonic injection, the PA should be driven at input power levels where the odd-order intermods are an increasing function of the input power and do not contain any sweet-spots which can result in asymmetry.

Also, as the PA is driven with two-tones with larger signal bandwidths, low-frequency memory effects [82] start becoming critical which results in asymmetry of the lower and higher sidebands for the signal. The PA is no longer symmetrical and the spectral regrowth can be lower or higher than that of the other side of the spectrum. When harmonic injection is performed on such a PA, the simultaneous reduction in both the upper and lower sidebands also becomes difficult and the spectral asymmetry is maintained. Nevertheless, the power levels of the intermodulation products reduces as compared to that of a class-AB PA.

As the input power level to the PA is increased from linear ($P_{in} = 10$ dBm) to saturation ($P_{in} = 16$ dBm), the amount of harmonic content and phase of the harmonics also changes. This results in amplitude and phase modulation (AM-AM and AM-PM) distortion. Therefore, with harmonic injection, the amount of phase shift required to achieve minima in the IMD products at these two power levels also differ. However, one should expect the phase shift required to produce nulls in the upper and lower IMD products at a single power level to be the same. But, even in this case, as shown in Fig.5.5, the phase differs by 10 to 20°. This is due to injection of two different frequencies in order to achieve nulls in both upper and lower spectral components.

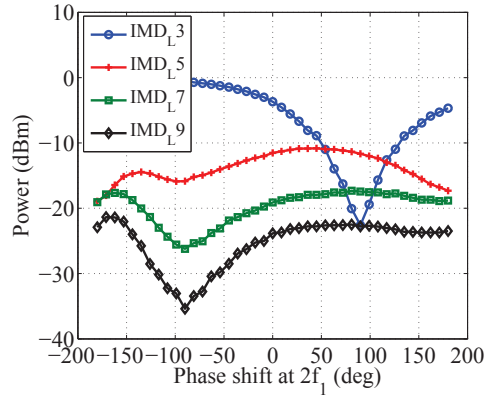

(a) IMD_L, 1 MHz tone spacing, $P_{in} = 10\,\text{dBm}$

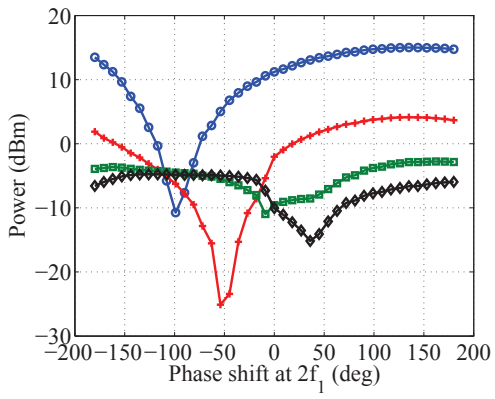

(b) IMD_L, 1 MHz tone spacing, $P_{in} = 16\,\text{dBm}$

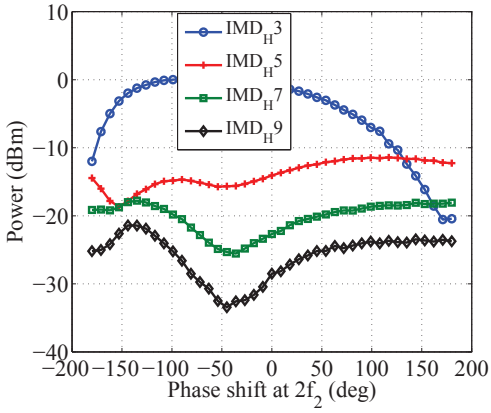

(c) IMD_H, 1 MHz tone spacing, $P_{in} = 10\,\text{dBm}$

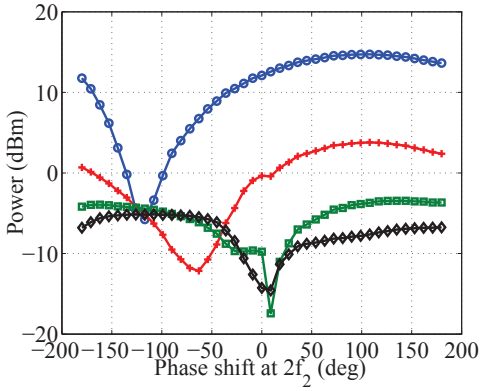

(d) IMD_H, 1 MHz tone spacing, $P_{in} = 16\,\text{dBm}$

Figure 5.5: Measured intermodulation distortion products in the upper and lower half of the spectrum for two tone signals with 1 MHz tone spacing

5.1.1 1 MHz TONE SPACING

Fig.5.5 shows the variation in the power levels obtained for odd-order intermodulation products with the phase shift at the injected second harmonic in both upper and lower halves of the spectrum. The figure compares the results for two different input drive levels with PA in linear region, i.e., $P_{in} = 10\,\text{dBm}$ and in saturation with $P_{in} = 16\,\text{dBm}$. Fig.5.5a - 5.5c show that at an input drive level of 10 dBm, the third order intermodulation products $IMD3_{L/H}$ achieve minimum points with the phase shift at the injected harmonic tones differing by 60°. Also, since the PA already exhibits a sweet spot condition for the fifth order intermods at this input drive level, the minima obtained in the fifth order intermods differ from the minimum point achieved in $IMD3$ by almost 180° in the phase shift required at the injected harmonic tone frequencies. The

higher order intermods such as $IMD7, 9...$ achieve null points with phase shifts close to minimum $IMD5$ levels. This is due to $IMD5$ harmonics affecting the power levels of higher order terms.

Refering to Fig.5.5, when the input drive level is increased to 16 dBm, the sweet spot condition for fifth order intermods no longer exhists. Hence, the minima obtained in $IMD3$ and $IMD5$ differs by only 50° in terms of phase shift at the injected harmonic tones. However, the higher order intermods such as $IMD7, 9...$ exhibit sweet spot conditions at this input drive level. Therefore, the phase shift required to achieve a minimum in these intermods differs by 180° from the phase shift required to achieve nulls at IMD3 products. Also, it is seen that the optimal phase shift at $2f_1$ and $2f_2$ only differs by 10° for minimum IMD3 and 5 products. Therefore, a symmetric reduction can be obtained in the odd order intermodulation products with harmonic injection at both $2f_1$ amd $2f_2$ simultaneously.

5.1.2 10 MHz tone spacing

Comparison of power levels achieved for odd order intermods at two different input drive levels for a tone spacing of 10 MHz is shown in Fig.5.6. In Fig.5.6a - 5.6c, it is seen that the low frequency memory effects in the PA are starting to affect the symmetry of the signal. The $IMD3$ products in upper and lower halves of the spectrum achieve minimum power levels at phase shifts which differ by 50° for the two injected harmonic tones. Again, the $IMD5$ products achieve nulls with phase shifts differing by 180° from minimum $IMD3$ points for input drive level of 10 dBm. For $P_{in} = 16$ dBm, it is seen that the phase shifts to obtain nulls in $IMD3$ and 5 differ by 50° where as there is asymmetry between the upper and lower $IMD7, 9$ minimum power level points. This asymmetry is partly due to the low frequency memory effects and also as the tone spacing of the fundamental frequency increases, the spacing between the harmonic tones now doubles. This results in a different optimal phase shift for minimizing upper and lower parts of the spectrum.

5.1.3 20 MHz tone spacing

Tone spacing of the input two tone signal when increased to 20 MHz results in asymmetrical behavior of the PA as seen in Fig.5.7. When harmonic injection is performed at the two harmonic tone frequencies, the phase shifts required to achieve minimum power levels at $IMD3$ differ by 100° in phase shifts for injected harmonics

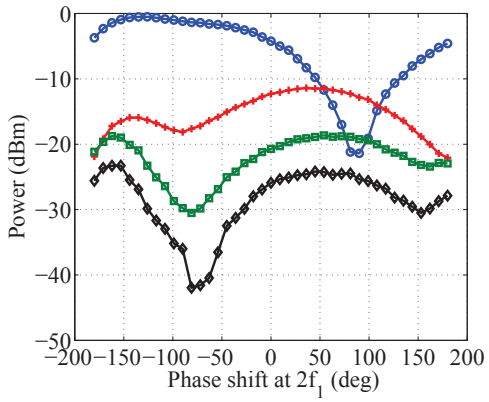

(a) IMD_L, 10 MHz tone spacing, $P_{in} = 10$ dBm

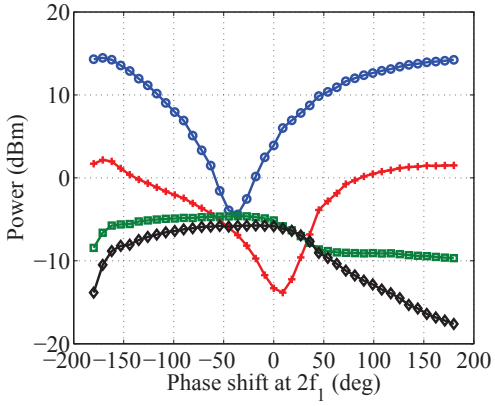

(b) IMD_L, 1 MHz tone spacing, $P_{in} = 16$ dBm

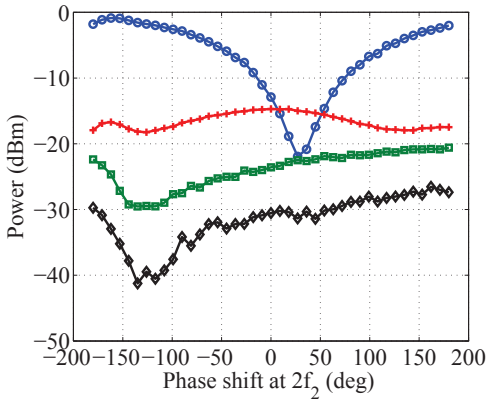

(c) IMD_H, 10 MHz tone spacing, $P_{in} = 10$ dBm

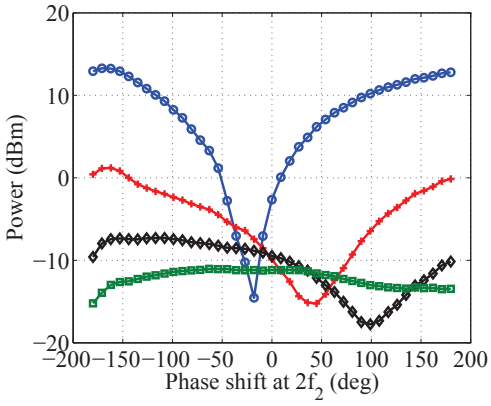

(d) IMD_H, 10 MHz tone spacing, $P_{in} = 16$ dBm

Figure 5.6: Measured intermodulation distortion products in the upper and lower half of the spectrum for two tone signals with 10 MHz tone spacing

for the upper and lower spectrum. Also, for input drive level of 10 dBm, a minimum point is obtained for $IMD5_L$ whereas $IMD5_H$ does not have a null point when the phase of the injected second harmonic is varied from 0 to 360°. Also, it is seen that the minimum power levels obtained for $IMD3, 5, ...$ for both upper and lower spectrum differ by 10 dBm for input drive level of 16 dBm. Therefore, as the tone spacing increases, the harmonically injected tone spacing doubles and the PA now becomes asymmetrical due to memory effects and variable phase shifts at the two injected frequency tones. It can be concluded that this technique will hence work for narrowband signals with bandwidths upto 10 MHz.

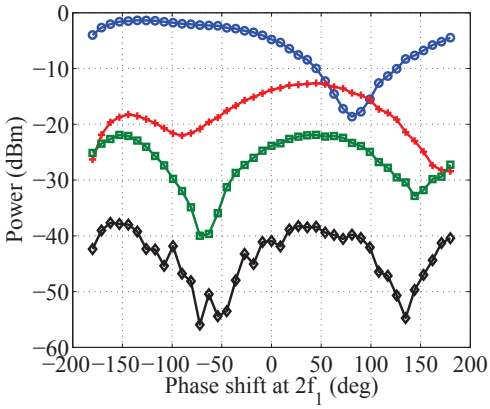

(a) IMD_L, 20 MHz tone spacing, P_{in} = 10 dBm

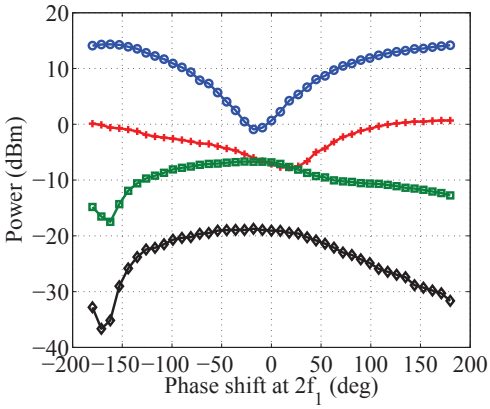

(b) IMD_L, 20 MHz tone spacing, P_{in} = 16 dBm

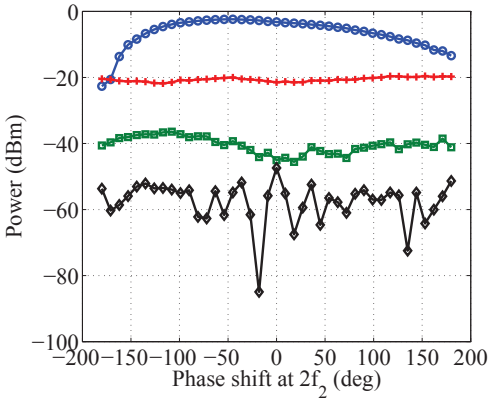

(c) IMD_H, 20 MHz tone spacing, P_{in} = 10 dBm

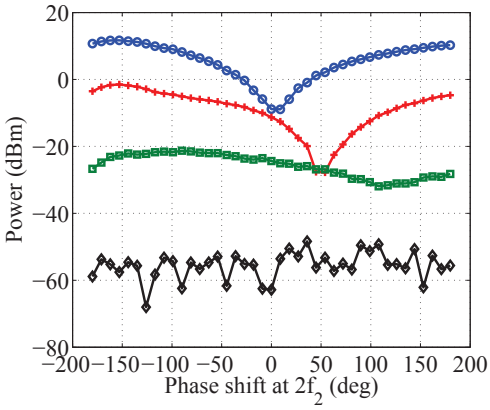

(d) IMD_H, 20 MHz tone spacing, P_{in} = 16 dBm

Figure 5.7: Measured intermodulation distortion products in the upper and lower half of the spectrum for two tone signals with 20 MHz tone spacing

5.2 Input power sweep

Optimization can be performed in order to achieve lowest third order or fifth order distortion products with input power sweep. The optimal injected 2^{nd} harmonic power which results in minimum $IMD3_L$ is shown in Fig.5.8 as a function of the input drive level. It is seen that the reduction in $IMD3_L$ using external second harmonic injection is greater than 15 dB for different input drive levels, whereas $IMD3_H$ at $2f_2$-f_1 and $IMD5_H$ at $3f_2$-$2f_1$ remain unaffected. The total drain efficiency of the PA which takes into account the amount of injected second harmonic as explained in [72] is improved from 53% for the two-tone class-A mode to 58% using harmonic injection at one tone. The total output power is seen to reduce by 0.5 dB along with 1 dB lower gain as compared to the class-A PA. The maximum efficiency improvement is seen to be 8% but

this results in a trade-off between high efficiency and linearity.

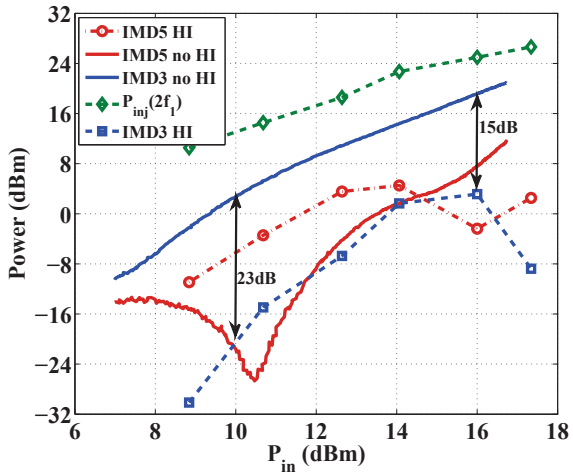

Figure 5.8: Comparison of power at $IMD3_L$ ($2f_1$-f_2), $IMD5_L$ ($3f_1$-$2f_2$) for HI-PA and PA without harmonic injection as a function of input drive level. The graph also shows the power injected at the second harmonic tone ($2f_1$) to achieve lowest $IMD3_L$.

Similarly, Fig.5.9 shows the power levels for IMD3 and 5 with second harmonic injection optimized for lowest fifth order distortion.

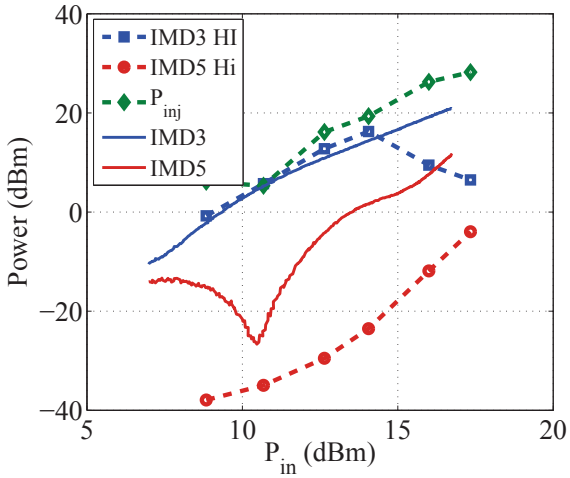

Figure 5.9: Comparison of power at $IMD3_L$ ($2f_1$-f_2), $IMD5_L$ ($3f_1$-$2f_2$) for HI-PA and PA without harmonic injection as a function of input drive level. The graph also shows the power injected at the second harmonic tone ($2f_1$) to achieve lowest $IMD3_L$.

It is seen that the reduction in $IMD3_L$ using external second harmonic injection is greater than 15 dB for different input drive levels, whereas $IMD3_H$ at $2f_2$-f_1 and $IMD5_H$ at $3f_2$-$2f_1$ remain unaffected. Fig.5.8 shows the reduction in power levels for $IMD3_L$ and $IMD5_L$ achieved for different fundamental input drive

levels along with the amount of injected $2f_1$ power.

For practical communication signals, the harmonic injection path needs to be modified in order to inject an exactly doubled spectrum of the signal. As seen in the two-tone measurements, injection at one harmonic tone only affects the distortion products which are a function of that harmonic tone frequency. Since, a modulated signal in general is a multi-tone signal, it will require a injected signal with twice the modulation bandwidth and RF carrier. This can be accomplished by baseband signal up-conversion.

The results show that a PA with harmonic injection in the output can be both efficient and linear. In the demonstrated results, we start with a class-AB PA, which is not perfectly linear. In fact, the theory shown in Ch.2 assumes that some second harmonic content is generated by the active device. If the transistor fails to generate second harmonic power and presents an impedance other than that of the fundamental frequency output termination, the necessary negative impedance cannot be synthesized using harmonic injection. In this case, harmonic injection at both the input and output of the transistor would be required.

For a modulated input signal, the third order nonlinearities have to be minimized since they create in-band distortion which is extremely difficult to filter. The third order distortion products are a function of the amplitude of second harmonic produced by the amplifier itself. Hence, a point in the amplitude and phase of the injected signal needs to be chosen to optimize linearity by a trade-off between the second and third harmonic content.

The main practical limitation on efficiency is the implementation of an efficient injector circuit. Fig.2.10 also shows that in order to achieve a significant improvement of $> 20\%$ in the total drain efficiency, the injection circuit efficiency should be more than 40% efficient along with the injection signal power 10 dB below the fundamental output power when the PA is operating at 1 dB compression point. But, this injection circuit efficiency does not contribute much to the total drain efficiency, if the PA is not operated close to saturation. It is seen that at lower input drive levels, the injected power required also reduces. Therefore, the injection circuit efficiency will now not play a significant role. This can be seen from Eq.6.1 where the DC power dissipated in the injected circuit is defined as a ratio of the injected RF power at the second harmonic and the injection circuit efficiency.

As seen in Fig.2.10, for an input drive level of 10 dB, the drain efficiency is improved from 35% for a

class-AB PA without harmonic injection to 48% for a PA with injection. But, the injection circuit efficiency does not affect the total efficiency and a flat response for total efficiency is achieved if the injection circuit efficiency is atleast 20%. As the PA compresses, the amount of power required for the second harmonic increases resulting in a higher impact of the injection circuit efficiency on the total drain efficiency of the PA.

This might present a challenge for very high power PAs, but is otherwise not a difficult constraint. In the prototype characterization presented in this paper, a passive doubler was used to produce the harmonic. This is not only inefficient, but not practical for amplifying a real signal, in which case significant distortion would be introduced. The linearity tests (Fig.3.6) show that a clean doubled frequency spectrum needs to be injected. Therefore, for signal amplification, a different approach is needed than was done for the CW tests in this paper. A topic of current research is integration of an up-converter in the injection circuit with a synchronized second baseband input. For very broadband signals, the phase control that achieves linearity might prove to be challenging. An interesting extension of the concept to a broadband HI-PA will require a three port injection network design with good harmonic isolation and low fundamental frequency loss over a broad frequency range.

5.3 Harmonic Balance Simulations

All the measurements presented above result from harmonic injection at one of the two second harmonic tones at the output of the PA. It is shown that each harmonic tone only affects the intermodulation products which are directly related to the injected tone. Therefore, simultaneous injection of both the harmonic tones should result in equal reduction of intermods on both sides of the spectrum. This idea has been validated using harmonic balance simulations in Advanced System Design (ADS) where a nonlinear model for the TriQuint TGF2023-01 discrete GaN on SiC die is used along with the designed input and output matching networks presented in Ch.4. A basic block diagram of the simulation setup is shown in Fig.5.10. Instead of terminating the output network in a 50Ω load, a fundamental tuner is utilized to perform load-pull at fundamental and intermodulation tones.

The harmonic balance simulation is setup to sweep the injected signal amplitude and phase along with load-pull at the fundamental tones to achieve maximum efficiency and minimum 3^{rd} and 5^{th} order IMD

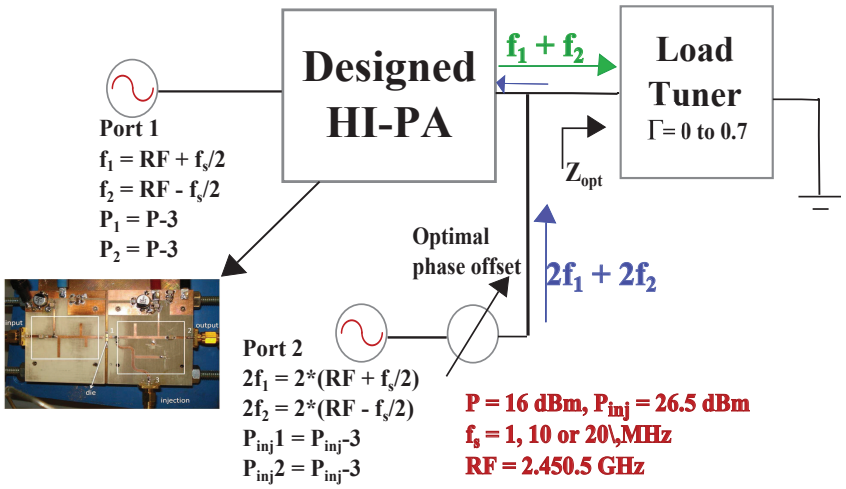

Figure 5.10: Harmonic balance simulations in ADS for harmonic injection at both the harmonic tone signals for the designed HI-PA with TriQuint 6 W GaN discrete die transistor having P_{out} = 36.28 dBm. A single harmonic balance source is used with two ports for fundamental and injected harmonic tone signals.

products. First, the load-pull is performed on the PA with no harmonic injection and the results are then compared to a PA with harmonic injection at both $2f_1$ and $2f_2$. The results are analyzed for tone seperations of 1, 10 and 20 MHz and an input drive level of P_{in} = 16 dBm which is the 1 dB compression point for the PA.

From Ch.1, it is known that waveform shaping is possible if short and open circuit impedances are presented at the even and/or odd harmonics at the virtual drain of the PA. Therefore, if load-pull to achieve maximum efficiency is performed on a PA without any harmonic terminations at the output, the optimum impedance points for the harmonics lie on the edge of the smith chart as shown in Fig.5.11a. Now, if we consider a two-tone signal at the input of the PA with a tone-spacing of 1 MHz and f_1 = 2.45 GHz, then load-pull for minimum 3^{rd} and 5^{th} order IMD products results in optimal impedance points at the fundamental tones also to be on the edge of the smith chart. This is because the IMD products are resultant of the even and odd-order nonlinearities from the PA [82].

Load-pull for maximum efficiency with two-tone input signal results in optimal impedance, Z_{opt} point for the fundmental tones to be close to 50Ω whereas for Z_{opt} for maximum linearity results in an impedance point to be on the edges of the smith chart. Therefore, trade-off is required between maximum efficiency and maximum linearity impedance points at the fundamental tone frequencies. However, selecting Z_{opt} = 14 + 12j Ω such that it lies in between minimum $IMD3$ point (Z_{opt} = 1.8+32j Ω) and maximum PAE point (Z_{opt} = 50.35-32j Ω) can result in almost 40% degradation in the PAE from 60% to 20% and a 4 dB reduction in

fundamental output power. Also, the harmonic balance simulations show that the minimum power levels obtained for $IMD3$ and $IMD5$ are -20.4 dBc and -33.95 dBc respectively for the optimum impedance points. Hence, this trade-off is not an efficient way to design the PA since there is severe degradation in the PAE and the intermodulation products are not minimized by a huge margin as shown in Fig.5.11.

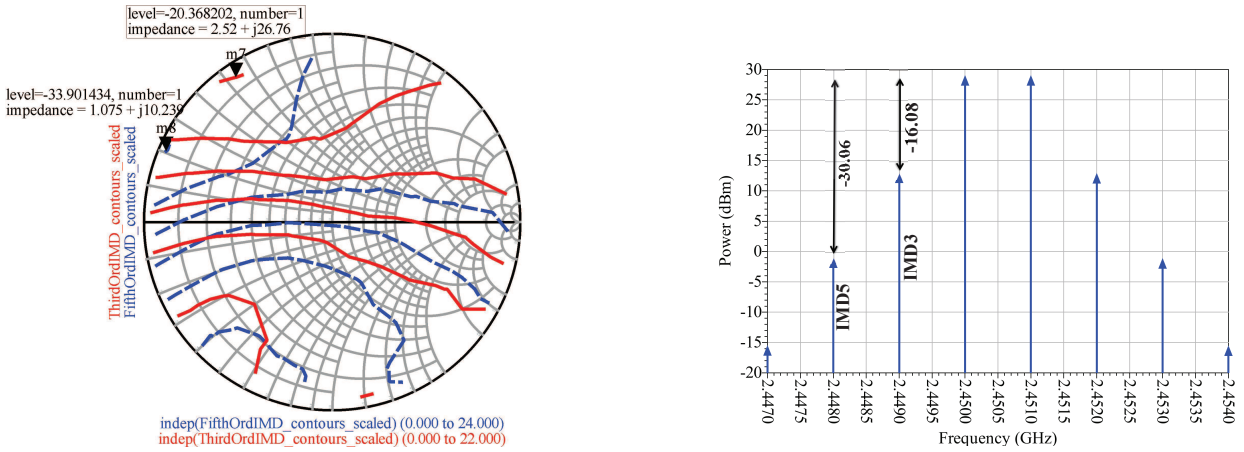

Figure 5.11: (a) Minimum $IMD3$ (red) and $IMD5$ (blue) contours for a class-AB without harmonic injection at the fundamental tones f_1 and f_2 with tone seperation of 1 MHz and total P_{in} = 16 dBm. (b) Spectral plot of the intermodulation distortion products for class-AB PA with load impedance, Z_{opt} = 14 + 12j Ω.

Next, the trade-off between efficiency and linearity in terms of Z_{opt} is studied for a class-AB PA with harmonic injection at both the harmonic tones i.e. $2f_1$ and $2f_2$. Equal power is maintained in the fundamental tones and the injected tones which is 3 dB less than the total power in both the frequency bands. Harmonic injection is performed with total injected power to be 9.5 dBc w.r.t. fundamental power and an optimal phase set for the injected tones. A single phase shifter is used to set the optimal phase at both the harmonic tones in the load-pull setup. Since second harmonic tone injection results in active impedance synthesis at the tone frequency, this affects the impedances at the IMD products as well. Also, phase reversal of 180° results in cancellation of IMD products as explained in section .2.3.1 and hence, the Γ_{opt} for maximum linearity now moves along the smith chart in phase and magnitude.

It is seen that the Z_{opt} for minimum $IMD5$ moves from the edges of the smith chart towards the center with a value of 89.856+j42 Ω shown in Fig.5.12 whereas Z_{opt} for minimum $IMD3$ moves from to 12+j19.6 Ω. The maximum efficiency point remains the same as that for class-AB PA without injection. Therefore, if an impedance is chosen in order to achieve resonably high efficiency and linearity, then at Z_{opt} = 68.707+29.466j

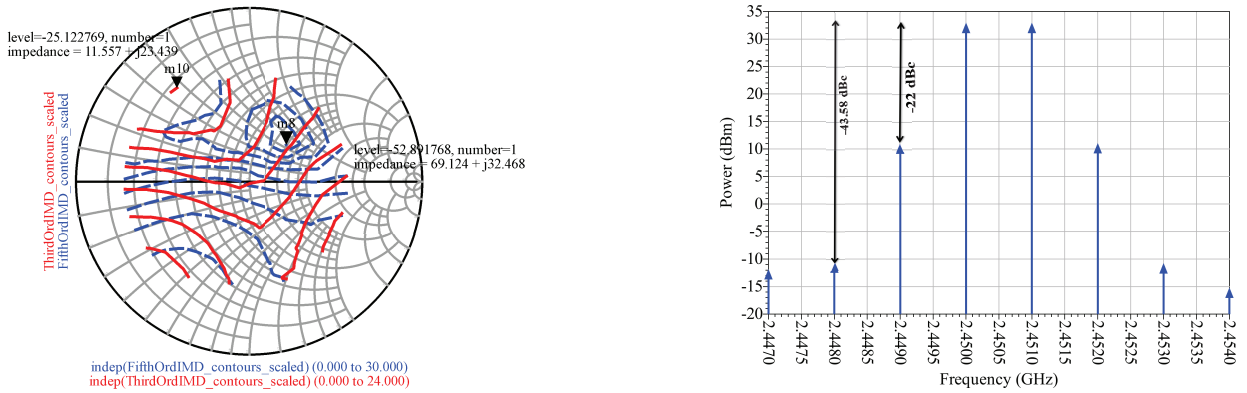

(a) (b)

Figure 5.12: (a) Minimum $IMD3$ (red) and $IMD5$ (blue) contours for HI-PA with optimal injection signal phase and amplitude for a fundamental tone seperation of 1 MHz and total P_{in} = 16 dBm. (b) Spectral plot of the intermodulation distortion products for HI=PA with load impedance, Z_{opt} = 68.707+29.466j Ω.

Ω, the values for $IMD3$ and $IMD5$ reduce by 5 dB and 10 dB respectively as compared to IMD power levels shown in Fig.5.11b and the efficiency drops by 15% relative to the maximum efficiency point for Z_{opt}. Also, there is a 0.8 dB drop in the fundamental output power as compared to 4 dB reduction in output power for class-AB PA without harmonic injection. Therefore, a non-expensive trade-off between efficiency and linearity is achievable with improved performance for the HI-PA compared to the class-AB PA without harmonic injection.

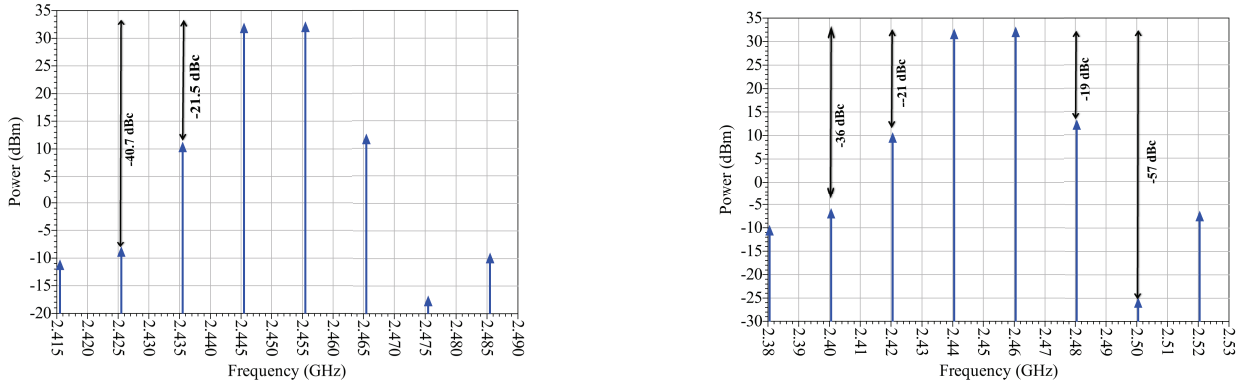

(a) (b)

Figure 5.13: Spectral plot of the intermodulation distortion products for HI-PA at Z_{opt} = 68.707+29.466j Ω with tone spacing of (a) 10 MHz and (b) 20 MHz.

Similar analysis is performed for HI-PA with tone spacing of 10 and 20 MHz where it is seen that as the tone spacing increases, the PA becomes asymmetric and the spectral components in both upper and

lower spectrum do not reduce equally. From Fig.5.13, as the tone spacing increases to 20 MHz, the upper and lower IMD spectral components do not reduce symmetrically. However, the power levels for these distortion products are still lower than a class-AB PA without harmonic injection. Therefore, this technique can result in high symmetrical linearity with considerable efficiencies for narrowband signals of bandwidths upto 10 MHz.

5.4 Conclusion

In summary, this chapter focuses on a study of linearity of harmonically-injected PAs. The behavior of odd order distortion products for fundamental two-tone signal with tone spacing from 1 to 20 MHz is studied in harmonically-injected PA. Harmonic injection is performed at one of the two harmonic tones at the output of the designed hybrid HI-PA resulting in reduction of distortion products which are directly related to the injected harmonic tone frequency.

Variations in both $IMD3$ and $IMD5$ w.r.t. amplitude and phase of the injected harmonic are presented where it is shown that the third and fifth order distortion products are reduced by more than 20 dB in linear region of the PA and 10 dB in saturation with a maximum efficiency improvement of 9%. This result matches with the results presented in Ch.4 where the reduction in third order nonlinearities for a CW signal are presented with harmonic injection resulting in a higher linearity for the PA.

It is shown that the phase required for both the harmonic tones to reduce the upper and lower sideband $IMD3$ products differs by 20° for tone spacings of 1 to 10 MHz. Also, as the tone spacing increases to 20 MHz, the PA asymmetry from low frequency memory effects results in variation of minimum power levels in the sidebands.

The analysis presented shows that simultaneous reduction in third and fifth order products can be achieved with harmonic injection at both harmonic tones if there are no sweet-spots present in the distortion products for the class-AB PA. The phase shift required in the injected harmonics to achieve maximum reduction in $IMD3$ and $IMD5$ products differs by 50° for tone spacings of 1-10 MHz.

Finally, harmonic balance simulations of variation in the optimum load for maximum linearity is presented showing that the trade-off required between efficiency and linearity for harmonically-injected PAs is less costly as compared to class-AB PAs with 15% reduction in total efficiency and 5 dB reduction in $IMD3$

for the harmonically-injected PA at a load selected to achieve the trade-off. The linearity investigation and measurement results that show reduction in IMD products for the HI-PA are presented in [83, 84].

Chapter 6

Supply Modulation Integration with Harmonically-Injected PA

The whole of science is nothing more than a refinement of everyday thinking.

—Albert Einstein

Machines are beneficial to the degree that they eliminate the need for labor, harmful to the degree that they eliminate the need for skill.

—W.H. Auden

Contents

6.1 Introduction

Modern communication systems utilize amplitude and phase modulation schemes with high peak-to-average ratios (PARs) and bandwidths. The primary challenge of a transmitter design is to achieve high efficiency and maintain linearity over the entire range of power levels and bandwidth [14, 15]. For example, Some of the solutions which address this requirement include outphasing (LINC), Doherty PA with DPD and envelope tracking PA with DPD [16, 17].

As shown in this thesis, second harmonic injected at the output of a power amplifier results in reduction of intermodulation distortion products or IMDs and high efficiency resulting in efficient and linear PAs.

In this chapter, the integration of supply modulation with second harmonic injection at the output of the PA is investigated in order to achieve highly efficient and linear power amplifiers for peak-to-average ratios (PARs) of $> 7\,\mathrm{dB}$. As shown in Ch.4 and 5,interaction of second harmonic with fundamental signal can result in mixing products with odd order behavior. In order to shape the fundamental waveform to obtain high efficiency, the injected signal has an optimal amplitude and phase w.r.t the fundamental signal. In addition, the mixing products at the optimal phase cancel out resulting in high linearity. Therefore, in order to achieve a linear and efficient PA for high PARs, the harmonically injected PA (HI-PA) is supply modulated in two different ways.

In the first approach, the input drive level is kept constant, the supply is varied simulatenously along with the amplitude of the injected second harmonic signal while maintaining the phase of the injected second harmonic to a constant optimal value. Nonlinear simulations performed in Advanced Systems Design (ADS) with a Modelithics nonlinear model of the TriQuint 6 W GaN on SiC device are shown along with

measurements validated with a proof-of-concept PA at a fundamental frequency of 2.45 GHz.

In the second approach, the input drive level is varied linearly with the supply and the ratio of the injected second harmonic power to the fundamental output power is maintained constant at 0.1. The phase of the injected second harmonic is set to an optimal value and the power varies linearly with input drive level and supply. Nonlinear simulations show that for a 6 dB PAR , a high drain efficiency of 80% is achieved along with a minimum point in the third order harmonic content, resulting in efficient and linear PA. The simulations are validated with measured results along with AM-AM and AM-PM measurements on the proof-of-concept PA at 2.45 GHz. Measured and simulated results show a high efficiency of 65% for a PAR of $\leq$ 7 dB along with 6 deg/dB reduction in the AM-PM distortion resulting in a highly efficient and linear PA for high Peak-to-Average ratio signals.

Finally, the requirements for an efficient supply modulator are discussed for both the approaches and a comparison is presented for supply modulator design for PAs with and without harmonic injection.

6.2 Theory

6.3 Nonlinear Simulations

In order to achieve a highly efficient and linear PA for high PARs, two approaches are presented in order to achieve high efficiency and linearity for $\leq$ 7 dB PARs using harmonic injection integrated with parital supply modulation at 2.45 GHz. In the first approach, the fundamental input drive level is kept constant with a simultaneous variation in the supply and the injected second harmonic power, $P_{inj}(2f_0)$, where as in the second approach, the input drive level is varied and a constant ratio is maintained between the output power at the fundamental, $P_{out}(f_0)$ and $P_{inj}(2f_0)$. In both approaches, there is a trade-off between the injection circuit efficiency and linearity. The harmonic balance simulations are performed in Agilent Advanced System Design (ADS) with a Modelithics non-linear model for the TriQuint 6-W GaN on SiC discrete device (TGF2023-01). A bias point in class-AB mode with $I_{DQ} = 130$ mA at $V_{DD} = 28$ V is chosen.

6.3.1 Approach I: Constant Input Drive

In this method, the simultaneous variation of the injected signal and drain supply achieves high efficiency for a 7 dB variation in output power with a constant input drive level as shown in Fig.6.1.

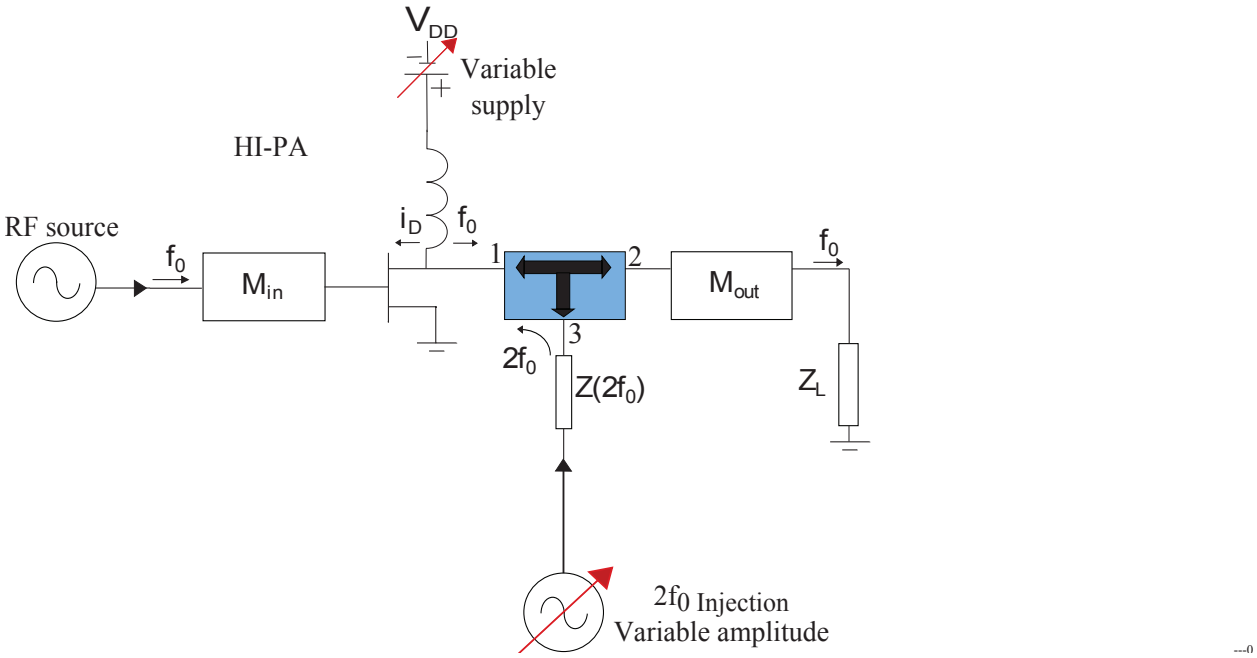

Figure 6.1: Block diagram of simulation setup in ADS for varying drain supply and injected second harmonic power in a class-AB PA with constant input drive power. The 3-port network at the output is a diplexer as shown in [7, 9].

First, an optimal phase for the $2f_0$ signal resulting in high efficiency and low third order harmonic content is chosen by simulating the HI-PA in class-AB bias at a constant fundamental input drive level of P_{in} = 16 dBm (P_{1dB}) and G = 21.5 dB. This phase is then set to the optimal value and the drain bias is varied from 10-35 V along with the injected second harmonic power level from -35 dBc to -10 dBc. The drain efficiency (η_D) for the HI-PA is calculated from Eq.2.25

$$\eta_D = \frac{P_{out}(f_0)}{P_{DC,f_0} + P_{inj}(2f_0)} \tag{6.1}$$

In Fig.6.2, dashed line B shows that a 7 dB PAR can be achieved with constant high η_D = 68% by varying V_{DD} from 10-25 V and $P_{inj}(2f_0)$ from 13-26 dBm. In HI-PA without supply variation, the horizontal line A is followed by applying a constant drain bias and fixed $P_{inj}(2f_0)$ in order to achieve high efficiency with only a minimal 0.5 dB variation in the fundamental output power. As seen from Fig.6.2, the required $P_{inj}(2f_0)$

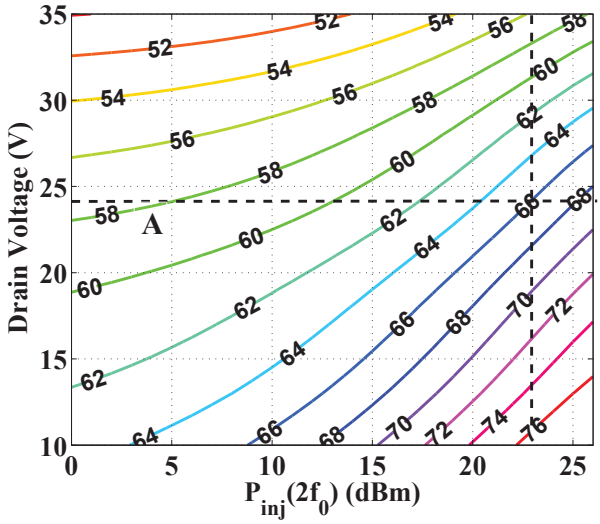

(a)

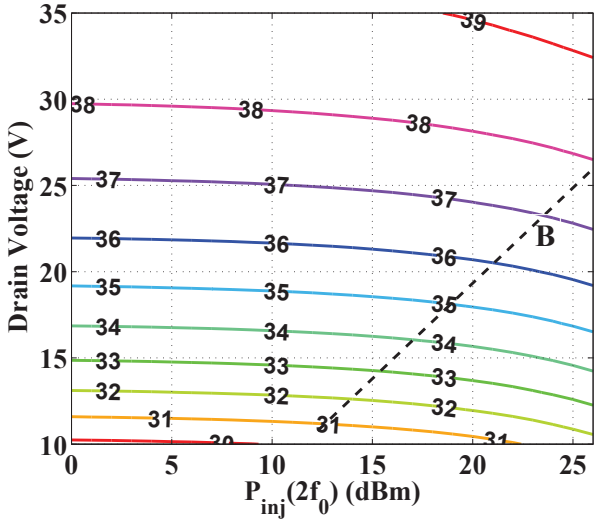

(b)

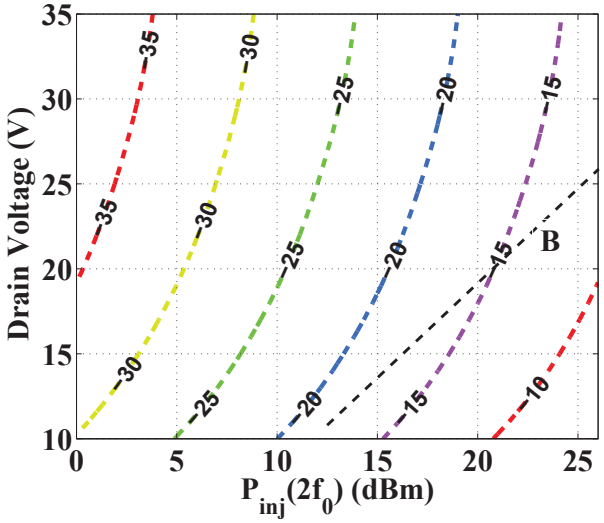

(c)

Figure 6.2: Simulated variation in (a) drain efficiency, η_D (%), (B) $P_{out}(f_0)$, in dBm, and (c) ratio $P_{inj}(2f_0)/P_{out}(f_0)$, in dBc, w.r.t. change in drain voltage and $P_{inj}(2f_0)$.

reduces at lower $P_{out}(f_0)$ in order to maintain constant high efficiency. Therefore, at lower power levels, the injection circuit efficiency is less critical whereas at higher power levels, (close to P_{1dB}), the injection circuit needs to be $\geq 40\%$ efficient in order to maintain high amplifier efficiency [9].

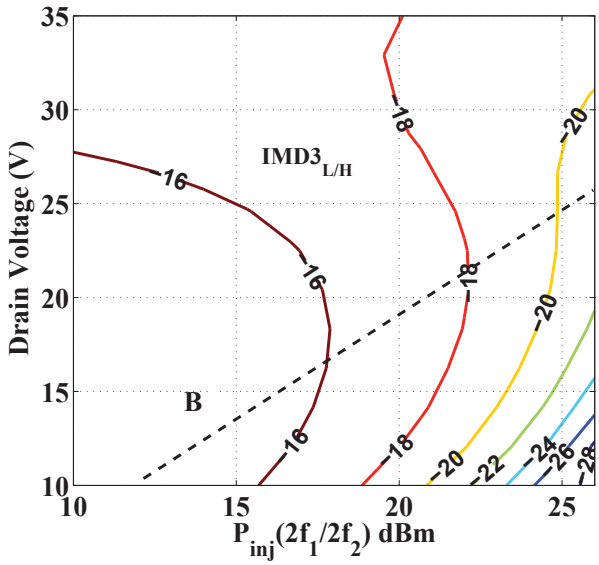

Figure 6.3: Variation in IMD3 with change in supply voltage and injected harmonic power. The input power is kept constant at 16 dBm. The contours show constant IMD3 levels for both sidebands and with a 1 MHz tone spacing.

As shown in [9, 71], high linearity can be achieved by maintaining an optimal power ratio, $P_{inj}(2f_0)/P_{out}(f_0)$ and phase of the injected signal. Here, this concept is further extended to integrate supply modulation with HI-PA. First, a study is performed with nonlinear simulations with a tone spacing of 1 MHz. Fig.6.3 shows that injection at both $2f_1$ and $2f_2$ with a fixed optimal phase results in a 5-12 dB reduction in both upper and lower IMD3 as compared to a PA without harmonic injection. It is also seen that for lower range of P_{out}, the ratio of P_{inj}/P_{out} is higher than 0.1 in order to achieve high linearity and efficiency. The design of the injection circuit can get challenging, since the efficiency of the injection circuit will now contribute more to the overall efficiency even at lower output power levels. Referring to the dashed line B in Fig.6.2, which describes the lookup table (LUT) in Fig.6.1, the simulated IMD3 curves show a 5 dB reduction at each power level. Thus, by proper control of both $P_{inj}(2f_0)$ and V_{DD}, both linearity and efficiency can be improved over a range of output power levels.

6.3.2 Approach II: Variable Input Drive

In a power amplifier, reduction in the supply voltage results in the 1 dB compression point shift to lower input drive levels as shown in Fig.6.4. Also, with increasing input drive levels and supply voltage, the amplitude and phase modulation distortion, AM-PM can be maintained constant from Fig.6.5.

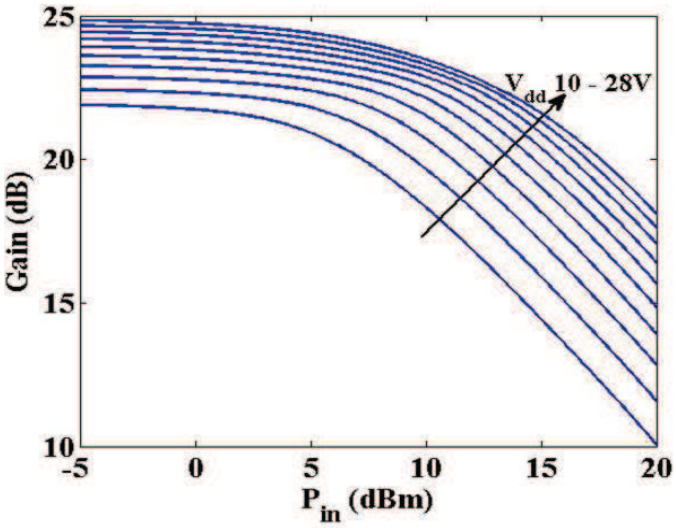

Figure 6.4: Gain characteristic of a class-AB PA with increase in input drive levels and suppy voltage from 10 to 28 V.

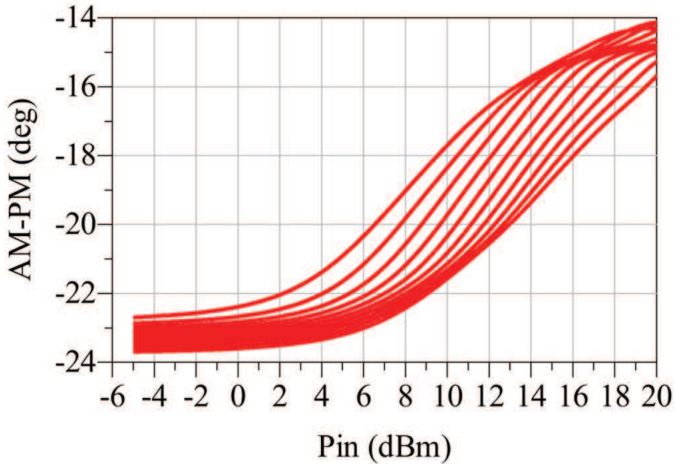

Figure 6.5: AM-PM characteristic of a class-AB PA with increase in input drive levels and suppy voltage from 10 to 28 V.

Therefore, in order to maintain constant gain or constant AM-PM distortion characteristic for high PARs, the supply voltage can be varied as a quadratic function of the input drive level shown in Fig.**??**. The constant

gain curve results in a 2° variation in the AM-PM distortion. However, if the AM-PM distortion is maintained constant, For. example, -21°, then the output power can be varied from 26 to 34 dBm with a 2 dB variation in the gain as seen in Fig.6.7. Also, if the constant AM-PM curve for variation in supply and input power is chosen, then the ratio between the injected 2^{nd} harmonic power and the fundamental output power will remain constant over the high PAR.

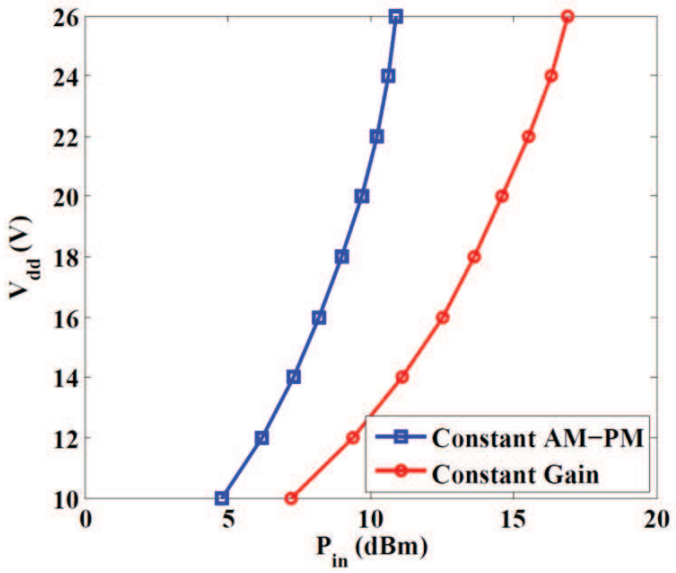

Figure 6.6: Quadratic approximation for supply voltage variation as a function of variation in the input drive level for constant gain and AM-PM characteristics.

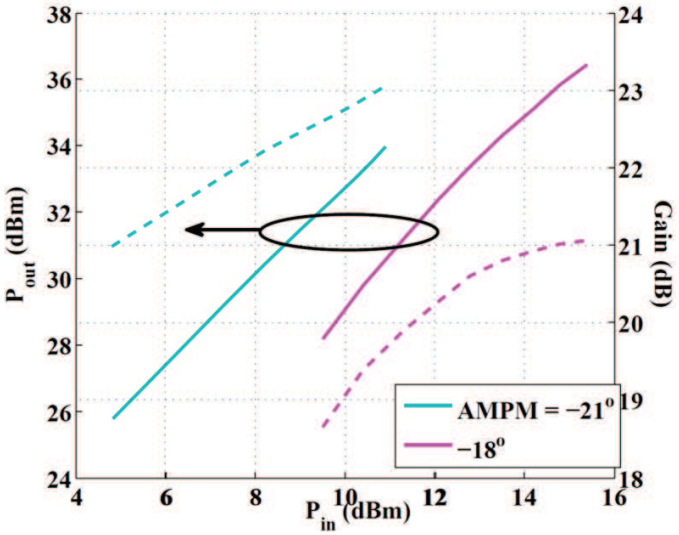

Figure 6.7: Variation in fundamental output power and gain with constant AM-PM distortion maintained in a PA with supply and input drive variation.

In the second approach, the fundamental input drive level is varied and a constant ratio of $P_{inj}(2f_0)/P_{out}(f_0)$ = 10.5 dB is maintained for each of the drive level along with a fixed optimal phase for the injected 2^{nd} harmonic as shown in Fig.6.8. This ratio gives the optimal value of the injected second harmonic power required to achieve high efficiency and linearity. The drain supply is then varied from 10-35 V for each of the input drive level. As seen in Fig.6.9, high efficiency of 75% is achieved for an output power variation of

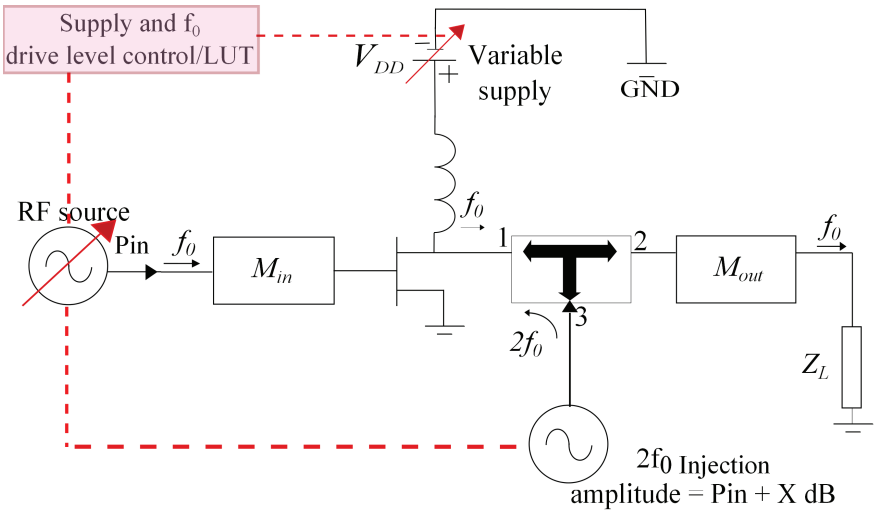

Figure 6.8: Block diagram of simulation setup in ADS for varying drain supply and fundamental input drive level in a class-AB PA. A constant ratio is maintained between $P_{inj}(2f_0)$ and $P_{out}(f_0)$.

7 dB when the supply is varied from 12-26 V and input power from 10-18 dBm. Also, since the input drive is varying, a constant gain of 20 dB is maintained over the 7 dB PAR resulting in high PAE as well.

In terms of linearity, the third order nonlinear product i.e. the output power at 3rd harmonic, $(P_{out}(3f_0))$, shows reduction at the peak efficiency points as shown in Fig.6.10. It is well known that lower third harmonic implies lower third order distortion products (IMD3) levels [75]. Hence, this approach results in high efficiency and linearity for all the output power levels. However, since the ratio between the instantaneous output power and injected power is now constant, the injection circuit efficiency is critical even at lower input drive levels. Two tone simulations show that IMD3 follows the same trend with $\leq$ -30 dBc reduction for a 7 dB variation in $P_{out}(f_0)$ and a constant gain of 19 dB.

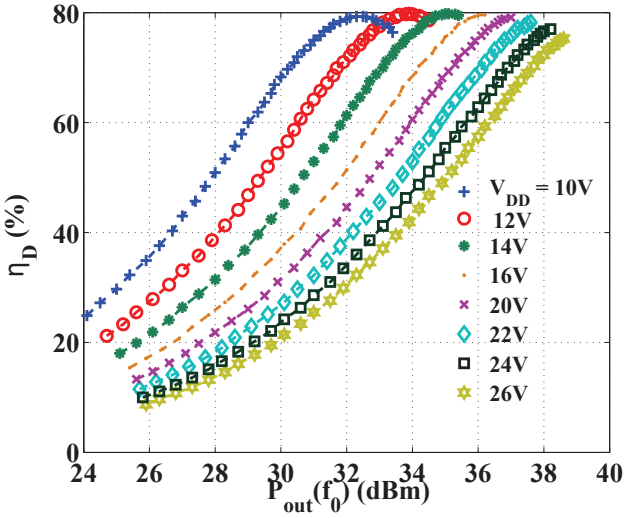

Figure 6.9: Simulated results for drain efficiency, η_D with simultaneous variation in fundamental input drive and drain supply voltage. The ratio, $P_{out}(f_0)/P_{inj}(2f_0) = 0.1$ for each input drive.

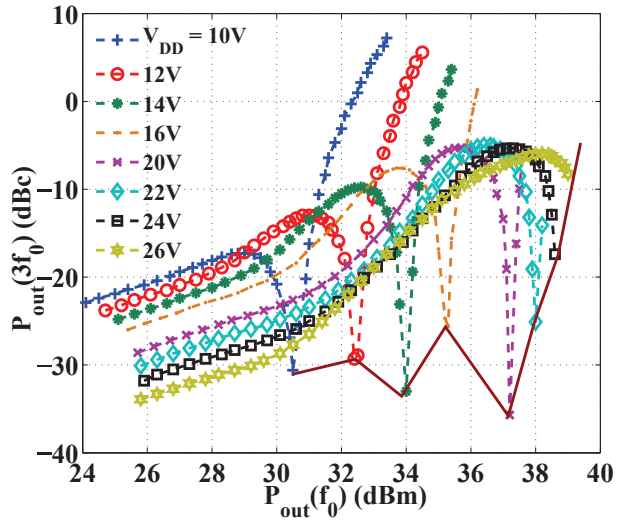

Figure 6.10: Simulated results for $P_{out}(3f_0)$ with simultaneous variation in fundamental input drive and drain supply voltage. The ratio, $P_{inj}(2f_0)/P_{out}(f_0) = 0.1$ for each input drive.

6.4 Measurements

The measurements are peformed on a harmonically-injected PA (HI-PA) proto-type designed using a 6 W discrete GaN on SiC die from TriQuint Semiconductor. The PA is designed at a fundamental frequency of f_0 = 2.45 GHz with a class-AB design at I_{dq} = 130mA and V_{dd} = 28 V. The output matching network of the PA incorporates a diplexer circuit in a non-50 Ω environment in order to inject the second harmonic into the

drain of the PA without affecting the fundamental output signal path. Detailed description of the PA design can be found in [9, 7, 66]. The PA has a small signal gain of 23 dB in class-AB mode with a drain efficiency, $\eta_D = 55\%$ at 1 dB compression. Note that all the measurements presented are calibrated at the output port of the designed amplifier.

6.4.1 Approach I

l The measurement setup consists of the HI-PA in a hybrid configuration with a TriQuint TGF2023-01 6-W discrete GaN die integrated with the input and output networks on a Rogers 4350B 30-mil substrate. The measurements include a total loss of 2 dB in the input and output networks of the PA. In order to validate approach I, the drain supply voltage and $P_{inj}(2f_0)$ are varied simultaneously with V_{DD} ranging from 12-32 V and $P_{inj}(2f_0)$ from -25 to -10 dBc with a fixed optimal phase for the injected second harmonic. Fig.6.11 shows

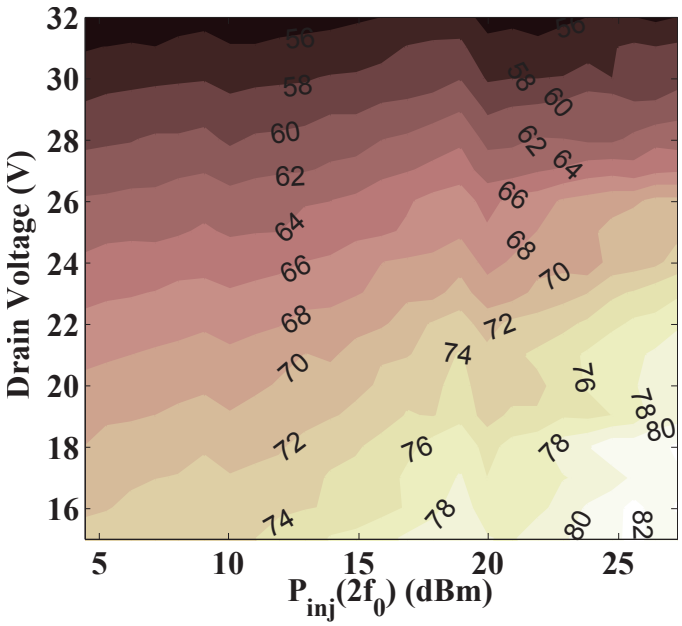

Figure 6.11: Variation in measured drain efficiency w.r.t. the drain voltage, V_{DD} and injected second harmonic power, $P_{inj}(2f_0)$. The amplifier has G = 19 dB at $P_{in} = 16$ dBm for a bias of $V_{DD} = 28$ V and $I_{DQ} = 130$ mA. The gain varies between 13 and 19 dB over the entire range of values.

measured drain efficiency curves for the HI-PA with supply modulation as a function of V_{DD} and $P_{inj}(2f_0)$, which compare well with the simulations in Fig.6.2. A 6 dB variation in $P_{out}(f_0)$ is achieved with a high η_D = 66%. As seen from Fig.6.11, the injected power required to achieve high efficiency for lower output power levels reduces. Hence, the injection efficiency for a transmitter at these power levels is not very important

and will not affect the total system efficiency. However, the gain varies by almost 6 dB over the entire range and a constant 10 dB reduction is seen in the third harmonic output power as compared to a class-AB PA with no harmonic injection.

Table 6.1: Measured parameters of supply modulated HI-PA.

$V_{DD}(V)$	$P_{inj}(dBm)$	$P_{out}(dBm)$	η_D	$R_{dd}(\Omega)$
12-18	16.6-26.28	30.9-34	72%	86.38-107.2
12-21.25	12.4-26.28	30.7-35	68%	83.3-107.4
12-23.25	12.4-26.28	30.65-36.5	66%	81.9-108
17-26.75	8.82-26.28	33.2-36.27	62%	86-110
21.75-30.5	8.82-26.28	34.8-37	58%	91.3-114

The measurements shown assume the injection efficiency to be 100% since the test bench setup consists of instrumentation equipment. Table 6.1 shows the measured parameters for the harmonic injection PA with supply modulation using approach I.

6.4.2 Approach II

In order to maintain linearity and constant gain over a high PAR, approach II explained in section 6.3.2 is validated, where the fundamental input drive is varied along with the drain supply of the harmonically injected PA. The ratio, $\frac{P_{out}(f_0)}{P_{inj}(2f_0)}$ is kept constant at a value of 10 dB for every input drive level. As shown in Fig.6.12, a constant gain of 17 dB is maintained for a 6 dB variation in the output power along with a -32 dBc reduction in the third order nonlinear harmonic content. The drain efficiency of the PA varies from 73% to 67% over a 6 dB change in the output power.

Note that in this case, the optimal phase of the injected harmonic is not varied with increasing drain voltage and input drive level. Next, the dynamic AM-PM distortion is measured as explained in [85]. Fig.6.13 shows the variation in output power as a function of input drive level and drain voltage for a harmonically-injected PA. It is seen that for a PA without supply variation, trajectory T1 can be followed where there is a 7 dB variation in output power with constant supply voltage of 28 V and variation in input drive level. However, in this case, high efficiency is only achieved at higher power levels as shown in Fig.6.15. If trajectory T2 is followed with harmonic injection, then a 10 dB variation in the output power is achieved with supply variation from 14 to 26 V and input power varied by 8 to 16 dB. Fig.6.15 shows that we can achieve high efficiency

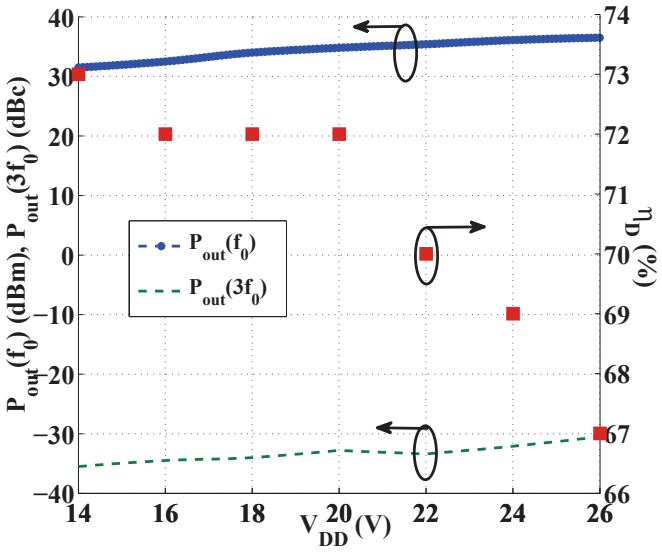

Figure 6.12: Measured $P_{out}(f_0)$ (dBm), $\eta_D(\%)$ and $P_{out}(3f_0)$ (dBc) for a harmonically injected PA with variable supply and input drive level. The ratio of $P_{out}(f_0)/P_{inj}(2f_0) = 10.5$ dB for each of the input drive levels.

ranging from 60 to 78% for a 10 dB variation in output power. Measured results shown in Fig.6.15 match closely with the simulated results shown in Fig.6.9 where we can see a constant high efficiency of 80% for a 6 dB variation in output power with drain voltage ranging from 16 to 26 V. As seen in Fig.6.14, if trajectory T2 is followed for supply modulation, the PA gain varies by 3 dB with gain of 19 dB for lower output power levels and 22 dB for higher power levels. Hence, as the peak of the signal increases in instantaneous power, the gain of the PA also increases.

It is clear that high efficiency can be achieved for a PAR of > 7 dB through the integration of supply modulation and harmonic injection. Approach II also is validated to acheive high linearity by measuring dynamic AM-PM data from the experimental setup as explained above. Measured AM-PM distortion for the class-AB PA with and without harmonic injection shows that as the supply voltage to the PA increases, the AM-PM distortion reduces by a maximum of 6 deg/dB for a harmonically-injected PA as compared to a PA without injection. Fig.6.16 shows the measured AM-PM distortion for the harmonically injected PA and the improvement in AM-PM over non harmonically-injected PA.

Measurements show that the AM-PM distortion is greatly reduced by a maximum of 6 deg/dB with harmonic injection hence resulting in a linear and efficient PA.

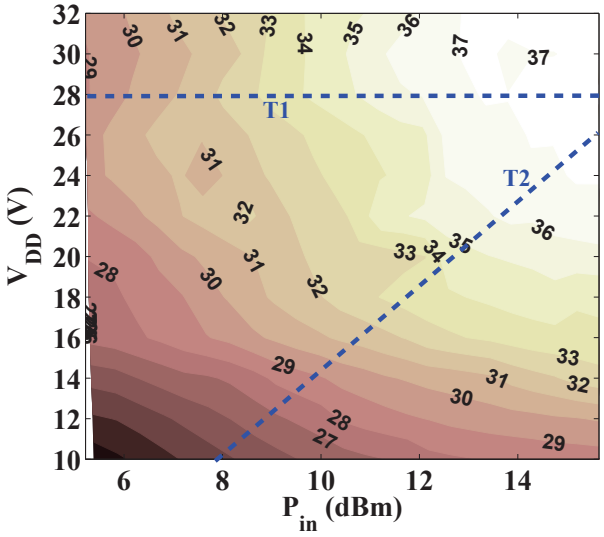

l

Figure 6.13: Measured variation in the fundamental output power, $P_{out}(f_0)$ as a function of the input drive level and supply voltage for a harmonically-injected PA with optimal amplitude and phase of the second harmonic.

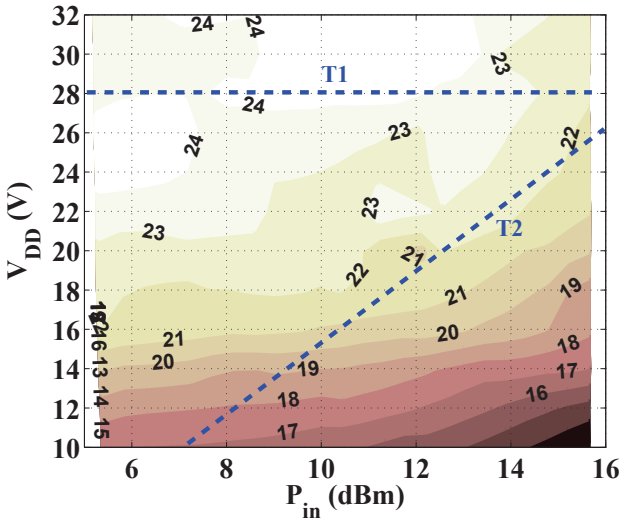

Figure 6.14: Measured variation in gain as a function of input power, P_{in} and supply voltage, V_{DD} for the harmonically-injected PA with supply variation.

The two main challenges in supply modulation integration are CPAE efficiency and the fact that the PA is a dynamic load to the supply [15]. The integration of supply variation with harmonic injection will require an efficient supply modulator where the total system efficiency can be calculated as follows:

$$\eta_{total} = \eta_{SM} \cdot \frac{P_{out}(f_0)}{P_{DC,f_0} + P_{DC,2f_0}} \tag{6.2}$$

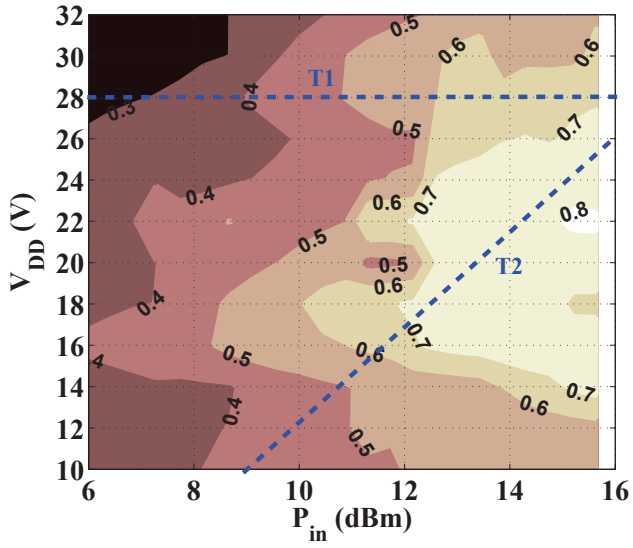

(a)

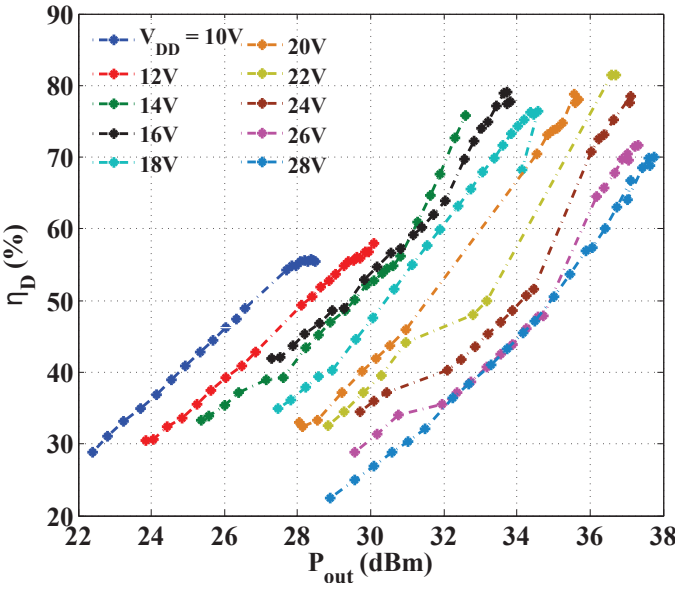

(b)

Figure 6.15: (a) Measured PAE contours as a function of the input drive level, P_{in} and supply voltage, V_{DD}, (b) Measured drain efficiency as a function of the output power and drain voltage showing constant high efficiency of 75% for a PAR of 6 dB.

where, $P_{DC,2f_0} = P_{inj}(2f_0)/\eta_{inj}$ and η_{SM} is the supply modulator efficiency. In order to design an efficient supply modulator, the PA supply sensitivity is shown in Fig.6.17, defined as

$$\zeta(\%) = \frac{\frac{\Delta V_{out}}{V_{out}}}{\frac{\Delta V_{DD}}{V_{DD}}} \cdot 100 \tag{6.3}$$

In approach I, for lower values of $P_{inj}(2f_0)$ and V_{DD}, the resultant error in output voltage into a 50 Ω load

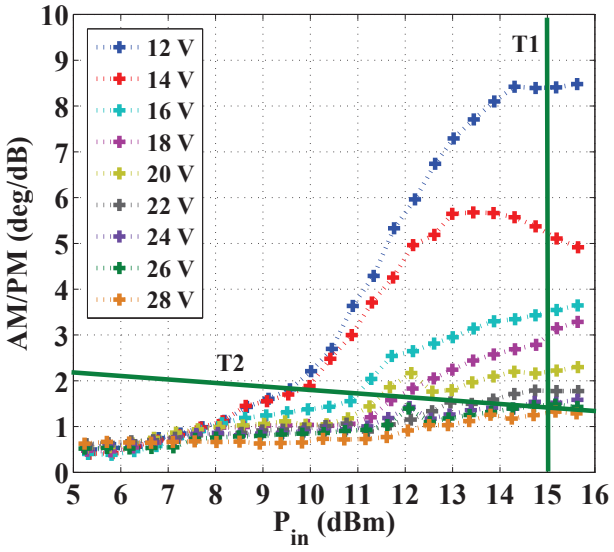

(a)

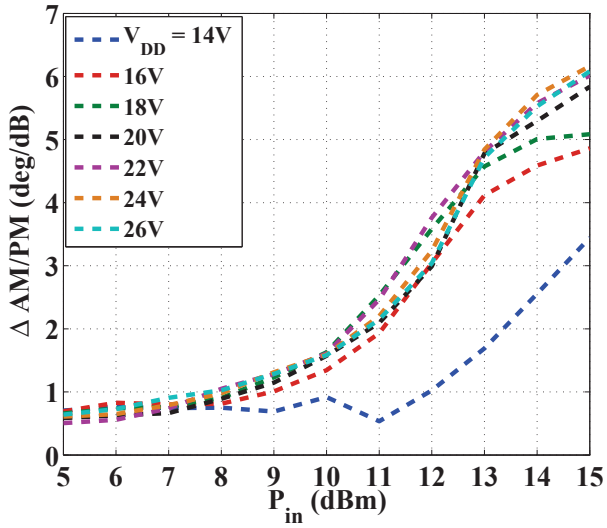

(b)

Figure 6.16: (a) dynamic AM-PM distortion for HI-PA with variation in input drive level and supply voltage. (b) Measured improvement in the AM-PM distortion of a harmonically-injected PA over a non harmonically-injected PA.

is as high as 95% and reduces to $\leq$ 40% for higher values of these parameters. Line B shows that the PA supply sensitivity for a 6 dB PAR drops from 95% to 60% as the output power increases to its peak value. The PA presents a dynamic load to the supply which can be defined as $R_{dd} = V_{DD}/I_{DD}$. For a harmonically injected PA, this load also has a dependency on the injected power at the second harmonic. Hence the value

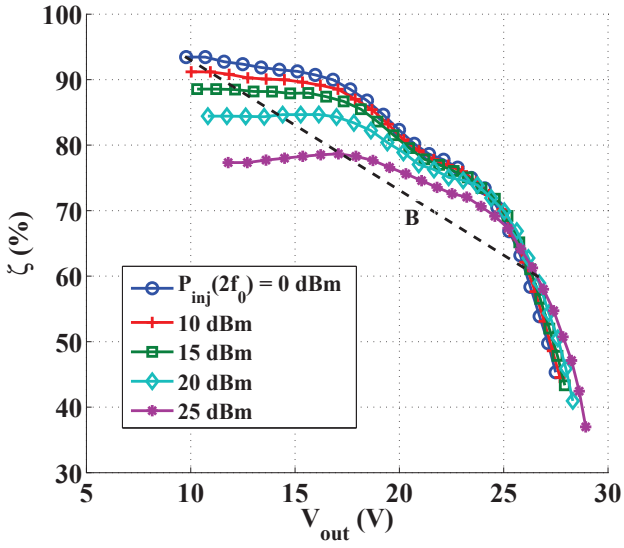

Figure 6.17: Simulated error in output voltage, V_{out} with 1 V error in drain bias voltage for various injected harmonic power levels (approach I).

of R_{DD} can be calculated as follows:

$$R_{dd} = \frac{V_{DD}}{I_{DD}} = \frac{V_{DD}^2}{P_{DC,f_0}} \tag{6.4}$$

Now, from (6.1), substituting for P_{DC,f_0}, the value of R_{dd} can be computed:

$$R_{dd} = \frac{V_{DD}^2 \cdot \eta_D}{P_{out}(f_0) - \eta_D \cdot P_{inj}(2f_0)} \tag{6.5}$$

In approach I, varying the drain supply with harmonic injection at a fixed input power results in a maximum 30% increase in the load presented by the PA to the supply modulator for a 6 dB variation in the output power as shown in the table 6.1.

Simulated results show that in approach II, the PA load defined in (6.5) remains almost constant at a value of 105Ω and varies by a small value of 2% when the drain bias is varied from 14-26 V and a constant gain is maintained over a 6 dB PAR with high efficiency. This small variation in R_{dd} means that the supply modulator design in this case is much less stringent than for a pure envelope tracking transmitter [15].

Measured static load variation is shown in Fig.6.18 where it is seen that if trajectory T2 is followed, then a 9% variation in the total load is seen from 110Ω to 120Ω. The trade-off involved in this approach is the efficiency of the injection circuit which now plays a critical role at lower power levels as well. Hence, the injection circuit would need to be designed for $\geq$ 40% efficiency over the entire 6-7 dB range of power levels.

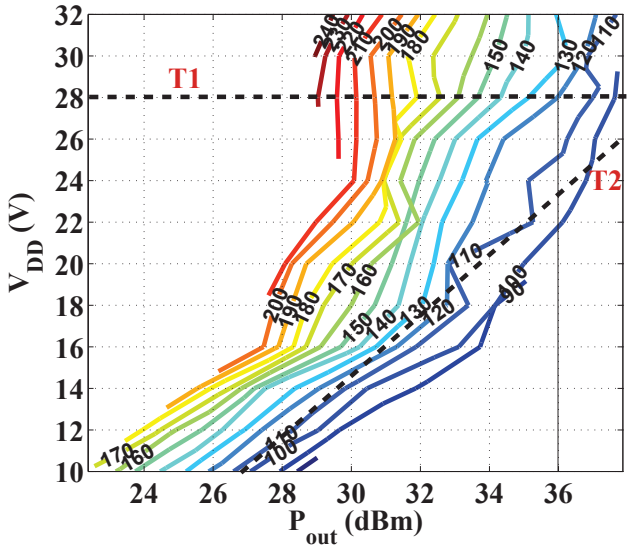

Figure 6.18: Measured static load presented by the PA to the supply as a function of the output power.

6.5 Discussion

A measure of linearity is AM-PM distortion in an amplifier because modern communication systems utilize phase based modulation schemes. These include but are not limited to various PSK standards for satellite communication links, WLAN, Bluetooth, Zigbee and RFID standard ISO14443. The ubiquity of phase modulation and the varying characteristics of phase distortion among different SSPA technologies and topologies make AM-PM distortion an important consideration in power amplifier design. If the input signal to the PA is assumed to the following:

$$x(t) = X(t).cos[2\pi.ft + \phi(t)] \tag{6.6}$$

The output of the PA exhibits nonlinear behavior both in amplitude and phase. Therefore, the output signal can be written as follows:

$$y(t) = G[X(t)].cos2\pi.ft + \phi(t) + \Phi[X(t)] \tag{6.7}$$

where $G[X(t)]$ and $\Phi[X(t)]$ represent the nonlinearites introduced in the amplitude and phase behavior of the PA. In order to understand the trade-off between efficiency and linearity for a harmonically-injected

PA with supply variation, dynamic AM-PM measurements are taken on the HI-PA with a constant ratio between the injected signal and output power of 10 dB and a fixed optimal phase for the injected harmonic for each input power and drain voltage sweep. The theoretical analysis of the dynamic AM-PM measurements is shown in [86, 85]. First, consider the AM-PM characteristics for a class-AB PA without harmonic injection as a function of drain bias and input drive level. In fig.6.19, the measured AM-AM and AM-PM data for this PA shows that the slope of the amplitude and phase distortion remains almost the same for drain voltages ranging from 10 to 32 V for the GaN PA. Although, as the drain voltage to the PA is increased, the PA compresses at higher input drive level. The AM-PM plot also shows that the nonlinear characteristic of the PA is preserved with variation in supply with the exception of degradation at a higher input power level. For example, in fig.6.19, a phase distortion of 4 deg/dB is obtained for drain voltages ranging from 12 to 32 V, but the input drive level at which this distortion is achieved increases with increase in the drain voltage. Therefore, for a PA with supply modulation, if the supply voltage varies linearly with the input drive level, then the compression and distortion characteristics of the PA remain the same.

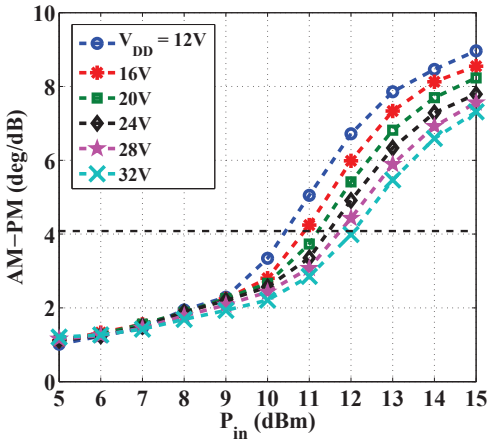

Figure 6.19: Measured dynamic AM-PM distortion for a class-AB GaN 6 W PA without harmonic injection. The plot shows the AM-PM distortion for various drain voltages as a function of the input drive level, P_{in}.

6.6 Conclusion

In summary, to the best of the author's knowledge, this is the first demonstration of a supply-modulated harmonic injection PA. We have demonstrated a 2.45 GHz GaN 6-W PA with η_D = 67-73% over a 6 dB PAR.

The gain remains constant and linearity is improved significantly. shows first time, the integration of supply variation with a harmonically-injected PA. Two different methods are presented to achieve high efficiency and linearity for high Peak-to-Average ratios of $> 6\,\mathrm{dB}$.

In the first method, harmonic balance simulations are presented with variation in supply and injected signal amplitude while keeping the input drive and relative phase of the injected harmonic at a constant optimal value. The simulated and measured results show constant total efficiency of 66% for a 6 dB variation in output power. The supply voltage and injected signal amplitude are varied linearly to achieve variation in output power. In the second method, the supply is varied with the input drive level by maintaining a constant ratio between the injected signal and the input drive level. The phase of the injected signal is again fixed to an optimal value. The simulated and measured results show total efficiencies of 70-80% for a 7 dB variation in outpput power. Measurements also show the reduction in third order nonlinearity i.e. $P_{out}(3f_0)$ by $> 15\,\mathrm{dB}$. AM-PM measurements also show reduction in phase distortion in the PA resulting higher linearity.

The analysis presented shows that the second method yields better trade-off characteristics between efficiency and linearity for the HI-PA, and is reported in [87].

Chapter 7

Contributions and Future Work

The whole of science is nothing more than a refinement of everyday thinking.

—Albert Einstein

Machines are beneficial to the degree that they eliminate the need for labor, harmful to the degree that they eliminate the need for skill.

—W.H. Auden

Contents

7.1 Introduction

This last chapter describes some directions for future work including preliminary results on a X-band MMIC harmonically-injected PA designed in the TriQuint high frequency GaN process. The motivation for the design is to demonstrate experimentally frequency scaling as well as high efficiency which includes the injection circuit efficiency. In addition, a proposed architecture for a complete communication transmitter using HI-PA is discussed. Finally, the contributions of this thesis are summarized.

7.2 X-Band MMIC Design

The design for the 10-GHz harmonically injected PA (HI-PA) in the TriQuint 0.15 μm GaN process is done in AWR Microwave office with the nonlinear model, design and layout rules guide provided by TriQuint Semiconductor for a GaN 12×100 μm gate periphery device. The first step in the design is to perform load-pull simulations on the device with the specific bias point in class-AB mode in order to design the input and output matching networks for the PA. Since, the aim here is to design a class-A PA which can then be made more efficient using harmonic injection, the bias point is chosen from the DC load line as shown in Fig.7.1.

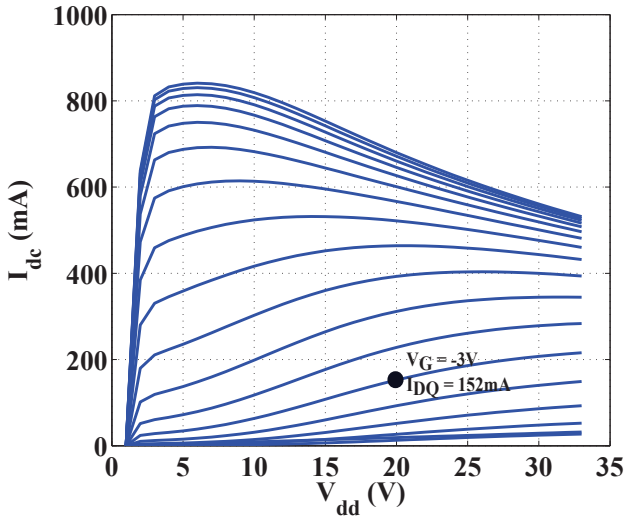

Figure 7.1: Simulated IV curves for the 12x100 μ periphery TriQuint GaN device. The bias point selected is shown in the figure with $I_{dq} = 152\,\text{mA}$.

Once the bias point is selected with $V_{dd} = 20\,\text{V}$, ideal load pull simulations result in the optimal output

impedance (Z_{out}) of the transistor for a class-A/AB mode of PA. A source pull is performed on the PA in order to achieve maximum small signal gain for the device at 10 GHz. This impedance is found to be Z_{in} = 3.0+5.1j Ω.

The input matching network is designed as a passive two-port network so that the gate of the device can be matched to Z_{in} along with low insertion loss and RF to DC isolation. Since the input network does not require components to handle large current densities, a spiral inductor is used as an RF choke along with resistance in series for stability. First, the input network is designed in AWR using ideal components in order to achieve the desired Z_{in} at port 2 of the two port input network. Once the desired impedance and $|S_{21}|$ is achieved with the ideal design, it is modified using on chip components using the $0.25\mu m$ process kit library in AXIEM EM simulator. A comparison of the impedance match achieved with both ideal and non-ideal MMIC components for the input matching network is shown in Fig.7.2 where port 1 of the input matching network is matched at 50 Ω and port 2 is matching to Z_{in} resulting in total insertion loss through the network of 0.5 dB. Also, the DC and bypass blocking capacitors provide a RF-DC isolation of $>$ 30 dB at 10 GHz.

Load-pull on the output is performed with the designed input matching network as shown in Fig.7.3 where the load-pull results in P_{out} = 35.9 dBm at an impedance of Z_{out} = 11+13j Ω. The output network design is divided in two parts with one low pass filter and one high pass filter network in parallel connected to a common node at the drain of the transistor. This network then represents a diplexer network design similar to the one shown in [7]. The filter networks are considered at passive two port networks with one port matched to Z_{out} and the other port matched to 50 Ω. Since the line lengths calculated for these networks are too long for the chip size, a combination of microstrip and capacitors is used to design the output diplexer network.

The simulated losses in both the low and high pass network is shown in Fig.7.4. In order to make this network compact, the DC blocking and bypass capacitors are integrated within line lengths along with a meandered section of wide microstrip line used as an RF choke which can handle the output current.

The simulated class-AB PA design results in 36.4 dBm output power at compression and 47% drain efficiency with a small signal gain of 15 dBm. The layouts for the designed networks are then integrated with that of the device in order to design the final chip layout as shown in Fig.7.6. The ideal design when tested with harmonic injection results in characteristics similar to the hybrid HI-PA presented in Ch.4. It is seen

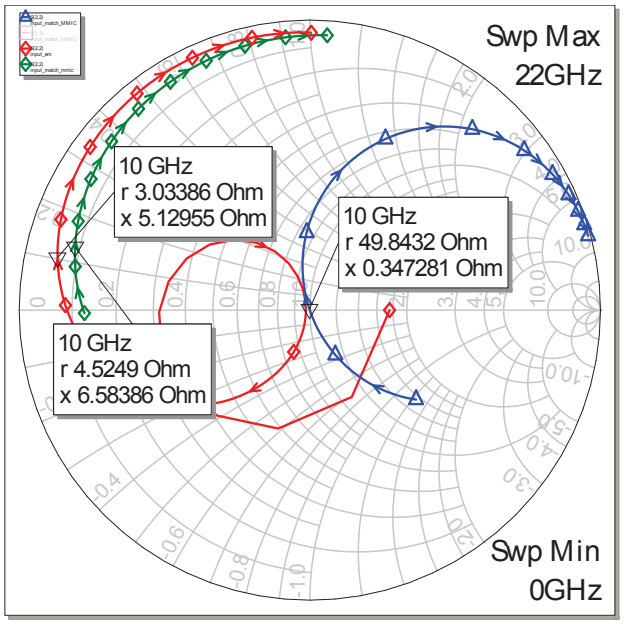

(a)

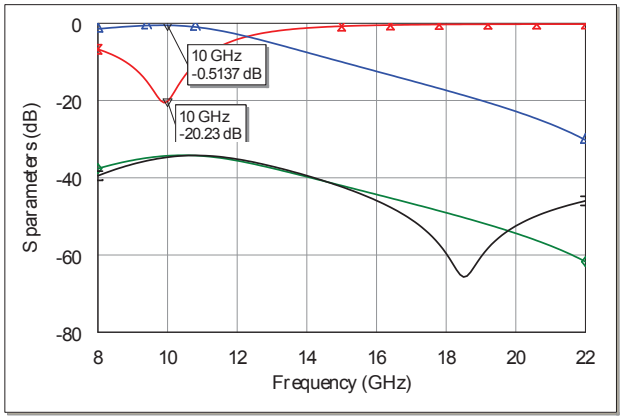

(b)

Figure 7.2: (a) Impedances for the ideal and non-ideal simulated input matching network with port 1 matched to 50 Ω (blue) and port 2 matched to Z_{in} (green - ideal, red- non-ideal). (b) Simulated S parameters for non-ideal input matching network.

that when the injected signal amplitude is maintained at 10 dBc w.r.t. fundamental output power at 1 dB compression, the output power at f_0 and $3f_0$ have peak and minimum points with a 0-360° relative phase shift at the injected second harmonic. The current also drops by > 100 mA as shown in Fig.7.5. This results in an efficiency improvement of $> 20\%$ with peak drain efficiency of 70% with > 4 W of output power.

The final layout of the designed chip is shown in Fig.7.6 where the main PA is the harmonically-injected PA at 10 GHz and the PA on the top left corner is a 20 GHz driver PA with $\eta_D > 60\%$ designed by Michael Coffey for this part of the project.

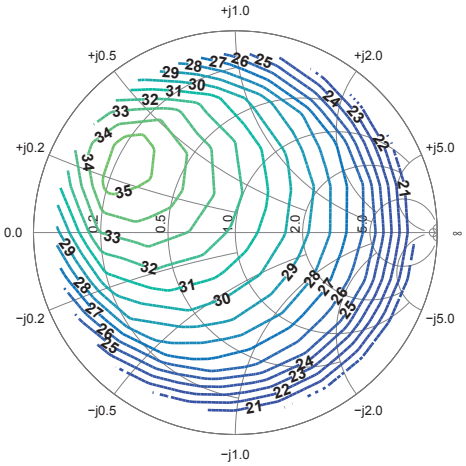

Figure 7.3: Simulated load-pull contours in order to obtain maximum output power, P_{out} at 10 GHz.

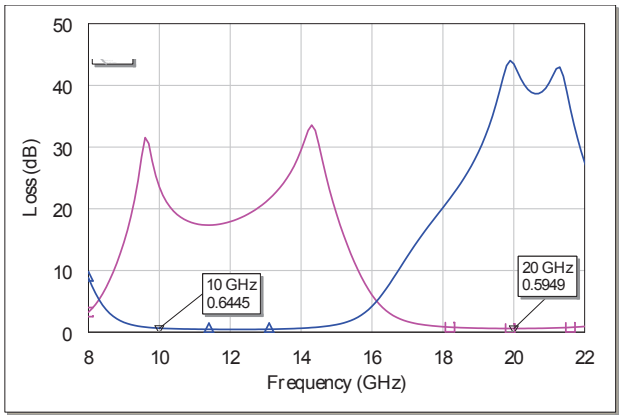

Figure 7.4: Simulated loss in the through and injection paths of the 3-port output diplexer network.

7.3 Measurements

The two PAs in Fig.7.6 are measured separately using fixtures which interface the MMIC to coaxial connectors as presented in [41]. The 10-GHz PA is measured without harmonic injection at a bias point of $V_{dd} = 20\,\text{V}$ and $I_{dq} = 70\,\text{mA}$ and the 20 GHz driver PA at a bias point of $V_{dd} = 15\,\text{V}$ and $I_{dq} = 20\,\text{mA}$. The 10-GHz HI-PA is then tested with 2^{nd} harmonic injection by optimizing the amplitude and phase of the injected $2f_0$ signal.

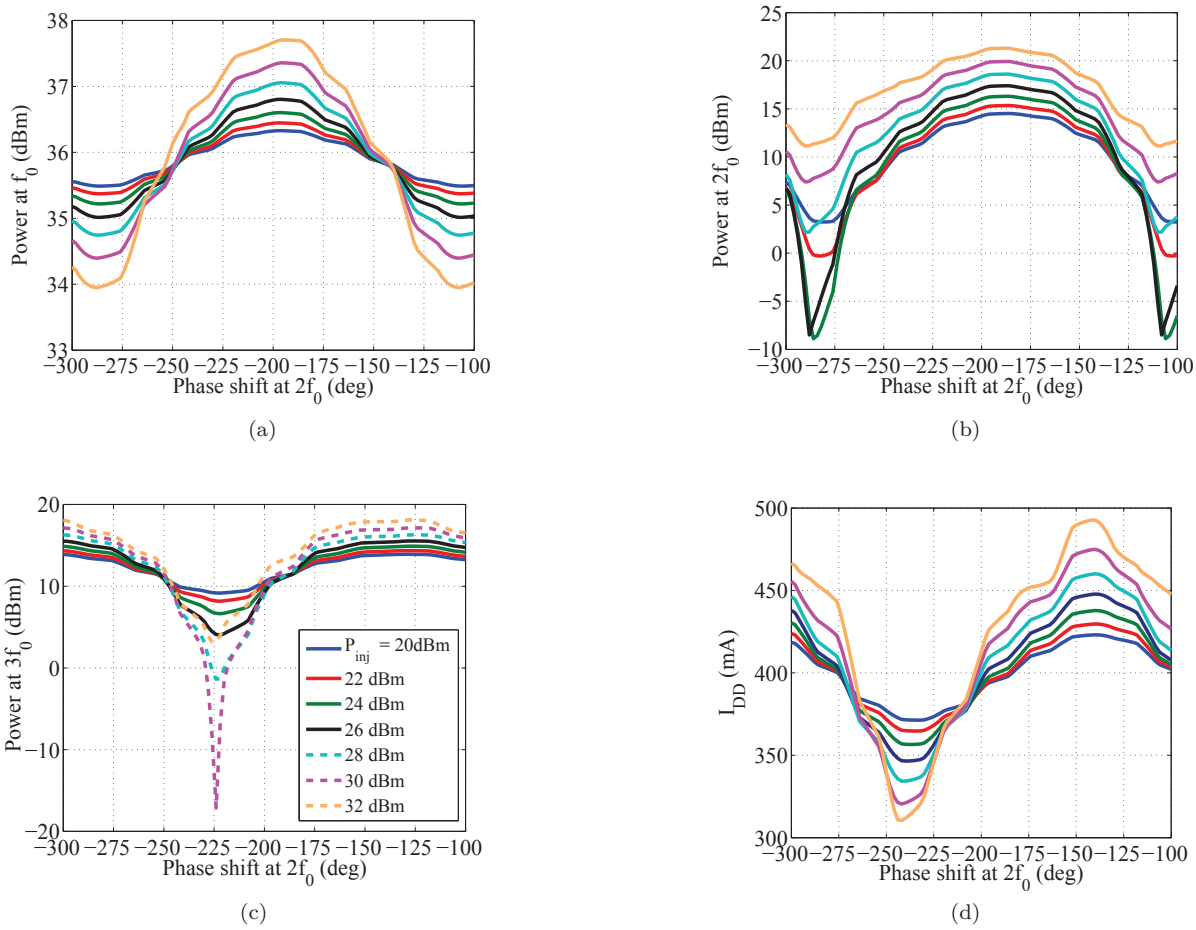

Figure 7.5: Ideal harmonic balance simulations showing variations in (a) fundamental output power, $P_{out}(f_0)$ (b) second harmonic output power, $P_{out}(2f_0)$ (c) third harmonic output power, $P_{out}(3f_0)$, and output drain current, I_{dd}, for the design HI-PA with phase of the injected harmonic swept from 0 to 360° and amplitude from -20 to -8 dBc w.r.t. fundamental output power.

f_0 CLASS-AB PA WITHOUT HARMONIC INJECTION

In class-AB, the PA achieves a maximum efficiency of 48.5% at $f_0 = 10.6$ GHz. A maximum P_{out} of 4 W or 36 dBm is achieved with a small-signal gain of 14 dBm. A comparison of the simulated vs. measured results for the f_0 PA are shown in Fig.7.7. It is seen that measurement and simulation match closely in terms of gain and efficiency even though the frequency is shifted by 600 MHz. A frequency sweep of the f_0 PA shows efficiency and output power in the X-band range as seen in Fig.7.8.

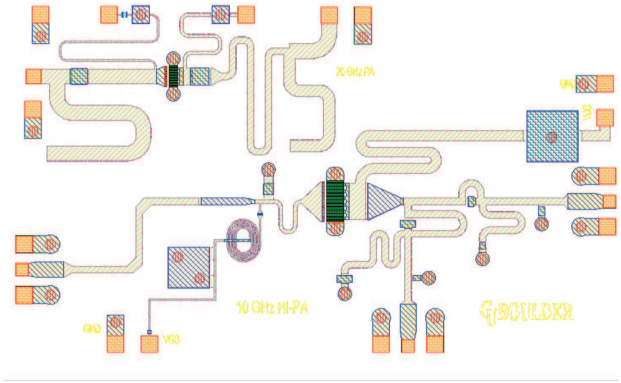

Figure 7.6: Final MMIC layout of the designed HI-PA (bottom) and 20 GHz driver PA (top).

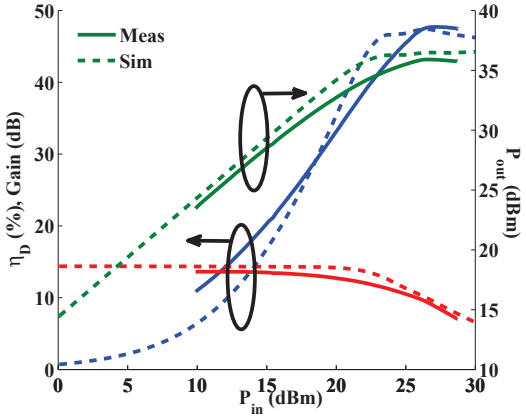

Figure 7.7: Comparison of the simulated (10 GHz) and measured (10.6 GHz) X-band class-A PA without harmonic injection in terms of drain efficiency,η_D, fundamental output power, P_{out} and gain at $V_{dd} = 20$ V and $I_{dq} = 130$ mA.

Second-harmonic Amplifier

The $2f_0$ PA is designed for 20 GHz and measured with class-AB bias with a maximum $P_{out} = 28.3$ dBm and PAE = 59% with a gain of 8 dB as shown in Fig.7.9. It is determined that the maximum power required at $2f_0$ for optimal second harmonic injection is approximately 27 dBm. Therefore, as seen from Fig.7.9, the injection PA is $> 50\%$ efficient at this power level. The high efficiency of the 20-GHz PA reduces the degradation of overall efficiency due to other microwave component losses in the injection path.

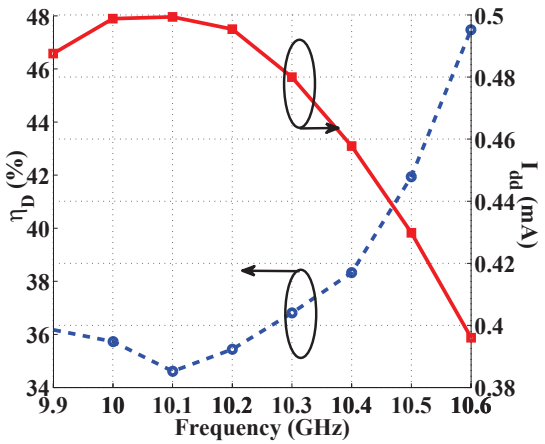

Figure 7.8: Class-AB PA performance in X-band without harmonic injection.

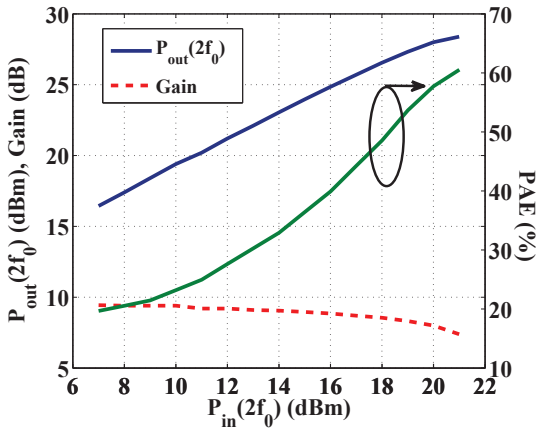

Figure 7.9: Measured response for the 20 GHz driver PA in terms of PAE (green), P_{out} (blue) and gain (red).

Harmonic Injection Test

The HI-PA when tested at 10 and 10.6 GHz with 2^{nd} harmonic injection at an input drive level of 23 dBm (close to P_{1dB}) results in a 15-point efficiency improvement along with a 60 mA reduction in the total drain current. At 1 dB compression, the maximum $P_{out}(f_0) = 35.79$ dBm with the drain current reduced from 0.39 A to 0.33 A at 10.6 GHz. The injected $2f_0$ power needed to achieve this 60 mA reduction in current is approximately 26.2 dBm. Due to the high process f_t [**?**], similar $2f_0$ driver PA efficiencies shown in Fig.7.9 can be obtained at 21.2 GHz. Therefore, at 10.6 GHz, an increase in the total efficiency from 48% to 70% can be achieved by taking into account the $2f_0$ driver PA efficiency at the required $2f_0$ injection power as shown in Fig.7.10.

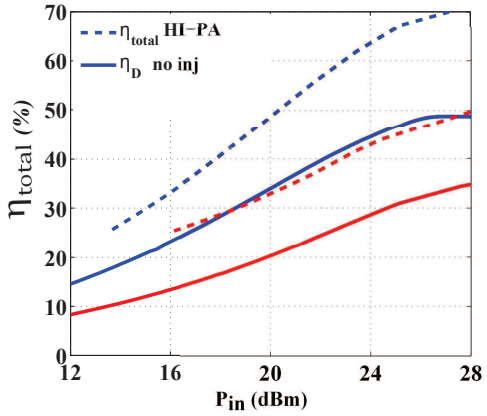

Figure 7.10: Measured and projected total efficiency, η_{total} of HI-PA as a function of fundamental input drive, $P_{in}(f_0)$ at 10 GHz (red) and 10.6 GHz (blue) with $P_{out}(f_0) = 3.5$ W.

7.4 Future Work

Some of the on-going work in the field on harmonically-injected PAs can be applied to communication system by analyzing the HI-PA with basic modulation schemes such as QPSK, 16-QAM, etc. The block diagram shown in Fig.7.11 shows the basic set-up required to analyze the HI-PA with a commuication signal modulation scheme. A linear and atleast 40% efficient injection PA is required in the injection path in order to provide a low distortion injection signal to the main PA. An up-converter (Eg. Hittite HMC819LC5) can be utilized in order to up-convert the input signal for injection. This upconverter has a high side-band rejection of -35 dBc resulting in linear signal and a conversion gain of 15 dBm. Base-band processing can be performed to create a base-band signal which has twice the bandwidth of the fundamental base-band signal. In this technique, the basic parameters to measure for the PA in terms of linearity are the Adjacent channel power ratio or ACPR and error vector magnitude or EVM.

The designed X-band MMIC PA can be measured with the 20 GHz driver PA integrated in hybrid and on-chip environment. Since the maximum output power of the 10 GHz PA is close to 4 W, the maximum power required at 20 GHz would be close to 27 dBm. The designed 20 GHz driver PA has a gain of 8 dB and a resultant efficiency of 60% at compression. The 10 GHz PA and the 20 GHz PA can be connected in a hybrid manner with fixturing provided by TriQuint Semiconductor shown in Fig.7.12 in order to measure the HI-PA. Analog voltage controlled phase shifter (Eg. Hittite HMC933LP4E) and RF sweeper can be used to control

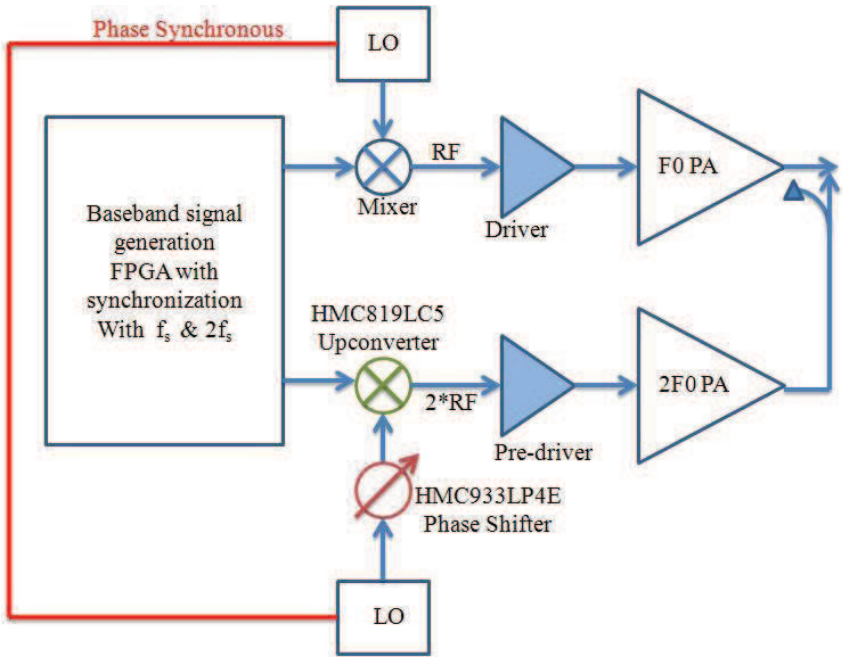

Figure 7.11: Block diagram describing measurement setup HI-PA with standard communication signal modulation schemes. An upconverter is used to create the injection signal along with a voltage controlled phase shifter to change the relative phase of the injected signal w.r.t. the fundamental signal.

the amplitude and phase of the injected harmonic signal.

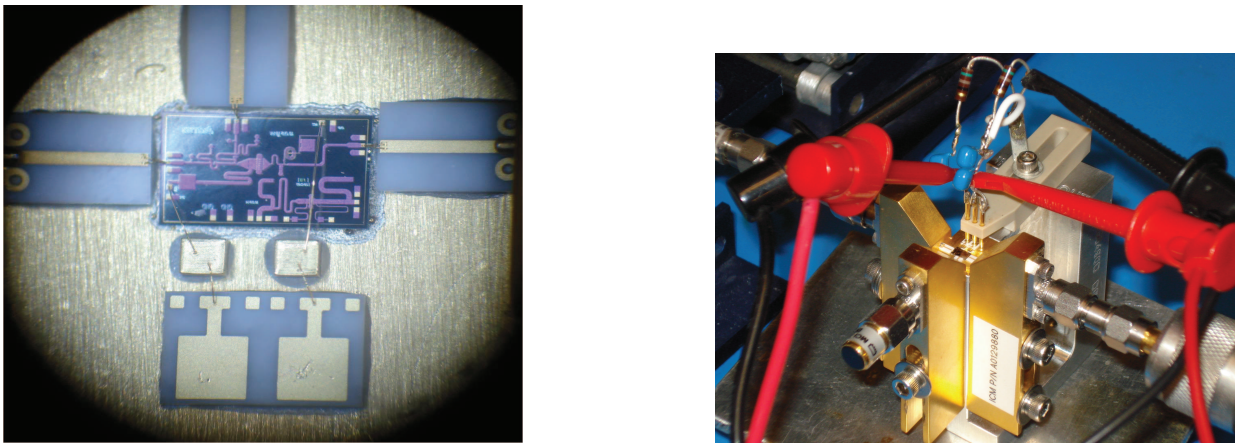

(a) (b)

Figure 7.12: (a) Fixturing for 10 GHz MMIC provided by TriQuint Semiconductor. Alumina lines with bond pads wire-bonded to the RF and DC pads on chip which is mounted on a copper molly substrate. (b) Measurement setup with launcher fixtures to measure the MMIC chip in 50 Ω environment.

The HI-PA can be measured in an integrated environment with the 20 GHz driver PA as designed and shown in Fig.7.13. A pre-driver is also designed at 20 GHz with a smaller gate periphery of 4x75 μ to provide high gain in the injection signal path. Hence, the phase shifter and amplitude control can be done in small-

signal regime which will allow the injection path to be more efficient. Since there is no coupler in the injection path of the diplexer network for power calibration, the characterization of the pre-driver and driver PAs needs to be performed first in order to understand the required input power level to achieve the maximum output power required from the driver PA. Once the 20 GHz PA characterization is done, the integrated HI-PA can be measured with an estimate of the injected signal amplitude.

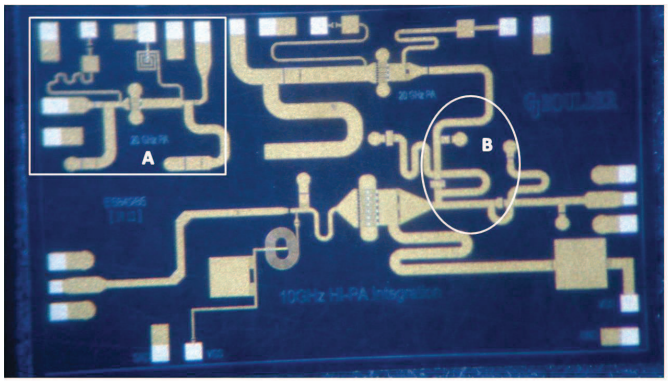

Figure 7.13: MMIC design for 10 GHz HIPA integrated with 20 GHz Driver PA using an integration in the output diplexer network (B). A pre-driver at 20 GHz designed for high gain in the injection path (A).

Some of the other work related to HI-PAs can be done in expanding the signal bandwidth and design of diplexer network for broad-band applications. Harmonic injection at higher even order harmonics can also be investigated to enhance efficiency and linearity in a PA. As seen in Ch.2, lot of work has been done to enhance linearity by injection at the input. Therefore, harmonic injection can be investigated with simultaneous injection at both input and output of the PA.

7.5 Contributions

Ch.2 presents theoretical analysis of achieving high efficiency and linearity for harmonically injected PAs with second harmonic at the output. Waveform shaping with addition of even and odd harmonics is analyzed along with intermodulation distortion (IMD) behavior for various classes of PA. Theoretical reasoning for asymmetrical reduction of IMD products is given with power series analysis for a PA in terms of drain current, i_d and transconductance, g_m.

In Ch.3, the theoretical concept of harmonic injection at the output of a class-A/AB PA is validated with

experimental results using commercial broadband amplifiers from Cree. The PA is measured in S-band at f_0 - 2.45 GHz with a diplexer network built for 50 Ω environment. Efficiency improvements of 15% are shown over the class-AB PA with η_D improving from 58% to 75%. Two-tone measurements also demonstrate linearity of the PA with >20 dB reduction in $IMD3$ products with harmonic injection at one of the two harmonic tones. The measurements are results are presented in [72].

In Ch.4, an integrated hybrid HI-PA is designed with the diplexer network integrated with output matching in a non-50 Ω environment. The PA is designed for class-AB mode of operation with large signal gain of 23 dB and $P_{out} = 5$ W. Characterization with 2^{nd} harmonic injection at the output of the PA is performed for optimization in linearity and efficiency. Variation in PA parameters such as P_{out} at fundamental and harmonics along with η_D, gain and Drain current, I_{dd} w.r.t. the amplitude and phase of the injected second harmonic is presented in [9].

- Efficiency enhancement shows maximum total efficiency improvement of 30% over class-AB PA with maximum $\eta_D = 89\%$ for the HI-PA. The power required at the injected harmonic to achieve this efficiency is -5.5 dBc.

- Linearity analysis is performed in terms of second and third harmonic content for the HI-PA. Optimization for minimum third harmonic content results in total efficiency improvement of 20% for a CW signal with max $\eta_D = 78\%$ and third harmonic reduction by > 15 dB in compression with the injected harmonic power 10 dBc w.r.t. fundamental output power. The total output power reduces by 0.26 dB w.r.t. class-AB PA.

In Ch.5, the behavior of odd order distortion products for fundamental two-tone signal is studied in harmonically-injected PA. Harmonic injection is performed at one of the two harmonic tones at the output of the designed hybrid HI-PA resulting in reduction of distortion products which are directly related to the injected harmonic tone frequency. It is shown that a corelation between CW and two-tone measurements can be done based on third order nonlinearity of the PA. Linearization of PA using harmonic injection at the output is presented in [83].

- Variation in both $IMD3$ and $IMD5$ w.r.t. amplitude and phase of the injected harmonic is presented.

This result is similar to the one presented for third harmonic at the output of the PA for CW tones in Ch.4. The third and fifth order distortion products are reduced by > 20 dB in linear region of the PA and > 10 dB in saturation.

- Reduction of distortion products is studied for harmonically injected PAs with tone spacings from 1-20 MHz. It is shown that the phase required for both the harmonic tones to reduce the upper and lower sideband $IMD3$ products differs by 20^{circ} for tone spacings of 1 to 10 MHz.

- The analysis presented shows that simultaneous reduction in third and fifth order products can be achieved with harmonic injection at both harmonic tones if there are no sweet-spots present in the distortion products for the class-AB PA. The phase shift required in the injected harmonics to achieve maximum reduction in $IMD3$ and $IMD5$ products differs by 50^{circ} for tone spacings of 1-10 MHz.

- Finally, harmonic balance simulations of variation in the optimum load for maximum linearity is presented showing that the trade-off required between efficiency and linearity for harmonically-injected PAs is less costly as compared to class-AB PAs with 15% reduction in total efficiency and 5 dB reduction in $IMD3$ for the harmonically-injected PA at a load selected to achieve the trade-off.

Ch.6 shows first time, the integration of supply variation with a harmonically-injected PA. Two different methods are presented to achieve high efficiency and linearity for high Peak-to-Average ratios of > 6 dB.

- In the first method, harmonic balance simulations are presented with variation in supply and injected signal amplitude while keeping the input drive and relative phase of the injected harmonic at a constant optimal value. The simulated and measured results show constant total efficiency of 66% for a 6 dB variation in output power. The supply voltage and injected signal amplitude are varied linearly to achieve variation in output power.

- In the second method, the supply is varied with the input drive level by maintaining a constant ratio between the injected signal and the input drive level. The phase of the injected signal is again fixed to an optimal value. The simulated and measured results show total efficiencies of 70-80% for a 7 dB variation in outpput power. Measurements also show the reduction in third order nonlinearity i.e. $P_{out}(3f_0)$ by > 15 dB. AM-PM measurements also show reduction in phase distortion in the PA resulting higher

linearity. The analysis of harmonically-injected PA with supply modulation is presented in [87] and a journal paper describing these results in detail is in preparation [88].

Finally, an X-Band MMIC is designed for an integrated HI-PA at 10 GHz with a 20 GHz driver PA in order to achieve 4 W of output power with $> 65\%$ efficiency at 10 GHz. The class-AB PA designed is 47% efficient at 10.6 GHz with a small-signal gain of 14 dB.

Bibliography

[1] "Solid state technologies." http://www.darpa.mil/uploadedImages/Content/Our_Work/MTO/Programs/Nitride_Electronic_NeXt-Generation_Technology/NEXT_2.jpg. xi, 5

[2] J. Hoversten, *Efficient and LInear Microwave Transmitters for High Peak-to-Average Ratio Signals*. PhD thesis, Dept of ECEE, CU- Boulder, 2010. xi, 8, 11, 12, 51

[3] F. Raab, P. Asbeck, S. Cripps, P. Kenington, Z. Popovic, N. Pothecary, J. Sevic, and N. Sokal, "Power amplifiers and transmitters for rf and microwave," *Microwave Theory and Techniques, IEEE Transactions on*, vol. 50, no. 3, pp. 814–826, 2002. xi, 14, 17, 18

[4] S. Nishiki and T. Nojima, "Harmonic reaction amplifier - a novel high-efficiency and high-power microwave amplifier," in *Microwave Symposium Digest, 1987 IEEE MTT-S International*, 9 1987. xii, 21, 22

[5] M. Wirth, A. Singh, J. Scharer, and J. Booske, "Third-order intermodulation reduction by harmonic injection in a twt amplifier," *Electronic Devices, IEEE Transactions on*, vol. 49, pp. 1082–1084, June 2002. xii, 22, 23, 24

[6] C. Aitchison and et.al., "Improvement of Third-Order Intermodulation Product of RF and Microwave Amplifiers by Injection," *Microwave Theory and Techniques, IEEE Transactions on*, vol. 49, pp. 1148–1154, June 2001. xii, 23, 24

[7] A. AlMuhaisen, S. Cripps, and et. al., "Novel wide band high-efficiency active harmonic injection power amplifier concept," in *Microwave Symposium Digest (MTT), 2010 IEEE MTT-S International*, pp. 664–667, may 2010. xii, xvii, 23, 24, 25, 42, 45, 52, 54, 91, 98, 110

[8] N. de Carvalho and J. Pedro, "Large- and small-signal imd behavior of microwave power amplifiers," *Microwave Theory and Techniques, IEEE Transactions on*, vol. 47, no. 12, pp. 2364–2374, 1999. xii, 32, 36

[9] A. Dani, M. Roberg, and Z. Popovic, "Pa efficiency and linearity enhancement using external harmonic injection," *Microwave Theory and Techniques, IEEE Transactions on*, vol. 60, pp. 4097 –4106, dec. 2012. xvii, 24, 70, 91, 93, 98, 119

[10] F. Raab, "Class-E, Class-C, and Class-F power amplifiers based upon a finite number of harmonics," *Microwave Theory and Techniques, IEEE Transactions on*, vol. 49, pp. 1462 –1468, Aug 2001. 2

[11] F. Raab et al., "Power amplifiers and transmitters for RF and microwave," *Microwave Theory and Techniques, IEEE Transactions on*, vol. 50, pp. 814 –826, Mar 2002. 2

[12] S. Kee, I. Aoki, A. Hajimiri, and D. Rutledge, "The class-e/f family of zvs switching amplifiers," *Microwave Theory and Techniques, IEEE Transactions on*, vol. 51, pp. 1677 – 1690, jun. 2003. 2

[13] M. Roberg and Z. Popovic, "Analysis of high-efficiency power amplifiers with arbitrary output harmonic terminations," *Microwave Theory and Techniques, IEEE Transactions on*, vol. 59, pp. 2037–2048, Aug. 2011. 2

[14] P. Asbeck and et. al., "Design options for high efficiency linear handset power amplifiers," in *Silicon Monolithic Integrated Circuits in RF Systems, 2009. SiRF '09. IEEE Topical Meeting on*, pp. 1 –4, jan. 2009. 2, 89

[15] J. Hoversten and et. al., "Codesign of pa, supply, and signal processing for linear supply-modulated rf transmitters," *Microwave Theory and Techniques, IEEE Transactions on*, vol. 60, pp. 2010 –2020, june 2012. 2, 89, 101, 104

[16] D. Kimball and et. al., "High-efficiency envelope-tracking w-cdma base-station amplifier using gan hfets," *Microwave Theory and Techniques, IEEE Transactions on*, vol. 54, pp. 3848 –3856, nov. 2006. 2, 89

[17] F. Raab, "Efficiency of outphasing rf power-amplifier systems," *Communications, IEEE Transactions on*, vol. 33, pp. 1094 – 1099, oct 1985. 2, 89

[18] M. Weiss, *Switched-Mode Microwave Circuits for High Efficiency Transmitters*. PhD thesis, Dept of ECEE, CU- Boulder, 2001. 3

[19] S. J. C. H. Theeuwen and J. Qureshi, "Ldmos technology for rf power amplifiers," *Microwave Theory and Techniques, IEEE Transactions on*, vol. 60, no. 6, pp. 1755–1763, 2012. 3

[20] P. Perugupalli, Y. Xu, and K. Shenai, "Measurement of thermal and packaging limitations in ldmosfets for rfic applications," in *Instrumentation and Measurement Technology Conference, 1998. IMTC/98. Conference Proceedings. IEEE*, vol. 1, pp. 160–164 vol.1, 1998. 3

[21] J.-M. Bosc, I. Percheron-Garcon, E. Huynh, P. Lance, I. Pages, J. M. Dorkel, and G. Sarrabayrouse, "Reliability characterization of ldmos transistors submitted to multiple energy discharges," in *Power Semiconductor Devices and ICs, 2000. Proceedings. The 12th International Symposium on*, pp. 165–168, 2000. 3

[22] J. Hudgins, G. Simin, and M. Khan, "A new assessment of the use of wide bandgap semiconductors and the potential for GaN," *2002 IEEE 33rd Annual IEEE Power Electronics Specialists Conference. Proceedings (Cat. No.02CH37289)*, vol. 4, pp. 1747–1752, 2002. 4, 5

[23] D. C. Dumka, C. Lee, H. Q. Tserng, and P. Saunier, "RF reliability performance of AlGaN = GaN HEMTs on Si substrate at 10 GHz," vol. 40, no. 24, pp. 24–25, 2004. 4, 5

[24] J. Technical and C. Services, "Advances in," vol. 90703, no. 1, pp. 5–8. 5, 7

[25] G. Meneghesso, G. Verzellesi, R. Pierobon, F. Rampazzo, A. Chini, U. K. Mishra, C. Canali, A. Member, E. Zanoni, and S. Member, "Surface-Related Drain Current Dispersion Effects in AlGaN âĂŞ GaN HEMTs," vol. 51, no. 10, pp. 1554–1561, 2004. 5

[26] A. Chini, F. Fantini, V. Di Lecce, M. Esposto, A. Stocco, N. Ronchi, F. Zanon, G. Meneghesso, and E. Zanoni, "Correlation between DC and rf degradation due to deep levels in AlGaN/GaN HEMTs," *2009 IEEE International Electron Devices Meeting (IEDM)*, pp. 1–4, Dec. 2009. 5

[27] A. M. Darwish, B. D. Huebschman, E. Viveiros, H. A. Hung, and S. Member, "Dependence of GaN HEMT Millimeter-Wave Performance on Temperature," vol. 57, no. 12, pp. 3205–3211, 2009. 5

[28] J. del Alamo, "Critical Voltage for Electrical Degradation of GaN High-Electron Mobility Transistors," *IEEE Electron Device Letters*, vol. 29, pp. 287–289, Apr. 2008. 6

[29] a. Prejs, S. Wood, R. Pengelly, and W. Pribble, "Thermal analysis and its application to high power GaN HEMT amplifiers," *2009 IEEE MTT-S International Microwave Symposium Digest*, pp. 917–920, June 2009. 6

[30] M. Faqir, G. Verzellesi, F. Fantini, F. Danesin, F. Rampazzo, G. Meneghesso, E. Zanoni, a. Cavallini, a. Castaldini, N. Labat, a. Touboul, and C. Dua, "Characterization and analysis of trap-related effects in AlGaNâĂŞGaN HEMTs," *Microelectronics Reliability*, vol. 47, pp. 1639–1642, Sept. 2007. 6

[31] G. Hemts, S. C. Binari, K. Ikossi, J. A. Roussos, W. Kruppa, S. Member, D. Park, H. B. Dietrich, D. D. Koleske, A. E. Wickenden, and R. L. Henry, "Trapping Effects and Microwave Power Performance," vol. 48, no. 3, pp. 465–471, 2001. 6

[32] M. Hosch, J. W. Pomeroy, A. Sarua, M. Kuball, H. Jung, and H. Schumacher, "Field Dependent Self-Heating Effects in High-Power AlGaN / GaN HEMTs," pp. 2–4, 2009. 6

[33] Y.-R. Wu and J. Singh, "Transient study of self-heating effects in AlGaN/GaN HFETs: Consequence of carrier velocities, temperature, and device performance," *Journal of Applied Physics*, vol. 101, no. 11, p. 113712, 2007. 6

[34] O. Jardel, G. Callet, J. Dufraisse, N. Sarazin, E. Chartier, T. Reveyrand, M. Oualli, and D. Lancereau, "Performances of AlInN / GaN HEMTs for Power Applications at Microwave Frequencies," no. September, pp. 49–52, 2010. 6

[35] G. H. Jessen, R. C. Fitch, J. K. Gillespie, G. Via, A. Crespo, D. Langley, D. J. Denninghoff, S. Member, M. Trejo, E. R. Heller, and A. Algan, "Short-Channel Effect Limitations on High-Frequency Operation of AlGaN / GaN HEMTs for T-Gate Devices," pp. 2589–2597, 2007. 6

[36] Y. Okamoto, T. Nakayama, Y. Ando, A. Wakejima, K. Matsunaga, K. Ota, and H. Miyamoto, "230 W C-band GaN-FET power amplifier," vol. 43, no. 17, pp. 16–17, 2007. 7

[37] H. Shigematsu, Y. Inoue, a. Akasegawa, M. Yamada, S. Masuda, Y. Kamada, a. Yamada, M. Kanamura, T. Ohki, K. Makiyama, N. Okamoto, K. Imanishi, T. Kikkawa, K. Joshin, and N. Hara, "C-band 340-W and X-band 100-W GaN power amplifiers with over 50-% PAE," *2009 IEEE MTT-S International Microwave Symposium Digest*, pp. 1265–1268, June 2009. 7

[38] K. Yamanaka, K. Iyomasa, H. Ohtsuka, M. Nakayama, Y. Tsuyama, T. Kunii, Y. Kamo, and T. Takagi, "S and c band over 100 w gan hemt 1-chip high power amplifiers with cell division configuration," in *Gallium Arsenide and Other Semiconductor Application Symposium, 2005. EGAAS 2005. European*, pp. 241–244, 2005. 7

[39] A. Margomenos, A. Kurdoghlian, M. Micovic, K. Shinohara, D. Brown, R. Bowen, I. Milosavljevic, R. Grabar, C. Butler, A. Schmitz, P. Willadsen, M. Madhav, and D. Chow, "70-105 ghz wideband gan power amplifiers," in *Microwave Integrated Circuits Conference (EuMIC), 2012 7th European*, pp. 199–202, 2012. 7

[40] M. Micovic, A. Kurdoghlian, A. Margomenos, D. Brown, K. Shinohara, S. Burnham, I. Milosavljevic, R. Bowen, A. Williams, P. Hashimoto, R. Grabar, C. Butler, A. Schmitz, P. Willadsen, and D. H. Chow, "92-96 ghz gan power amplifiers," in *Microwave Symposium Digest (MTT), 2012 IEEE MTT-S International*, pp. 1–3, 2012. 7

[41] S. Schafer, M. Litchfield, A. Zai, C. Campbell, and Z. Popovic, "X-Band MMIC GaN Power Amplifiers Designed for High-Efficiency Supply-Modulated Transmitters," in *Microwave Symposium Digest (MTT), 2013 IEEE MTT-S International*, pp. 1–3, 2013. 7, 112

[42] S. Cripps, *RF Power Amplifiers for Wireless Communications*. 685 Canton St. Norwood, MA 02062: Artech House Publishers, 2nd ed., May 2006. 10, 52, 58

[43] M. Roberg, *Analysis & Design of Non-Linear Amplifiers for Efficient Microwave Transmitters*. PhD thesis, Dept. of ECEE, CU-Boulder, 2012. 11, 24, 25, 31, 37, 42, 44, 52, 54, 56

[44] Y. Y. Woo, Y. Yang, B. Kim, and S. Member, "Analysis and Experiments for High-Efficiency Class-F and Inverse Class-F Power Amplifiers," vol. 54, no. 5, pp. 1969–1974, 2006. 12

[45] F. Raab, "Class-f power amplifiers with maximally flat waveforms," *Microwave Theory and Techniques, IEEE Transactions on*, vol. 45, no. 11, pp. 2007–2012, 1997. 12

[46] A. Rudiakova and V. Krizhanovski, "Driving waveforms for class-f power amplifiers [gaas mesfets]," in *Microwave Symposium Digest. 2000 IEEE MTT-S International*, vol. 1, pp. 473–476 vol.1, 2000. 12

[47] M. VasicÌĄ, O. Garcia, J. Oliver, P. Alou, D. Diaz, J. Cobos, A. Gimeno, J. Pardo, C. Benavente, and F. J. Ortega, "High efficiency power amplifier based on envelope elimination and restoration technique," in *Energy Conversion Congress and Exposition (ECCE), 2010 IEEE*, pp. 3833–3840, 2010. 17

[48] H. Chireix, "remnaining amiplifier. *," vol. 23, no. 11, pp. 1370–1392, 1935. 17

[49] F. Raab, "Efficiency of outphasing rf power-amplifier systems," *Communications, IEEE Transactions on*, vol. 33, no. 10, pp. 1094–1099, 1985. 17

[50] B. Kim, J. Kim, I. Kim, J. Cha, and S. Hong, "Microwave doherty power amplifier for high efficiency and linearity," in *Integrated Nonlinear Microwave and Millimeter-Wave Circuits, 2006 International Workshop on*, pp. 22–25, 2006. 17

[51] J. Esch, "High-efficiency doherty power amplifiers: Historical aspect and modern trends," *Proceedings of the IEEE*, vol. 100, no. 12, pp. 3187–3189, 2012. 17

[52] T. Liu, Y. Ye, Z. Fan, X. Zeng, and F. Ghannouchi, "Linearization of wideband rf doherty power amplifiers with complex dynamic nonlinearities," in *Communications and Networking in China, 2008. ChinaCom 2008. Third International Conference on*, pp. 974–977, 2008. 18

[53] C. Liu, H. Xiao, Q. Wu, and F. Li, "Linear rf power amplifier design for wireless signals: a spectrum analysis approach," in *Acoustics, Speech, and Signal Processing, 2003. Proceedings. (ICASSP '03). 2003 IEEE International Conference on*, vol. 4, pp. IV–568–71 vol.4, 2003. 18

[54] K. Gard, H. Gutierrez, and M. Steer, "Characterization of spectral regrowth in microwave amplifiers based on the nonlinear transformation of a complex Gaussian process," *IEEE Transactions on Microwave Theory and Techniques*, vol. 47, pp. 1059–1069, July 1999. 18

[55] P. Medrel, T. Reveyrand, a. Martin, P. Bouysse, J.-M. Nebus, and J. Sombrin, "Time domain envelope characterization of power amplifiers for linear and high efficiency design solutions," *Wamicon 2013*, pp. 1–6, Apr. 2013. 18

[56] Y.-S. Lee, M.-W. Lee, S.-H. Kam, and Y.-H. Jeong, "Advanced design of high-linearity analog predistortion doherty amplifiers using spectrum analysis for wcdma applications," in *Radio and Wireless Symposium (RWS), 2010 IEEE*, pp. 140–143, 2010. 19

[57] J. Moon, J. Son, J. Kim, I. Kim, S. Jee, Y. Y. Woo, and B. Kim, "Doherty amplifier with envelope tracking for high efficiency," in *Microwave Symposium Digest (MTT), 2010 IEEE MTT-S International*, pp. 1086–1089, 2010. 19

[58] D. Willems et al., "High efficiency harmonic injection power amplifier," December 1991. 21

[59] Z. Zivkovic and A. Markovic, "Increasing the efficiency of the high-power triode hf amplifier -why not with the second harmonic?," *Broadcasting, IEEE Transactions on*, vol. BC-32, no. 1, pp. 5 –10, 1986. 21

[60] Z. Zivkovic-Dzunja and A. Markovic, "Plate and grid modulated hf high-power tuned amplifier with increased efficiency," *Broadcasting, IEEE Transactions on*, vol. 35, pp. 97 –107, Mar. 1989. 21

[61] A. Juhas, L. Novak, and S. Kostic, "Signals with flattened extrema in balance power analysis of hfhpta: theory and applications," *Broadcasting, IEEE Transactions on*, vol. 47, pp. 38 –45, Mar. 2001. 21

[62] C.-W. Fan and K.-K. Cheng, "Theoretical and experimental study of amplifier linearization based on harmonic and baseband signal injection technique," *Microwave Theory and Techniques, IEEE Transactions on*, vol. 50, no. 7, pp. 1801–1806, 2002. 22

[63] S. Kusunoki, K. Kawakami, and T. Hatsugai, "Load-Impedance and Bias-Network Dependence of Power Amplifier With Second Harmonic Injection," *Microwave Theory and Techniques, IEEE Transactions on*, vol. 52, pp. 2169–2176, Sept. 2004. 22

[64] M. R. Moazzam and C. Aitchison, "A low third order intermodulation amplifier with harmonic feedback circuitry," in *Microwave Symposium Digest, 1996., IEEE MTT-S International*, vol. 2, pp. 827–830 vol.2, 1996. 23

[65] H. Matsubara, F. Kawanabe, and T. Nojima, "A 2-ghz band experiment on efficiency enhancement of a

gan power amplifier using 2nd harmonic injection," in *Microwave Conf., APMC. Asia-Pacific*, pp. 1 –4, 2008. 23

[66] A. AlMuhaisen, P. Wright, J. Lees, P. Tasker, S. Cripps, and J. Benedikt, "Wide band high-efficiency power amplifier design," in *Microwave Integrated Circuits Conference (EuMIC), 2011 European*, pp. 184–187, Oct 2011. 23, 42, 45, 52, 98

[67] H. R. Bae, C. S. Cho, and J. W. Lee, "Efficiency enhanced class-e power amplifier using the second harmonic injection at the feedback loop," in *Microwave Conference (EuMC), 2010 European*, pp. 1042 –1045, 2010. 23

[68] A. Telegdy, B. Molnar, and N. Sokal, "Class-em switching-mode tuned power amplifier-high efficiency with slow-switching transistor," *Microwave Theory and Techniques, IEEE Transactions on*, vol. 51, pp. 1662 – 1676, june 2003. 24

[69] A. Ramadan, T. Reveyrand, A. Martin, J. M. Nebus, P. Bouysse, L. Lapierre, J. F. Villemazet, and S. Forestier, "Experimental study on effect of second-harmonic injection at input of classes f and f-1 gan power amplifiers," *Electronics Letters*, vol. 46, no. 8, pp. 570–572, 2010. 24

[70] Z. Zivkovic and A. Markovic, "Third harmonic injection increasing the efficiency of high-power hf amplifiers," *Broadcasting, IEEE Transactions on*, vol. BC-31, no. 2, pp. 34 –39, 1985. 24

[71] J.G.Wolhlbier, J.H.Booske, and I. Dobson, "On the physics of harmonic injection in a travelling wave tube," *Plasma Science, IEEE Transactions on*, vol. 32, pp. 1073–1085, June 2004. 24, 93

[72] A. Dani, M. Roberg, and Z. Popovic, "Efficiency and linearity of power amplifiers with external harmonic injection," in *Microwave Symposium Digest (MTT), 2012 IEEE MTT-S International*, pp. 1 –3, june 2012. 25, 49, 79, 119

[73] P. Colantonio, F. Giannini, and E. Limiti, *High Efficiency RF and Microwave Solid State Power Amplifiers*. The Atrium, West Sussex, UK: J. Wiley and sons publications, 2009. 25, 58

[74] I. J. Bahl, *Fundamental of RF and Microwave Transistor Amplifiers, Ch. 12, pp. 332-333*. 111 River street, Hoboken, New Jersey: J. Wiley & Sons, 2009. 33, 58, 62

[75] P. B. Kenington, *High-Linearity RF Amplifier Design, Ch. 2, pp. 21-85*. 685 Canton street, Norwood, MA: Artech House publications, 2000. 33, 63, 67, 96

[76] J. Aikio and T. Rahkonen, "Detailed analysis of imd in an ldmos rf power amplifier," in *Microwave Symposium Digest, 2005 IEEE MTT-S International*, pp. 4 pp.–, 2005. 36

[77] N. de Carvalho and J. Pedro, "Large signal imd sweet spots in microwave power amplifiers," in *Microwave Symposium Digest, 1999 IEEE MTT-S International*, vol. 2, pp. 517–520 vol.2, 1999. 36

[78] F. G. Paolo Colantonio and E. Limiti, *High Efficiency RF and Microwave Solid State Power Amplifiers*. The Atrium, Southern Gate, Chichester, West Sussex, PO198SQ, UK: John Wiley and Sons, 2009. 37

[79] "Cree cgh40006p datasheet." http://www.cree.com/rf/products/general-purpose-broadband-28-v/packaged-discrete-transistors/cgh40006p. 43

[80] S. Pajic, *Robust design methodology for class-E amplifiers for microwave applications*. PhD thesis, Dept of ECEE, CU- Boulder, 2005. 51

[81] "6 watt discrete power gan on sic hemt, part tgf2023-01." http://www.triquint.com/products/p/TGF2023-2-01. 51

[82] J. Voulevi and T. Rahkonen, *Distortion in RF Power Amplifiers*. 685 Canton street, Norwood, MA: Artech House Publications, 2003. Chp. 3, Memory Effects in RF Power Amplifiers. 75, 83

[83] A. Dani and Z. Popovic, "Linearization of efficient harmonically-injected pas," in *Power Amplifiers for Wireless and Radio Applications (PAWR), 2013 IEEE Topical Conference on*, pp. 31–33, 2013. 87, 119

[84] "Linearization of efficient harmonically-injected pas." PA Symposium, University of San Diego, Sept 2012. 87

[85] C. Clark, C. P. Silva, A. A. Moulthrop, and M. S. Muha, "Power-amplifier characterization using a two-tone measurement technique," *Microwave Theory and Techniques, IEEE Transactions on*, vol. 50, no. 6, pp. 1590–1602, 2002. 99, 106

[86] J. Laico, H. McDowell, and M. C.R., "A medium power travelling-wave tube for 6000-mc radio relay," *Bell System Technical Journal*, vol. 35, pp. 1285–1346, Nov. 1956. 106

[87] A. Dani, M. Coffey, and Z. Popovic, "Efficient linear supply-modulated pa with harmonic injection," in *European Microwave Conference, EuMC 2013, Nuremburg, Germany*, pp. 1–4, 2013. 107, 121

[88] A. Dani, M. Coffey, and Z. Popovic, "Efficient and linear supply modulated pa with harmonic injection for high pars," *To be submitted to Microwave Theory and Techniques, IEEE Transactions on*, 2013. 121